

Stability of 41 metal - boron systems at 0 GPa and 30 GPa from first principles

A.G. Van Der Geest[‡], A.N. Kolmogorov[‡]

[‡] State University of New York - Binghamton, USA

Corresponding author: A.N. Kolmogorov <kolmogorov@binghamton.edu>

(Dated: February 13, 2018)

A multitude of observed boron-based materials have outstanding superconducting, mechanical, and refractory properties. Yet, the structure, the composition, and the very existence of some reported metal boride (M-B) compounds have been a subject of extensive debate. This density functional theory work seeks to set a baseline for current understanding of known metal boride phases as well as to identify new synthesizable candidates. We have generated a database of over 12,000 binary M-B entries for pressures of 0 and 30 GPa producing the largest scan of compositions and systems in this materials class. The 175 selected crystal structures include both observed prototypes and new ones found with our evolutionary ground state search. The metals considered are: Al, Ag, Au, Ba, Be, Ca, Cd, Co, Cr, Cs, Cu, Fe, Hf, Hg, Ir, K, La, Li, Mg, Mn, Mo, Na, Nb, Ni, Os, Pd, Pt, Rb, Re, Rh, Ru, Sc, Sr, Ta, Tc, Ti, V, W, Y, Zn, and Zr. Based on the formation energy calculated at zero pressure and temperature 4 new M-B phases or structures have been predicted, while a number of previously reported compounds have been shown to be unstable. At 30 GPa, changes in the convex hulls are expected to occur in 18 out of 41 M-B systems, which is used to indicate regions of the periodic table (for metal borides) that require further investigation from the community. Analysis of the collected information has revealed a nearly linear relationship between the magnetic moment per atom and the metal content for all the Fe-B, Co-B, and Ni-B structures within 0.15 eV/atom of the stability tie line. Both GGA-PBE and LDA-PW functionals were used to provide an understanding of the systematic error introduced by the choice of the exchange-correlation functional.

I. INTRODUCTION

Boron forms compounds with nearly all metals and defines a remarkable variety of morphologies in compounds, including 3D polyhedron frameworks, 2D nets, and 1D chains^{1,2}. The richness and the complexity of metal boride structures can be traced back to the behavior of pure boron. Namely, the tendency of the second-row element to form covalent bonds sets boron apart from the neighboring nearly-free-electron metals in the periodic table, such as magnesium or aluminum³. At the same time, the three valence electrons are insufficient to fill up all the bonding states in stable covalent structures adopted by tetravalent elements, such as carbon or silicon³. The resulting frustration makes boron a metalloid with arguably the most complex non-magnetic elemental ground state under normal conditions⁴⁻⁶. For example, the stability of the known ambient-pressure α -B and β -B polymorphs along with the recently discovered high-pressure γ -B polymorph has been subject of numerous recent studies⁴⁻⁸.

Not surprisingly, mixing boron with metals of different size and valence has created a large class of inorganic compounds with diverse mechanical and electronic properties, some of which have been uncovered only in recent years⁹⁻¹⁴. The most striking example is the 2001 discovery of a phonon-mediated superconducting transition in a well-known binary compound, MgB₂, at a record-breaking 39 K¹⁰. The research generated by this breakthrough has identified unusual non-centrosymmetric superconductors (Li₂(Pd,Pt)₃B^{11,12,15,16} and Ru₇B₃¹³) and has led to a number of predicted conventional superconducting boron-based materials (Li_xBC¹⁷, LiB^{18,19},

Li-TM-B¹⁹, and Fe-B⁵). One of the proposed new materials, FeB₄, has been synthesized recently and appears to be the first superconductor designed entirely on the computer¹⁴. Due to the super hardness of pure boron²¹, metal borides have also attracted attention as candidate cheap hard materials²². ReB₂²³ and CrB₄⁶ have been suggested to have unusually high hardness, but further investigations have indicated that they are not super hard²⁵⁻²⁷. A lot of recent work has been dedicated to related transition-metal borides, such as WB₃/WB₄²⁸⁻³² and the Mo-B system³³⁻³⁵. The chemical inertness and low volatility of metal borides have also allowed for their commercial use as refractory materials³⁶, thermionic emitters^{37,38}, and steel strengthening agents³⁹. It is worth noting that the strongest permanent magnets include a small amount of boron in a complex Nd-Dy-Fe-B compound⁴⁰.

Over the last decades the techniques used to investigate metal boride structures have varied greatly. Leading up to and during the 1960's a majority of the known metal borides were synthesized for the first time⁴¹⁻⁴³. Development of chemically intuitive semi-empirical electronic structure methods during the 1970's and 1980's has been instrumental for building structural and binding models for selected compounds. Examples include the studies of the La and Y hexaborides⁴⁴, Mn and Cr tetraborides⁴⁵, and several other Cr borides⁴⁶. Advances in density functional theory (DFT)⁴⁷⁻⁴⁹ during the 1990's into the 2000's enabled characterization of materials through systematic calculations of their stability across the periodic table. For example, Oguchi⁵⁰ studied binding trends for the AlB₂ prototype, while Kolmogorov and Curtarolo⁵¹ rationalized the stability of several metal boride structures.

Screening large libraries of *known* crystal structures and various compositions has emerged as an increasingly popular approach to not only identify new materials, but to also check the reliability of DFT-based methods^{52–57}. Curtarolo *et al.*⁵² showed that formation energy evaluated with DFT at zero temperature is a reliable criterion for compound existence giving a 92.4% agreement (97% with experimental error removed) with experiment for 80 binary metal systems. A number of computational frameworks have been developed, such as AFLOW⁵⁸ or the Materials Project⁵⁵, that enable high-throughput screening of available inorganic databases for new materials with targeted properties⁵⁹.

Other search techniques seek to identify new stable materials crystallizing in yet unknown configurations. The problem of global crystal structure optimization (from scratch) has been addressed with the introduction of such approaches as evolutionary algorithms^{60–63}, minima hopping^{64–66}, random searches⁶⁷, or particle swarm optimizations^{68,69}. Ground state searches for large systems are typically carried out at fixed compositions due to high computational cost, although variable-composition optimization has also been proposed⁷⁰. Meredig and Wolverton⁷¹ have developed techniques, called FPASS, to combine the experimentally known properties of structures such as space group and lattice constant with evolutionary algorithms to determine the atomic structure of unrefined powder diffraction files. Synthesis and characterization of complex high-pressure phases of B^{72,73} and CaB₆⁴ have illustrated (i) the advantages of the evolutionary approach to constructing large ground states from scratch and (ii) the considerable benefits of incorporating prior structural information into the searches. Complementary ground state searches at selected compositions beyond the known prototypes have been performed in several detailed studies of binary M-B systems. Some of the predictions have already been confirmed, such as the incompleteness of the previous structural model of the known CrB₄ compound^{5,6,75} and the existence of a new FeB₄ material (meta)stable under normal conditions^{5,14,75}, while others are awaiting confirmation, such as the possibility of new Li-B^{18,76,77}, Fe-B^{5,75}, Mo-B³⁴, W-B³², and Ca-B^{4,7} phases under ambient or high pressures.

The next natural step in the investigation of this class of materials is a systematic scan of all relevant metal-boron binary systems with a combination of high-throughput and evolutionary-type calculations. The generation of the largest *ab initio* database for metal borides has given us an opportunity to (i) identify new stable candidate materials for further investigation; (ii) establish trends across M-B systems and compositions; and (iii) expand the series of benchmark studies^{52–57} that reveal the current capabilities of DFT-based methods for guiding materials research. Known metal boride structures found in the Inorganic Crystal Structure Database (ICSD)⁷⁹ were considered along with new structures generated from our evolutionary search. The studied set of

s-p and transition metals is: Al, Ag, Au, Ba, Be, Ca, Cd, Co, Cr, Cs, Cu, Fe, Hf, Hg, Ir, K, La, Li, Mg, Mn, Mo, Na, Nb, Ni, Os, Pd, Pt, Rb, Re, Rh, Ru, Sc, Sr, Ta, Tc, Ti, V, W, Y, Zn, and Zr. We carried out calculations at both ambient (0 GPa) and high (30 GPa) pressure. The value of 30 GPa was chosen to bracket the pressure range of up to \sim 25 GPa in which facile materials synthesis can be carried out with multi-anvil cells. In addition, materials with a certain degree of covalent bonding synthesized under such moderate pressures have been known to remain metastable once quenched down to normal conditions (γ -B⁷, CaB₆⁴, FeB₄^{14,75}). The combined library of 175 structure types calculated for 41 M-B systems under at least 2 pressures contains over 12,000 entries.

We would like to stress that the set of identified *more* stable phases at selected compositions, especially under high pressures, are not necessarily *the* ground states: the aforementioned examples on CaB₆^{4,7}, WB₃/WB₄^{28,32,80}, and FeB₄^{5,14} have illustrated that reliable determination of materials ground state requires an enormous number of calculations. In particular, our detailed studies of individual M-B systems^{4,5,57,75} showed that the vibrational entropy term in Gibbs energy calculated at elevated temperature can noticeably affect the zero-temperature relative stability and shift the pressure-induced phase transformations by a few GPa. Therefore, we view our findings as a guide for future comprehensive studies of select systems. We also note that since this paper overviews work on metal borides carried out over the last 60+ years, it was necessary to place an emphasis on referencing larger reviews of the materials systems (such as Massalski *et al.*⁹, Rogl *et al.*⁸¹, Rogl and Schuster⁸², Rudy⁸³) over studies of individual materials.

II. STRUCTURE DETERMINATION METHODS

The structures considered within this work were determined in two ways. The first one was a scan of the Inorganic Crystal Structure Database (ICSD)⁷⁹ for relevant metal-non-metal structure types, critical assessment of available M-B binary phase diagrams⁹, and an overview of recently published studies on individual M-B systems. Since the presence of (meta)stable B-rich intercalated compounds or M-rich alloys rarely affects the stability of ordered M-B compounds away from the edges of the phase diagram, we did not consider M_xB_{1-x} phases with compositions $x < 0.08$ or $x > 0.85$. The second approach was to perform evolutionary ground state searches for selected fixed compositions with Module for *Ab Initio* Structure Evolution (MAISE)⁴ software code developed by the authors. The unconstrained optimization was seeded with both random and known structures. Due to the considerable computational cost of density functional theory (DFT) calculations, the evolutionary searches were carried out for a small set of chosen compositions primarily to investigate existing discrepancies between experiment and theory (i.e. W-B). For a list of

compositions see the Supplemental Material⁸⁴.

Nearly all of the collected 175 structures in our library have been considered for each M-B system. The few exceptions were very large structures, over 40 atoms per unit cell, that were clearly unnatural for certain metal classes. For example, our selected tests showed that complex ground states in alkali and alkaline-earth metal-boron systems had very large positive formation energies for TM-B binaries. The resulting database has been generated in a high-throughput fashion using the MAISE-based framework described in the Supplementary Material⁸⁴.

Following the determination of structures relevant to M-B systems these structures were studied with DFT. For this study the thermodynamic stability due to phase separation of each material composition was determined through a construction of the convex hull for each M-B system. The enthalpy of formation per atom ($H_f^{M_nB_m}$) for each system was determined using:

$$H_f^{M_nB_m} = (H_{tot} - n\mu_M - m\mu_B)/(n + m). \quad (1)$$

Here H_{tot} is the total enthalpy of the material composition, n is the number of M atoms, m is the number of B atoms, μ_M is the chemical potential of the lowest energy bulk metal phase, and μ_B is the chemical potential of α -B for 0 GPa and γ -B for 30 GPa. For a discussion on our selection of α -B for 0 GPa see the authors previous work⁵. The $H_f^{M_nB_m}$ is then used to construct a convex hull with the stable (metastable) structure defining (being 20 meV/atom above) the corresponding tie line. These determined stable and metastable structures are then compared to literature and the ICSD to determine discrepancies between experiment and computation.

III. CALCULATION METHODS

All of the energy calculations and structural optimizations, including those within the MAISE software, were performed using the *ab initio* software VASP⁸⁵. The MAISE evolutionary search settings were similar to those described in our previous studies^{5,7}. The projector augmented-waves⁴⁹ formalism was used to treat the core electrons. All the compounds considered in this study were calculated using the GGA-PBE⁴⁷ exchange correlation functional. The resulting stable and metastable compounds were then calculated using the LDA-PW⁴⁸ functional. Finally, a few select systems were verified with ultrasoft potentials⁸⁶. For a majority of the systems the stability or metastability of a compound as determined with the two functionals were the same. The specific differences found between the GGA and LDA results are discussed in more detail in Section VI. The same potentials are used regardless of the pressure considered. A plane wave basis set with an energy cutoff of 500 eV was used with a dense Monkhorst-Pack k-point mesh^{87,88} selected specifically for each structure. Formation energies are expected to be numerically converged to within

1-2 meV/atom. The stress tensor is optimized to the value of the specified pressure (0 GPa or 30 GPa). Compounds containing the five magnetic elements (Cr, Mn, Fe, Co, Ni) were calculated both with and without spin polarization. The known antiferromagnetic elements (Cr and Mn) were also treated with antiferromagnetic initial conditions. The antiferromagnetic initial conditions were constructed by identifying planes in each of the a_1 , a_2 , and a_3 directions and alternating the spin either within a plane or between neighboring planes. For compounds with odd number of magnetic elements super cells of the form $2x2x1$ were created to allow for in-plane spin variation. For the Sc-B system phonon calculations were performed to determine the dynamic stability of the cF52-ScB₁₂ (SG#225) phase. We used the finite displacement methods in the PHON⁸⁹ code for these calculations.

IV. RESULTS AND ANALYSIS

The calculations of the 41 metal boride systems found that around 191 stable phases and that 184 metastable phases exist. The formula, formation energy, stability (distance to the tie line), and Pearson symbol for both the GGA-PBE and LDA-PW functionals are shown in Tables II (stable compounds) and III (metastable compounds). The Wyckoff positions of the stable structures (and select metastable structures) are in the Supplemental Materials⁸⁴. The metal-boride systems were analyzed for both ambient (0 GPa) and high (30 GPa) pressures. The changes between 0 GPa and 30 GPa manifest both as same composition phase transitions or as known/new compositions becoming stable/unstable due to phase separation. Individual analysis of how the M-B systems change with pressure is discussed in Section VI. We have also adopted the following naming convention: a *system* denotes a combination of elements, a *compound* specifies a material at a particular composition, a *structure (type)* represents a unit cell and atomic positions for unspecified elements, and a *phase* corresponds to a compound in a particular structure.

Generation of the large datasets at the two pressures made it possible for us to examine pressure-induced changes in the number or type of stable compounds across the whole set of considered metal boride systems as shown in Fig. (1). It should be noted though that the selective application of the evolutionary searches disproportionately increased the likelihood of identifying new stable phases under pressure at the studied compositions, e.g. in the Ca-B system. One can distinguish three sets of metal-boron systems showing similar response to applied pressure. For the alkali-metal block, we observed not only an increased number of stable borides under higher pressure but also phase transformation of all stable ambient-pressure compounds with the exception of tP136-Li₃B₁₄. For the columns IIIB-IVB in the TMs, we did not see any phase changes or change in number of stable phases between the two pressures except for La, which had one

Li	3	6	Be	1	1	B	
						E	
			i	j			
Na	1	3	Mg	3	2	Al	1
K	1	3	Ca	2	4	Sc	3
						Ti	3
						V	6
						Cr	5
						<i>Mn</i>	4
						Fe	5
						Co	3
						<i>Ni</i>	1
						Cu	3
						Zn	0
							0
Rb	0	3	Sr	3	1	Y	1
						Zr	5
						Nb	6
						Mo	2
						Tc	3
						Ru	3
						Rh	2
						Pd	2
						Ag	0
						Cd	0
Cs	0	1	Ba	1	1	La	2
						Hf	3
						<i>Ta</i>	6
						W	4
						Re	4
						Os	2
						Ir	2
						Pt	1
						Au	3
						Hg	0
							0

FIG. 1: The elements considered in this M-B structure study. Included with each (non-B) element is the number of stable phases at 0 GPa (lower left) and 30 GPa (lower right) for the corresponding M-B system. B is in green (bold), while blue (italic) represents systems with new phases or structures predicted in this study.

more stable compound at 30 GPa. For the columns IB and IIB in the TM_s, there were no stable compounds at either pressure. In contrast to the three sets, the alkaline-earth and columns VB-VIIIB in the TM_s did not exhibit common distinguishable trends within themselves. These metal-boron systems were found to have many competing phases which made it difficult to determine the convex hull, let alone count the pressure-induced phase changes. The finite-temperature contributions and DFT systematic errors are likely to have the most impact on the relative stability of close lying phases in these systems and should be investigated in future studies.

In order to rationalize the stability of individual compounds we performed a meta-analysis of the formation energies of all the stable compounds at ambient pressure. Figs. (4-8) show the collection of all individual M-B tie lines and reveal clear general trends in stability as a function of the metals electron count. The formation energies of the compounds in each system starts low for metals with a low valency and decreases in formation energy (becoming more stable) until the metals with a valency of 4 electrons (Ti, Zr, and Hf) is reached after which the formation energy increases until no stable systems exist for columns VB-VIIIB transition metals. This demonstrates that metal boride systems with metals that are closer to column IVB are more stable with the metals furthest from N=4 being unstable. Fig. (2) shows the tie lines of each system combined by column in the periodic table valency and plotted versus formation energy. The plot shows that the instability of noble metal borides observed previously for selected layered structures^{50,51} is a more general trend holding for a much larger set of configurations. It is worth noting that the Cs-B and Rb-B systems do not contain stable compounds at ambient pressures. It is expected to be caused by the large atomic size of Cs and Rb, which is supported by the existence of stable structures for Cs and Rb at higher pressures due to compression of boron frameworks around the large atoms.

Interestingly, the Pt-B system has been found to be the only considered M-B binary that destabilizes at ele-

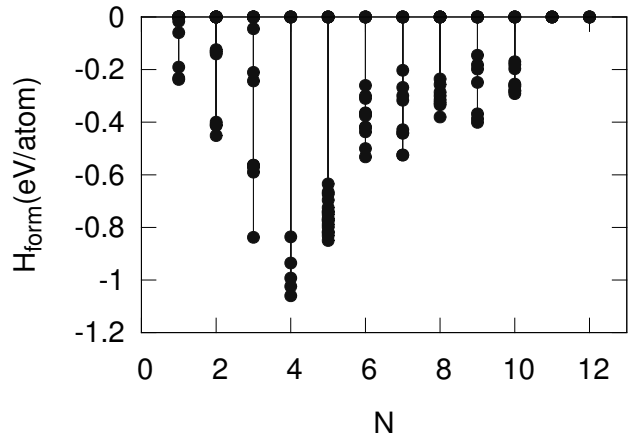


FIG. 2: Tie lines of each metal boride system at P = 0 GPa versus the electron count (column in the periodic table) of the metal. A minimum formation enthalpy is observed for N = 4.

vated pressures. We have checked that the finding is not sensitive to the choice of the exchange-correlation functional (GGA or LDA) or the pseudo-potential (PAW or ultrasoft⁸⁶), i.e., in all these cases the Pt-B compounds under pressure show reduced magnitudes of formation enthalpy. Explanation of this puzzling result will require further study.

Another interesting trend observed within this large data set was a nearly linear relationship between the magnetic moment per atom and the metal content above a certain saturation point for the considered ferromagnetic TM-B systems (TM = Fe, Co, Ni), as seen in Fig. (3). Only relevant structures with negative formation enthalpy and within 0.15 eV/atom of the convex hull were taken into account to exclude unrealistic configurations. The decrease in the metal concentration is expected to result in the decrease in the magnetic moment per atom, but the well-defined linear trend is rather surprising given the large variety of structural morphologies in the considered structure set. In fact, we did not observe such a clear correlation when we examined (i) the magnetic moment per *metal* atom as a function of composition; (ii) the magnetic moment per atom as a function of the metal-metal distance; or (iii) the antiferromagnetic moment per atom for any of the Cr, Mn, Fe, Co, Ni - B systems. The saturation point is seen to increase from 20% metal for Fe to 50% for Co and 75% for Ni. It must be noted for Ni that the limited amount of structures above 80% metal content reduces the size of the dataset. However, the results are still consistent across the Fe-Ni set.

The observed correlation can be helpful for the rational design of material properties. For example, the theoretical and experimental results indicate that the recently discovered FeB₄ compound is likely a phonon-mediated superconductor. The finding is unusual considering that

irons strong itinerant magnetic moment either prevents the superconducting transition altogether or defines it through spin fluctuations⁹⁰. In case of FeB_4 , the observed T_c of 3 K was much lower than the calculated value of 15-20 K. The original superconductivity calculations indicated that the phonon-mediated T_c would be particularly sensitive to the electron count due to the sharp drop of density of states (DOS) near the Fermi level. If the phonon-mediated scenario is correct electron doping of FeB_4 with Co or Ni should increase the T_c considerably by moving the Fermi level into the high DOS peak while not making the compound magnetic, according to Fig. (3).

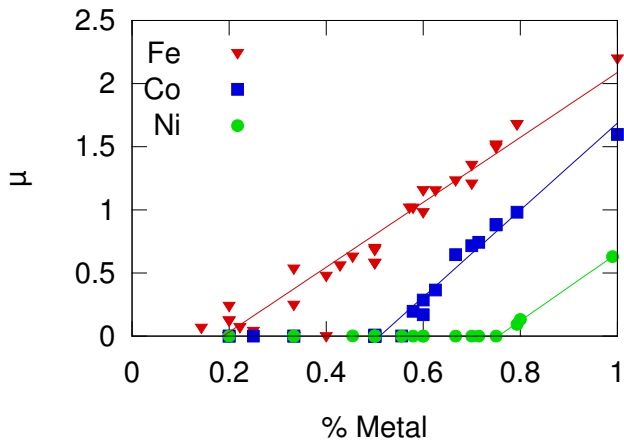


FIG. 3: A plot of the magnetic moment per atom (boron and metal) versus the metal content of all structures considered with a negative formation energy within 0.15 eV/atom of the tie line for Fe (triangles), Co (squares), and Nickel(circles). Increasing the cutoff energy above 0.15 eV/atom increases the noise of the data sets without greatly effecting the resulting fits, especially for the 33% and 50% compositions, where many structure types were studied. The fits to these data sets are red for Fe, blue for Co, and green for Ni.

This extensive study of metal borides has identified several new phases at ambient pressure and many new ones at high pressure. The recently proposed and confirmed phases in our previous studies^{4-7,51} are briefly discussed here but not referred to as new. Considering that the vast majority of experiments have been carried out under normal conditions, our comparison analysis has been dedicated primarily to ambient-pressure metal borides. Nevertheless, the lattice parameters and Wyckoff positions of all stable and selected metastable calculated materials are included in the Supplemental Material⁸⁴ for both 0 GPa and 30 GPa. 4 previously unreported phases at 0 GPa have been calculated to be stable with respect to phase separation. The new ambient pressure materials are summarized in Table I and classified based upon whether they are a new compound and whether they are new (from MAISE) or previously known structures. Here we discuss these newly predicted structures.

TABLE I: The stability of the newly predicted materials by functional and whether the composition is new and whether the structure was previously known. The distance to the tie line dH is negative if the new structure is more stable.

Material	Compound	Structure	dH (meV/atom) (GGA/LDA)
mP20-MnB ₄	Known	New	(-2 / -2)
oS20-Ta ₂ B ₃	New	Known	(-2 / -7)
mS28-Ni ₅ B ₂	New	Known	(-4 / +3)
tP16-NaB ₃	New	Known	(+6 / -3)

The exact structure of MnB_4 has remained a puzzle ever since the synthesis of the compound in 1970⁹¹. It has been argued^{45,92,93} that the structure should be a monoclinic distortion of an oI10 (SG#71) configuration originally proposed for CrB_4 ⁹⁴. Our previous work demonstrated that the oI10- CrB_4 (SG#71) and oI10- FeB_4 (SG#71) phases are dynamically unstable^{5,75} and later experiments confirmed the derived lower-symmetry oP10 (SG#58) phase^{14,27,95}. Here, the oI10 \rightarrow oP10 distortion was found to lower the energy of MnB_4 as well (by 10 meV/atom). Additional evolutionary searches have produced even more stable configurations related to oI10, e.g., an antiferromagnetic oF80- MnB_4 (SG#43) phase 6 meV/atom below oP10. A new non-magnetic mP20 (SG#14) structure, 8 meV/atom below oP10, is proposed to be the ground state structure for MnB_4 . The monoclinic structure of MnB_4 was recently independently described by Bykova and co-authors based on unpublished single crystal X-ray diffraction data⁹⁶. Table I in the Supplemental Material⁸⁴ contains the cell parameters and Wyckoff position of this compound.

Three additional compounds are proposed here in the Ta-B, Ni-B, and Na-B systems (see Supplemental Material for cell sizes and Wyckoff positions⁸⁴). The oS20-Ta₂B₃ (SG#63) phase of the V_2B_3 prototype is seen just below the tie line (by 2 meV/atom) defined by hP12-TaB₂ (SG#194) and oI14-Ta₃B₄ (SG#71)^{97,98}. We noted an unusual sensitivity of the relative energy of competing TaB₂ polymorphs to the choice of the DFT approximation: hP3 (SG#191) is below hP12 by 15 meV/atom in the GGA while hP12 is below hP3 by 12 meV/atom in the LDA (and literature^{98,99}). However, in both cases oS20-Ta₂B₃ (SG#63) appears as marginally stable. The proposed Ni-B compound is mS28-Ni₅B₂ (SG#15), 4 meV/atom below the tie line defined by tI12-Ni₂B (SG#140)¹⁰⁰ and oP16-Ni₃B (SG#62)¹⁰¹ in the GGA and 3 meV/atom above the tie line in the LDA. Considering the (near) stability shown with the two functionals, the compound is a viable candidate to exist. The identified new tP16-NaB₃ (SG#127) phase (of the tP16-Li₂B₆ prototype) is calculated to be stable with the LDA functional at 3 meV/atom below the tie line defined by oS46-Na₃B₂₀ (SG#65) structure and bulk Na. However, the GGA-PBE functional calculates NaB₃ to be 6 meV/atom above this tie line.

Along with these newly proposed compounds we were able to confirm another compound that was recently proposed in literature. Liang *et al.*³² used an evolutionary search for the WB_3 composition and found an hR24 (SG#166) structure to be more stable than the hP16 (SG#194) structure previously considered^{28,30,31,80}. Our calculations based on both high-throughput and evolutionary searches confirm that the hR24 structure is 8 meV/atom more stable than the hP16 structure. In fact, this structure is one of the three metastable ones that was predicted by Zhang *et al.*³⁴ in 2010 during their detailed evolutionary search of the Mo-B system. The Mo-B and W-B systems are discussed in more detail in Section VI.

This study also provides evidence against both theoretically and experimentally predicted/reported structures. Both hP3-AuB₂ (SG#191) and hP3-AgB₂ (SG#191) phases have been reported¹⁰². However, the stability of these structures has been questioned either due to the difficulty of synthesis and the instability over extended periods^{103,104} or due to positive formation energies⁵¹. Our calculations demonstrate that none of the noble metal - boron systems contain any stable phases. Another reported phase we found unstable was mP16-NiB₃ (SG#14) proposed by Caputo *et al.*¹⁰⁵. The mP16 structure, generated from the parameters in Ref.¹⁰⁵, relaxed by 283 meV/atom in our VASP calculations, but its final formation energy remained positive at 0.132 meV/atom. Our evolutionary search at the NiB₃ composition identified a considerably more stable mS32 (SG#12) structure, 179 meV/atom below mP16, but still 77 meV/atom above the tie line. Finally, tP20-RbB 4 (SG#127) (of the UB 4 prototype) has been predicted as a previously unobserved stable phase¹⁰⁶. However, our calculations show this structure to be unstable with a positive formation energy of 0.253 eV/atom.

The overall correspondence between the calculated and observed sets of stable compounds is rather difficult to quantify. If we compare the number of experimentally seen phases (excluding intercalated compounds, those that are too large to be simulated with DFT, and high temperature or high pressure polymorphs) with the number of phases that are calculated with either LDA or GGA to be stable we see that 75.5% of the experimental phases are stable in the DFT. The number increases to 77.2% if we also include, as in Ref.⁵², the agreement between observed and calculated immiscibility. Each of the 8 immiscible systems correctly found to be immiscible was counted, conservatively, as one hit (Au and Ag are considered as immiscible systems due to the lack of a reported stable structure in the literature). However, this number might not accurately reflect the discrepancies between our DFT calculations and experiment because there are 4 newly predicted phases here. Therefore, if we instead track the number of discrepancies between theory and experiment and divide it by the total number of compounds (those reported experimentally and those newly predicted here) the agreement rate is 76.3%. It is important to note that both experiment and computation

contribute to the error in this agreement rate. Therefore, to gain a better understanding of the computational error, we removed the discrepancies that deviated from the tie line by more than 50 meV/atom. Since this cutoff is higher than the expected numerical/systematic errors and the missing finite temperature contributions, these disagreements are likely due to formation of truly metastable phases or errors in the interpretation of the experimental data. This adjustment increases the agreement rate to 83.6%. When the experiment is similarly compared to just GGA (LDA) the percentage is 79.6% (81.6%).

The estimated agreement rate of 83.6% (75.2%) obtained for the metal borides excluding (including) non-computational discrepancies is lower than the corresponding value of 97.3% (92.4%) reported by Curtarolo *et al.*⁵² for 80 metal alloys. The lower agreement percentage seen in this metal boride study is not unexpected considering that (i) the synthesis/characterization of metal borides is complicated by their structural complexity and high melting temperatures and (ii) the DFT errors for materials relative stabilities are more likely to cancel out for metal alloy structures, which have more closely matched charge densities.

V. CONCLUSIONS

In summary, the resulting dataset for ambient-pressure *s-p* and TM boride systems:

- demonstrates that the formation energy of the stable compounds of a system is lowest for metals with a valence of 4 with the stability of the systems decreasing on either side of this valence until the noble metals are completely unstable;
- demonstrates a linear relationship between the magnetic moment per atom and the metal content for the ferromagnetic Fe, Co, and Ni-based compounds with negative formation energy within 0.15 eV/atom of the system's tie line; the linear fits give 20%, 50%, and 75% as minimal values of the Fe, Co, and Ni content for the relevant compounds to be magnetic;
- includes one proposed new mP20-structure (SG#14) (as the true ground state of MnB_4) and three new candidate compounds (oP10-Ta₂B₃ (SG#63), mS14-Ni₅B₂(SG#15), and tP16-NaB₃ (SG#127));
- serves as a benchmark for the DFT calculations of crystal structure stability of 83.6% agreement between calculated and expected stable metal borides.
- singles out Pt-B as the only considered system with pressure-induced *destabilization* of binary compounds.

Finally, this study illustrates the need to go beyond the previously known structures to correctly characterize each of the metal boride systems and to search for new materials. The study of column VB-VIIB TM borides at ambient pressure is a strong example of this. However, it is within the high pressure regime that opportunities for the discovery and prediction of new materials are particularly likely.

VI. SYSTEM DESCRIPTIONS

A. *s-p* metals

The convex hulls for the alkali, and alkaline-earth metals are in Fig. (4), while the convex hull for Al is in Fig. (5).

1. *Li-B*

Vojteer *et al.*¹⁰⁷ has stated that three phases of Li-B have been well quantified with many other phases compositions being either undetermined or undeterminable. The three quantified structures correspond to the Li_2B_6 , Li_3B_{14} , and $\text{LiB}_{0.88}$ compositions. The boron framework comprised of B_6 octahedra in $M_n\text{B}_6$ is typically stabilized by a single large metal atom per cP7 unit cell ($n = 1$). Two small Li^+ ions fit into each cavity causing the B_6^{2-} units to rotate and break the cubic symmetry. The resulting tetragonal structure (SG#127) has been observed to host Li in the $4h$ and $4f$ Wyckoff sites with 0.80 and 0.20 occupancies, respectively¹⁰⁸. As in the study of Chepulkii and Curtarolo¹⁰⁶, we simulated the structure with the majority $4h$ sites fully occupied and confirmed the stability of the tI16- Li_2B_6 (SG#127) phase. The tI160- Li_3B_{14} (SG#122) phase based on B_8 and B_{10} units¹⁰⁹ has multiple Li sites with fractional occupancies of 0.50 or 0.40. We were able to retain the 3:14 composition in a tetragonal tP136 cell (SG#81) by populating 50% of metal sites and picking an atomic arrangement with the most natural Li-Li distances. The simulated phase was found to be soundly stable without the inclusion of the configurational entropy contribution. Determination of the morphology and the exact composition of the nearly stoichiometric LiB_x compound required a set of extensive studies discussed and performed by Kolmogorov and Curtarolo⁵¹. The simplest proposed representations of the linear boron-chain structure were $\alpha\text{-LiB}$ ^{110,111} and $\beta\text{-LiB}$ ¹¹². However, the structural models are not suitable for interpretation of powder XRD data as the fitting leads to unphysically short B-B distances. An insightful solution proposed by Wörle and Nesper in 2000¹¹¹ was that the off-stoichiometry is a result of incommensurability of the B and Li sub-lattices. A computational study of LiB_x by Kolmogorov and Curtarolo⁵¹ illustrated that maximum stability occurs at compositions close to $x \approx 0.90$ in excellent agreement

with experiment. An established linear dependence between x and the easy-to-measure $c_{\text{Li}-\text{Li}}$ provided a simple recipe for monitoring the compound's composition and suggested that the $x = 0.8 - 1.0$ range of stability is greatly overestimated. An unusual feature of the Li-B phase diagram near the 1:1 composition is that LiB_x has a small but finite range of stability at $T = 0$ K and may be changed post-synthesis¹¹³. The commensurate hP15- Li_8B_7 (SG#187) representation of LiB_x defines the convex hull in this work.

At $P = 30$ GPa our DFT calculations show that 6 structures are stable. In agreement with our previous study⁵¹, the region of LiB_x stability shifts further away from 1:1 with pressure and hP7- Li_4B_3 (SG#187) takes the place of Li_8B_7 . The tP136- Li_3B_{14} compound retains the same structure, while the hP15- LiB_3 phase becomes unstable and is replaced by the tI10- LiB_4 (SG#139) phase. Among the considered structures on the B- and Li-rich sides, new oS28- LiB_6 (SG#65) and oS12- Li_2B (SG#63) compounds become stable. The 1:1 ground state is a previously proposed 'metal sandwich' hP8- LiB (SG#194) phase. This stoichiometric layered phase was predicted to be a close superconducting analog to MgB_2 ¹⁸. The first attempts to synthesize it were unsuccessful, but recent computational studies^{77,114,115} have reproduced the stability of the proposed 'metal sandwich' phases at this pressure. The investigations of the Li-B system under higher pressures^{77,114,115} have revealed a number of interesting ground states across the full composition range.

2. *Na-B*

The Na-B system has had several phases suggested including oS46- Na_3B_{20} (SG#65)¹¹⁶, oS28- NaB_6 ⁹, NaB_{15} ¹¹⁷, NaB_{16} ⁹, and mS64- Na_2B_{29} (SG#8)¹¹⁸. However, Albert *et al.*¹¹⁸ has shown that Na_2B_{29} is the correct composition for the NaB_{15} and NaB_{16} compounds, which are known to be stable at non-zero temperatures. Moreover, they are intercalated structures so are not considered in our calculations. The NaB_6 compound is now known to only be stable with the inclusion of C to form NaB_5C ^{119,120} or as the oS46- Na_3B_{20} (SG#65) phase^{1,116}. Therefore, the stable Na_3B_{20} compound seen here agrees with the known experimental ground state. However, our LDA calculations indicates a possibly stable phase, tP16- NaB_3 (SG#127), which is of the Li_2B_6 prototype.

The ambient-pressure oP23- Na_3B_{20} phase becomes unstable at higher pressure giving way to the more common nearby MB₆ composition, implying that both C inclusion and increased pressure can stabilize the NaB_6 phase. Also, at 30 GPa two other phases are calculated to be stable, tP16- NaB_3 (SG#127) and mP12- NaB_2 (SG#10).

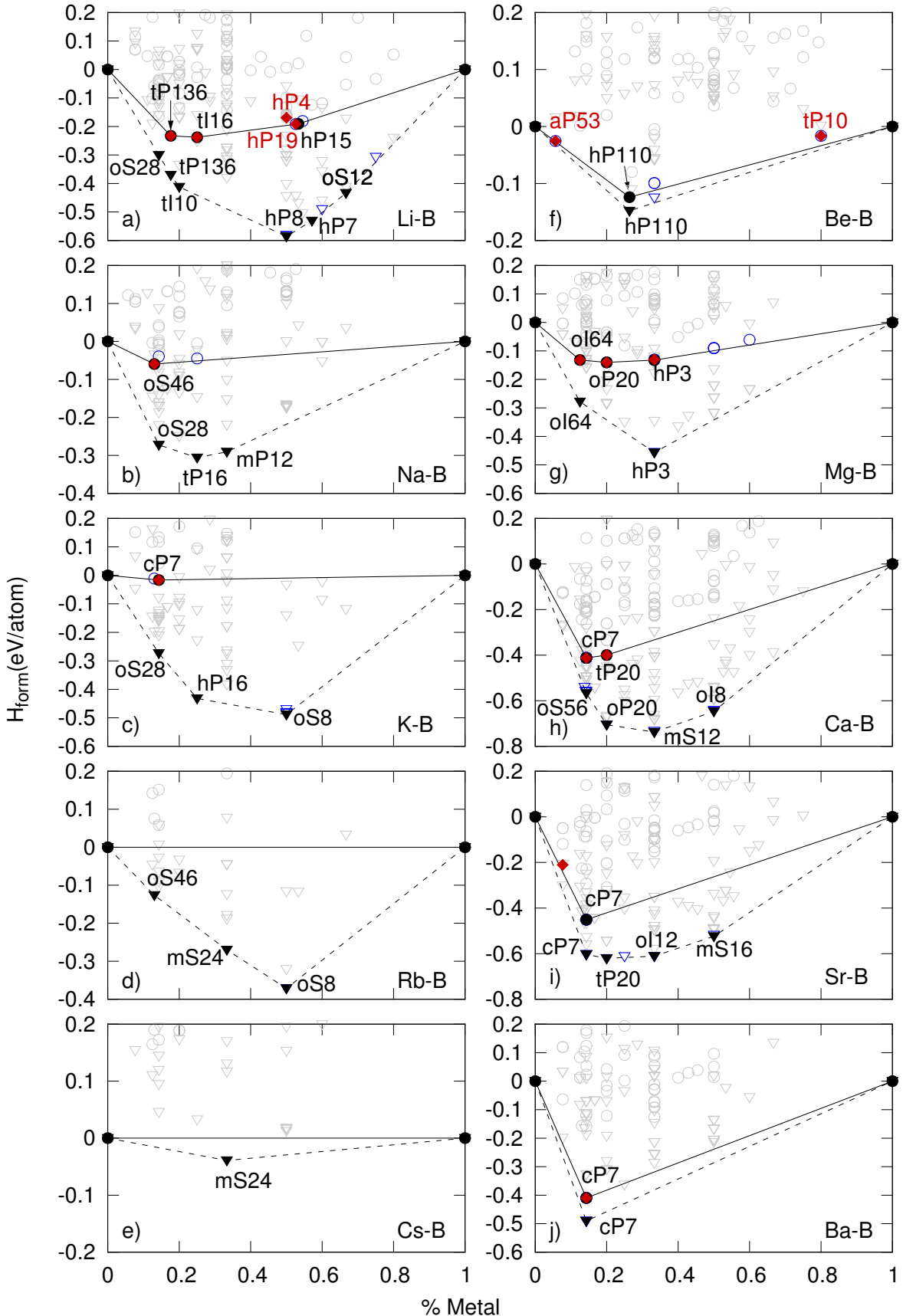


FIG. 4: The tie lines and convex hulls of the alkali (Li through Cs) and alkali-earth (Be through Ba) metals. Circles are 0 GPa calculations, triangles are 30 GPa calculations, and diamonds are 0 GPa reported experiments. Black shapes are stable, gray shapes are unstable, and blue shapes are marginally-stable systems. Black labels are stable Pearson symbols from this work, while red labels are the Pearson symbols from experiment. If the label corresponds to both this work and literature the label is black.

3. K-B

Experimentally, the K-B system contains a single phase, cP7-KB₆ (SG#221)¹²¹. This agrees with our calculations, although the phase's formation energy is found to be barely negative (see Fig. 4). Application of high pressure is expected to induce phase transformation, as one of the metastable structures found with MAISE for CaB₆, oS28-(SG#65), stabilizes over cP7. Further, two new phases form at 30 GPa, namely the hP16-KB₃ (SG#194) and oS8-KB (SG#63). The oS8 structure has a common morphology for this M-B composition composed of linear B chains.

4. Rb-B

The Rb-B system contains no intermediate phases as predicted in our calculations at ambient pressures. However, at 30 GPa oS46-Rb₃B₂₀ (SG#65), mS24-RbB₂ (SG#12), and oS8-RbB (SG#194) are all seen to be stable.

5. Cs-B

The Cs-B system contains no intermediate compounds, which matches our results. Within our calculations, at P=30 GPa, mS24-CsB₂ (SG#12) is the only phase observed (for both pressures) to have a negative formation energy after running an evolutionary search.

6. Be-B

The Be-B system is a complex system with many metastable and uncertain phases⁹, especially within the high boron content compositions. Walsh *et al.*¹²² identified the following set of Be-B phases: cF12-Be₂B (SG#225), hP117-BeB₂ (SG#191), tP196-BeB₂ (SG#76), and possibly tP10-BeB₄ (SG#129). Hermann *et al.*¹¹⁴ used ab initio techniques to explain the uncertainty in the literature about the boron-rich Be-B phases in the 20-33% composition range. They found the BeB_{~2.75} compound, represented as hP110-Be₂₉B₈₁ (SG#187), to be the most stable within this region with other slight variations in stoichiometry possible due to partial occupancy of Be sites. In agreement with the follow-up paper of Hermann *et al.*¹¹⁴, we observe hP110-Be₂₉B₈₁ to be the only stable Be-B compound with tP10-BeB₄ (SG#129) and aP53-Be₃B₅₀ (SG#1) metastable by 17 meV/atom and 1 meV/atom, respectively. We also had constructed, using chemical reasoning, a cF12-BeB₂ (SG#216) phase with the diamond B¹⁻ network stabilized by the insertion of the small Be²⁺ cations, which has been recently proposed by Hermann *et al.*¹¹⁴ as the lowest-energy BeB₂ structure at 0 GPa and stable at very high pressures¹¹⁵. However, our evolutionary

search at 0 GPa has uncovered a considerably more stable oS12 (SG#63) structure, 85 meV/atom below cF12 and only 13 meV/atom above the tie line. The new structure (see the Supplemental Materials⁸⁴) is comprised of hexagonal buckled B sheets with Be sitting above the middle of a B hexagon in one layer and on top of a B-B bond in another. The high-temperature cF12-Be₂B (SG#225) structure seen in the literature is unstable by 44 meV/atom in our calculations. At 30 GPa we calculate that the hP110-Be₂₉B₈₁ structure is the only stable structure in agreement with Hermann *et al.*¹¹⁵ who predicted the first changes in the Be-B convex hull occurring between 20 and 80 GPa.

7. Mg-B

The known Mg-B ground states are the hP3-MgB₂ (SG#191)¹²³, oP20-MgB₄ (SG#62)¹²⁴, oI64-MgB₇ (SG#74)¹²⁵ phases, perfectly matching the calculated set. The theoretical metal sandwich structures^{18,51} were originally identified for the Mg-B system. Both MgB and Mg₃B₂ composition with additional layers of Mg are metastable at 0 GPa, and neither is stabilized at higher pressures. Therefore, the only seen change at 30 GPa is that oP20-MgB₄ becomes unstable.

8. Ca-B

The ambient and high-pressure Ca-B phases have been systematically explored in recent studies^{4,7}. Under normal conditions, cP7-CaB₆ (SG#221) and tP20-CaB₄ (SG#127) have been observed experimentally¹²⁶⁻¹²⁸. Stability of CaB₄ has been the subject of debate¹²⁹, but the recent^{7,106} and the present calculations indicate that the compound is thermodynamically stable at 1 bar.

Application of gigapascal pressure leads to the appearance of a number of new ground states. At the 1:6 composition alone, the cP7 structure becomes dynamically unstable and gives way to unexpectedly complex oS56 (SG#63) and tI56 (SG#139) structures⁴. The latter was supported by powder XRD data and is one of the largest structures found without *any* structural input from experiment⁴. The most recent DFT analysis showed that addition of B stabilizes the parent tI56-CaB₆ phase (SG#139) further⁷. One of the possible derived phases, tP57-CaB_{6.125} (SG#123), could be the ground state for pressures above 32 GPa⁷. At the 1:4 composition, the metallic ThB₄-type structure destabilizes with respect to the semiconducting MgB₄-type structure. New stable superconducting compounds appear at the 1:2 and 1:1 compositions⁷. Our resulting convex hull at 30 GPa is defined by oS56-CaB₆(SG#63), oP20-CaB₄ (SG#62), mS12-CaB₂ (SG#71), and oI8-CaB (SG#74).

9. *Sr-B*

The Sr-B system is known to contain the cP7-SrB₆ (SG#221) compound¹³⁰, as seen in our calculations in Fig. (4i). The cP7-SrB₆ (SG#221), tP20-SrB₄ (SG#127), oI12-SrB₂ (SG#71), and mS16-SrB (SG#15) structures are all calculated to be stable structures at 30 GPa. Established correlations between the metal ion size and the structure stability for boron-rich compounds⁷ indicate that the large-size Sr and Ba ions will keep the known cP7 structure stable up to at least 40 GPa with respect to considered polymorphs.

10. *Ba-B*

The Ba-B system has been experimentally reported to have cP7-BaB₆ (SG#221) as its only stable compound¹³¹. This matches the cP7-BaB₆ (SG#221) phase from our database at ambient pressures and 30GPa. As discussed for Sr-B, the cP7 structure is particularly stable due to the large size of the Ba ion⁷.

11. *Al-B*

Al is the only considered non-alkali/alkaline-earth *s-p* metal. Our Al-B convex hull is in Fig. (5), while the most recent phase diagram is from Duschanek and Rogl¹³². Observed Al-B phases include hP3-AlB₂ (SG#191)¹³³, oC88-AlB₁₀ (SG#60)⁹, tP216-AlB₁₂ (SG#94)¹³² (α), AlB₁₂ (SG#74)⁹ (β), and oP384-AlB₁₂ (SG#19)^{9,132} (γ). However, both AlB₁₀, and β AlB₁₂ are high temperature phases⁹. Our calculations do not include the AlB₁₀₊ structures due to our chosen limits on intercalation. Therefore, we can only comment upon the stability of hP3 structure, which appears stable at both ambient and high pressures.

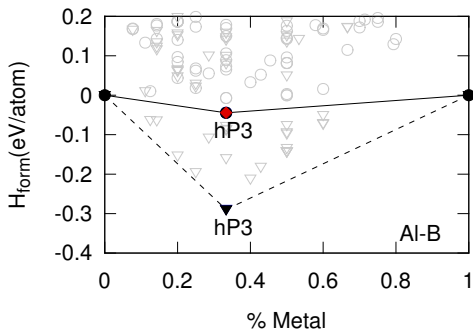


FIG. 5: The convex hull of the Al-B system. Circles are 0 GPa calculations, triangles are 30 GPa calculations, and diamonds are 0 GPa reported experiments. Black shapes are stable, and gray shapes are unstable. Black labels are stable Pearson symbols from this work. If the label corresponds to both this work and literature the label is black.

B. Row 3 transition metals

The convex hulls of the 3d TMs are in Fig. (6).

1. *Sc-B*

The Sc-B system is known to have hP3-ScB₂ (SG#191) as a stable phase¹³⁴, which agrees with our database. ScB₁₅ (SG#76) and ScB_{19-19.5} (SG#92) have been observed experimentally^{135,136}, but are not simulated here due to the large sizes of the intercalated structures. At the ScB₁₂ composition, two related⁹ intercalated structures have been reported: cF52-ScB₁₂ (SG#225)¹³⁷ and tI26-ScB₁₂ (SG#139)¹³⁸. According to our calculations at 0 GPa, cF52 is thermodynamically stable and its tI26 derivative relaxes back to the cubic configuration. At 30 GPa, cF52 is found to have multiple imaginary phonon modes which makes the identification of nearby dynamically stable derivatives a challenging problem as discussed in Ref.⁷. The proposed 'metal sandwich' hP8 structure^{18,51} is only 16 meV/atom above the tie line at 0 GPa but becomes less stable at higher pressures. The 1:12 and 1:2 phases define the convex hull at 30 GPa as well.

2. *Ti-B*

The Ti-B system is a well understood system with three compounds reported. These oP8-TiB (SG#62)¹³⁹, oI14-Ti₃B₄ (SG#71)⁹, and hP3-TiB₂ (SG#191)⁹⁹ phases all match well with those calculated in this study and shown in the phase diagram of Nakama *et al.*¹⁴⁰. The phases remain stable at 30 GPa.

3. *V-B*

The V-B system is also a well understood system with a large number of reported stable compounds. The hP3-VB₂ (SG#191), oS20-V₂B₃ (SG#63), oI14-V₃B₄ (SG#71), oS22-V₅B₆ (SG#65), oS8-VB (SG#63), and tP10-V₃B₂ (SG#127) phases have been seen experimentally^{99,141-147} and all agree with those obtained in our database. The set illustrates nicely the evolution of the boron bonding morphology from the flat 2D sheets in VB₂, to mixtures of strips and chains for the intermediate V-B compositions, to purely 1D chains in VB, and finally to unlinked sites in V₃B₂. The perfect agreement between theory and experiment can be attributed to the cancellation of errors in the calculated relative stabilities for the series of closely related structures. The set of stable V-B phases is unchanged at 30 GPa.

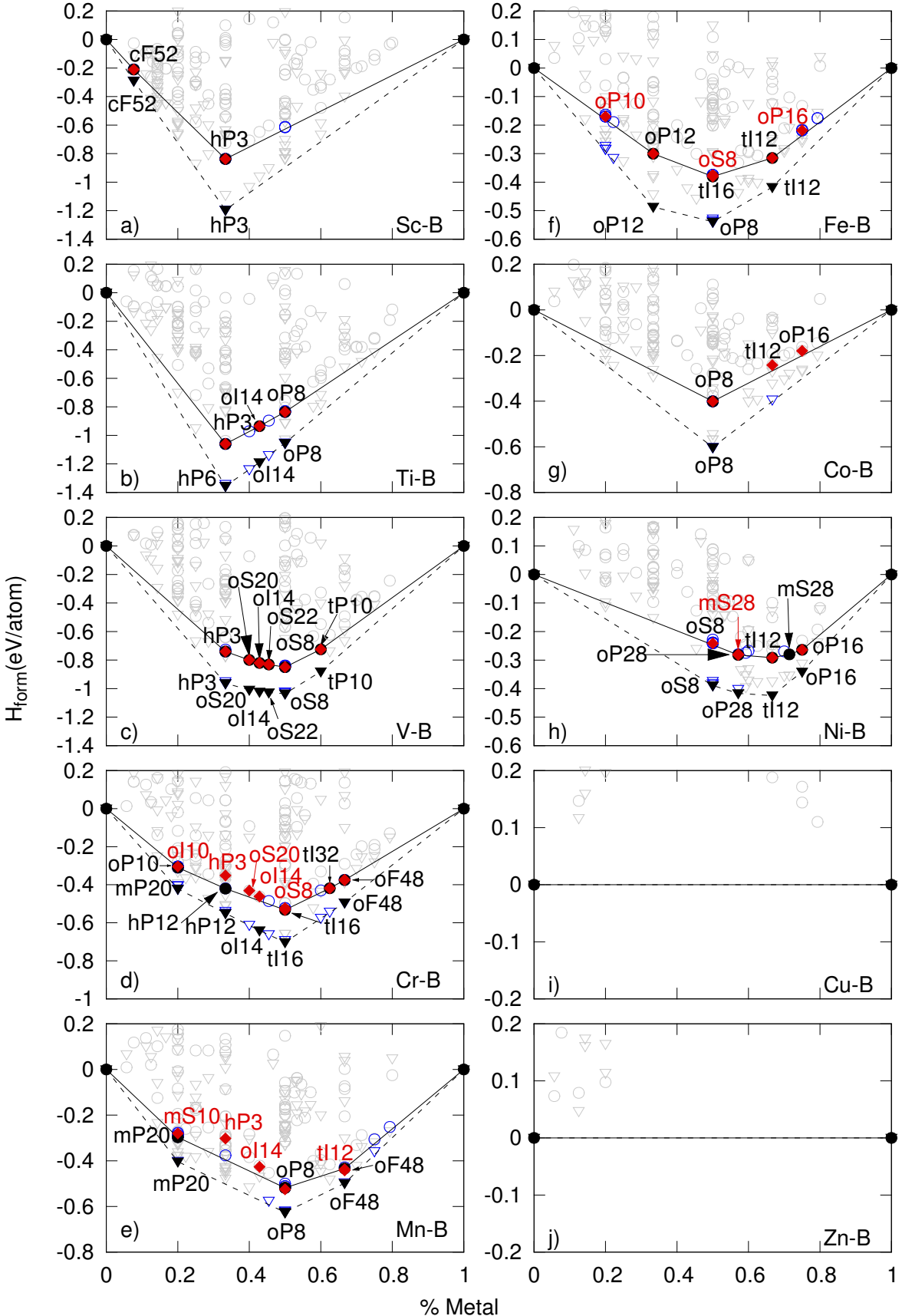


FIG. 6: The tie lines and convex hulls of the 3d TM (Sc through Zn). Circles are 0 GPa calculations, triangles are 30 GPa calculations, and diamonds are 0 GPa reported experiments. Black shapes are stable, gray shapes are unstable, and blue shapes are marginally-stable systems. Black labels are stable Pearson symbols from this work, while red labels are the Pearson symbols from experiment. If the label corresponds to both this work and literature the label is black.

4. Cr-B

Our review of the Cr-B system reveals several discrepancies between theory and experiment and highlights the need for further analysis of some reported Cr-B compositions. The theory-guided revision of the CrB_4 structural model illustrates the value of expanding crystal structure searches beyond the known prototype databases. Andersson and Lundström⁹⁴ synthesized CrB_4 over 40 years ago, and based on powder diffraction data, solved its structure as oI10 , which was used until very recently⁹⁵. Kolmogorov *et al.*⁵ and Bialon *et al.*⁷⁵'s calculations showed oI10 (SG#71) to be dynamically unstable and predicted a derived oP10 (SG#58) structure with a considerably distorted boron network to be the true ground state. The brand-new oP10 structure has indeed been confirmed for CrB_4 by recent experiments^{6,27} (see the Fe-B section for more related information). The $\text{tI32-Cr}_5\text{B}_3$ phase reported in literature¹⁴⁸⁻¹⁵⁰ is stable in our database. However, CrB_2 has been reported to adopt the hP3 (SG#191) configuration (the AlB_2 prototype with flat boron layers)^{150,151}, while our calculations indicate that the structure is unstable by 70 meV/atom with respect to hP12 (SG#194) (the WB_2 prototype with a mixture of flat and buckled boron layers). The majority of literature on CrB reports an oS8 (SG#63) structure^{9,46,82,152,153} with the exception of Papesch *et al.*¹⁵⁴ who observed a tI16 (SG#141) structure. According to our calculations, tI16 is the ground state with oS8 being metastable by 10 meV/atom. The $\text{oI14-Cr}_3\text{B}_4$ (SG#71) composition of the Ta_3B_4 prototype has been seen in literature^{9,155}, but is found to be 22 meV/atom above the tie line in our calculations matching the experimental expectation of it being a high temperature phase⁸². However, this structure becomes stable at 30 GPa within our database. Originally, the Cr_2B structure was reported to be tI12 (SG#140)¹⁴⁹, but has since been described to be $\text{oF48-Cr}_2\text{B}$ (SG#70)^{9,150,156}. The latter structure matches both the GGA and LDA calculations of this study. Cr_2B_3 was reported by Okada *et al.*⁴⁶ as oS20 (SG#63), which is unstable (by 34 meV/atom) in our calculations. It is worth noting that all of the stable structures in the Cr-B system seen within our DFT calculations were nonmagnetic. At 30 GPa, our calculations show that mP20-CrB_4 (SG#58), hP12-CrB_2 (SG#194), $\text{oI14-Cr}_3\text{B}_4$ (SG#71), tI16-CrB (SG#141), and $\text{oF48-Cr}_2\text{B}$ (SG#70) are the stable phases.

5. Mn-B

The Mn-B system, just as Cr-B, contains a series of discrepancies between theory and experiment that suggest the need for further investigation. The most recent reinvestigation of the full Mn-B system was from Smid *et al.*¹⁵⁷. The $\text{oF40-Mn}_4\text{B}$ (SG#70) phase reported in Ref. ¹⁵⁸ has since been described as a vacancy structure of orthorhombic Mn_2B (SG#70)^{9,159,160}.

An additional high-temperature tI12 (SG#140) structure has been reported in the literature for the Mn_2B composition¹⁶¹. Our calculations support these experimental findings placing the $\text{tI12-Mn}_2\text{B}$ (SG#140) polymorph 5 meV/atom above the $\text{oF48-Mn}_2\text{B}$ (SG#70) ground state at $T = 0$ K. The calculated stability of oP8-MnB (SG#62) is also consistent with experiment¹⁵⁸. However, the experimentally observed $\text{oI14-Mn}_3\text{B}_4$ (SG#71)¹⁵⁸ phase is 45 meV/atom above the tie line in our DFT calculations. The experimental hP3-MnB_2 (SG#191) (AlB_2 prototype)^{9,162} phase is also determined to be unstable by nearly 100 meV/atom. The hP6 (SG#194) (ReB_2 prototype) structure is found to be far more energetically favorable than hP3 , in agreement with previous DFT calculations¹⁶³, but it is not clear whether or not hP6 is really stable being 20 meV/atom above and 10 meV/atom below the tie line in the GGA and the LDA, respectively. Our evolutionary search at the MnB_4 composition produced a new mP20 (SG#14) structure which we propose to be the true ground state. This finding appears to agree with the results of an independent experimental study by Bykova and co-authors based on unpublished single crystal X-ray diffraction data⁹⁶. Sections IV, Cr-B, Fe-B, and Ref.⁵ give more information on the relationship between the other related mS10 (SG#12)⁹³, oI10 (SG#71)⁹⁴, and oP10 (SG#58)^{5,75} structures proposed for the MnB_4 , CrB_4 , and $\text{FeB}_4/\text{CrB}_4$ compounds, respectively. At 30 GPa mP20-MnB_4 (SG#14), oP8-MnB (SG#62), and $\text{oF96-Mn}_2\text{B}$ (SG#70) are stable in our study.

6. Fe-B

The Fe-B system has been overviewed and explored in the author's previous studies^{5,75}. Two stable compounds, oP8-FeB (SG#53) and $\text{tI12-Fe}_2\text{B}$ (SG#140), appear in the experimental phase diagram¹⁶⁴, but synthesis of metastable FeB_{49} ¹⁶⁵, a solid solution of 5% Fe in B (FeB_{19})¹⁶⁶, and Fe-C analogs, $\text{cF116-Fe}_{23}\text{B}_6$ (SG#225) and $\text{tI32-Fe}_3\text{B}$ (SG#82), have also been reported^{39,167,168}. In good agreement with experiment, our DFT calculations indicate stability of $\text{tI12-Fe}_2\text{B}$ (SG#140) and metastability of $\text{cF116-Fe}_{23}\text{B}_6$ (SG#225) and $\text{oP16-Fe}_3\text{B}$ (SG#62) by 19 meV/atom and 18 meV/atom, respectively. Three phases of Fe_3B , $\text{oP16-Fe}_3\text{B}$ (SG#62) prototype Fe_3C , $\text{tI32-Fe}_3\text{B}$ (SG#82) (prototype Ni_3P), and $\text{tP32-Fe}_3\text{B}$ (SG#86) (prototype Ti_3P), have been reported with the Fe_3C prototype determined to be a metastable phase, while the Ni_3P and Fe_3P prototypes are high temperature phases¹⁶⁸. This agrees with our results of 24 meV above the tie line for tI32 , 104 meV for tP32 , and 18 meV for oP16 . As discussed by Kolmogorov *et al.*⁵, two experimentally observed FeB polymorphs, oP8 (SG#62) and oS8 (SG#63) are slightly above (by at least 5 meV/atom) a tI16 structure in the GGA, but are favored (by at least 10 meV/atom) in the LDA. The evolutionary ground state

search of Kolmogorov *et al.*⁵ unexpectedly produced two viable ground states at 1:2 and 1:4 compositions. The predicted oP12 structure for FeB₂ (SG#62) comprised of B chains rather than B layers was found to be over 30 meV/atom below the α -B \leftrightarrow oP8-FeB tie line. The previously unobserved oP10 structure for FeB₄ (SP#58) was shown to be a high-*T* ground state and to have the potential to be a phonon-mediated superconductor. The two proposed compact phases were shown to stabilize further under high pressures⁷⁵. The oP10-FeB₄ phase has just been synthesized under medium pressures and appears to be the first realized superconductor designed entirely on the computer^{5,14}. This experimental study has also led to the discovery of another new iron boride¹⁴, Fe₂B₇, with a complex oP72 (SG#55) structure^{8,169}, but our calculations show that the compound is metastable by about 10 meV/atom in the 0-30 GPa range. *Ab initio* predictions of metastable compounds at such an unusual composition and with such a large unit cell would have been no less than an act of clairvoyance. Nevertheless, the original DFT study⁵ indicated the likely existence of new Fe-B compounds and successfully guided the experiment to discovery of new materials in a seemingly well-studied binary system.

At 30 GPa, the only change in the set of the ground states is the stabilization of oP8-FeB over the competing oS8 and tI16 polymorphs. After initially gaining in stability at pressures up to 20 GPa, P10-FeB₄ eventually becomes less stable when the tie line is defined by γ -rather than α -B.

7. Co-B

Our DFT calculations show that one compound, oP8-CoB (SG#62)¹⁰⁰, is stable in the Co-B system, while references to two more additional compounds exist in the literature. We found tI12-Co₂B (SG#140)¹⁷¹ and the oP16-Co₃B (SG#62)¹⁰⁰ phase to be unstable, but not far from the tie line, by 25 meV/atom and 21 meV/atom, respectively. The oP8-CoB (SG#62) compound is also the only compound calculated to be stable at 30 GPa for Co-B.

8. Ni-B

The compounds in the Ni-B structures match up fairly well between those reported in literature and those calculated to be stable here. Experimentally, both an orthorhombic and a monoclinic form of Ni₄B₃ have been seen¹⁰¹, which is consistent with the calculated stability of oP28-Ni₄B₃ (SG#62) and the metastability of mS28 (SG#15) (by 2 meV/atom). Malik *et al.*¹⁷² discuss the off-stoichiometric nature of oP28 and the resulting stability of mS28. The tI12-Ni₂B (SG#140)¹⁰⁰ and the oP16-Ni₃B (SG#62)¹⁰¹ reported phases match those from the current study. At the 1:1 composition the oS8 (SG#63)

structure has been reported¹⁷³. According to our calculations, the three competing structures, oS8 (SG#63), oP8 (SG#62), and tI16 (SG#141) are all metastable with the oS8 structure being 5 meV/atom (1meV/atom) above the tie line for GGA (LDA). The GGA calculations indicate the possible stability of the new Ni₅B₂ compound with a mS28 (SG#15) structure (metastable by 3 meV/atom in LDA). Therefore, this composition is worth future investigation to determine whether the GGA or LDA calculations correctly predict the structure. Finally, Caputo *et al.*¹⁰⁵ predicted a stable monoclinic NiB₃ (SG#14) structure through computational work based upon experimental work. As discussed in Section IV we do not find the NiB₃ structure suggested by Caputo *et al.*¹⁰⁵ to be stable nor did we find another stable structure. At 30 GPa the newly predicted mS28-Ni₅B₂ phase is unstable, while the oS8-NiB, oP28-Ni₄B₃, tI12-Ni₂B, and oP16-Ni₃B phases remain stable. At the Ni₄B₃ composition the metastable mS28 structure is destabilized to 15 meV/atom above oP28.

9. Cu-B

The Cu-B system contains no intermediate compounds⁹. This matches with our results at both pressures, which show all calculated structures have positive formation energies.

10. Zn-B

No known intermediate compounds are found for the Zn-B system⁹. This agrees with our convex hulls for both 0 GPa and 30 GPa which shows all formation energies are positive.

C. Row 4 Transition metals

Fig. (7) contains the tie lines of the 4d TM.

1. Y-B

All known compounds in the Y-B system are boron-rich. The hP3-YB₂ (SG#191)¹⁷⁴, tP20-YB₄ (SG#127)¹⁷⁵, and cP7-YB₆ (SG#221)¹⁷⁶ phases have common M-B structures. Of these three phases, cP7-YB₆ was found to not be stable (at 31 meV/atom above the tie line) within our calculations. The set of intercalation compounds is comprised of cF52-YB₁₂⁴³, YB₂₅¹⁷⁷, YB₅₀¹⁷⁸, and YB₆₆¹⁷⁹. Of these complex phases, only cF52-YB₁₂ (SG#225)⁴³ was considered, and it was found to be stable. No additional phases are calculated to be stable at 30 GPa.

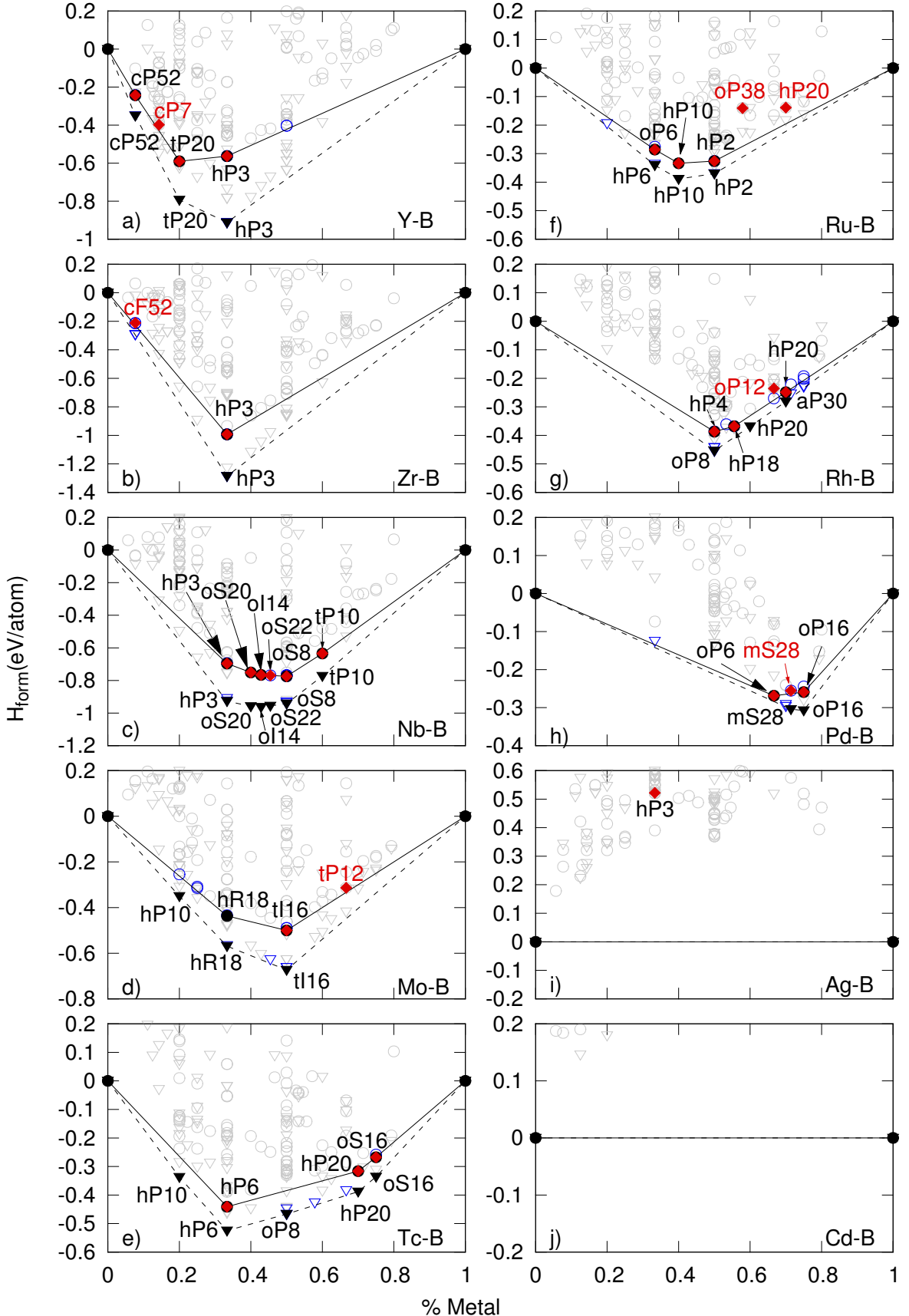


FIG. 7: The tie lines and convex hulls of the 4d TM (Y through Cd). Circles are 0 GPa calculations, triangles are 30 GPa calculations, and diamonds are 0 GPa reported experiments. Black shapes are stable, gray shapes are unstable, and blue shapes are marginally-stable systems. Black labels are stable Pearson symbols from this work, while red labels are the Pearson symbols from experiment. If the label corresponds to both this work and literature the label is black. For Nb the oS22 is included with a black (stable) label due to the LDA data plotted shows it as metastable

2. Zr-B

The Zr-B system contains two phases⁹, hP3-ZrB₂ (SG#191)⁹⁹ and cF52-ZrB₁₂ (SG#225)⁴³. The hP3-ZrB₂ phase is stable in our calculations, while cF52-ZrB₁₂ is metastable (at 18 meV/atom above the tie line). Rogl and Potter¹⁸⁰ discussed the metastability of both oP8-ZrB (SG#62) and oI14-Zr₃B₄ (SG#71), which we found to be in reasonable agreement with our calculations, which are 70 meV and 43 meV above the tie line respectively. The ground state does not change at 30 GPa.

3. Nb-B

The Nb-B and V-B systems contain the exact same set of stable structures noted in the V-B section to display an underlying relationship across the composition range. The reported Nb-B phases, hP3-NbB₂ (SG#191), oS20-Nb₂B₃ (SG#63), oI14-Nb₃B₄ (SG#71), oS22-Nb₅B₆ (SG#65), oS8-NbB (SG#63), and tP10-Nb₃B₂ (SG#127)^{9,99,143,181-183} match our calculated ground states at 0 GPa and remain stable at 30 GPa. It is worth noting that Nb₃B₂ was reported¹⁸⁴ to possibly be vacancy- or surface-stabilized contrary to our calculated result.

4. Mo-B

The Mo-B system has received a lot of recent attention due to the potential high hardness of related Mo- and W-based borides^{31,34,35,185}. Zhang *et al.*³⁴ performed evolutionary searches at specific compositions and found that the convex hull consists of known M-B structures. After performing evolutionary searches and large scans of known M-B structures, we have obtained a matching set of the ground states. However, not all of the calculated stable structures agree with experimentally observed ones. The reported tI12-Mo₂B phase (SG#140)¹⁸⁶ is not stable (at 20 meV/atom above the tie line) within our calculations or those of Zhang *et al.*³⁴. Theory also indicates the stability of hR18-MoB₂ (SG#166)^{34,35}, while the only experimentally reported (high-temperature) structure at this composition is hP3 (SG#191)^{9,186}. It is unlikely that temperature effects could stabilize the hP3 structure found to be over 160 meV/atom above hR18 at zero temperature. The hR21-Mo₂B₅ phase has been studied both experimentally¹⁸⁶ and theoretically³³. According to our calculations and those of Zhang *et al.*³⁴, the phase is unstable by over 0.4 eV/atom and the lowest-energy structure at the Mo₂B₅ composition (24 meV/atom above the tie line) is hP14 (SG#194) suggested by Zhang *et al.*³⁴. These authors also found a metastable hR24 (SG#166) structure (13 meV/atom above the tie line in our calculations) with an evolutionary search for MoB₃³⁴, which matches

the structure predicted with an evolutionary search for WB₃ by Liang *et al.*³². This is not consistent with the experimental observation of the hP16-Mo_xB₃ phase (SG#194)¹⁸⁷ that appears unstable computationally^{34,35} (19 meV/atom above the tie line in our calculations). One more metastable phase predicted by Zhang *et al.*³⁴ is hP10-MoB₄ (SG#194) (8 meV above the tie line in our database), energetically preferred over the previously reported hP20-MoB₄¹⁸⁸ phase, which is also dynamically unstable^{34,35}. Finally, two polymorphs of MoB, the α tI16-MoB (SG#141)^{9,189} phase and the high temperature β oS8-MoB-(SG#64) phase^{190,191}, have been reported, which agrees with the stability of the former and the metastability of the latter (by 11 meV/atom) in our calculations. The most recent phase diagram for Mo-B is from Ref.⁸². It includes the disputed Mo_{1-x}B₃ composition, which is discussed in more detail for the W-B system. At 30 GPa the hR18-MoB₂ and tI16-MoB phases remain stable, while the previously metastable hP10-MoB₄ becomes stable.

5. Tc-B

The Tc-B system contains the hP6-TcB₂ (SG#194), hP20-Tc₇B₃ (SG#186), and oS16-Tc₃B (SG#63)¹⁹² phases matching out calculated ground states. At 30 GPa, the oP8-TcB (SG#62) phase is seen to be stable along with the hP10-TcB₄ (SG#194) structure of the MoB₄ prototype. The ambient pressure structures remain stable as well at 30 GPa.

6. Ru-B

The most recent Ru-B phase diagram is in Rogl and Schuster⁸². Among the reported hP2-RuB (SG#187)⁹, hP10-Ru₂B₃ (SG#194)^{193,194}, oP6-RuB₂ (SG#59)¹⁹⁵, and hP20-Ru₇B₃ (SG#186)¹⁹⁶ phases, only the last one is found to be unstable (by 57 meV/atom) in our calculations. An oP38-Ru₁₁B₈ (SG#55)^{82,197} phase has also been reported, but does not appear in Massalski *et al.*⁹ and is 134 meV/atom above the tie line in our database. At 30 GPa, hP2-RuB (SG#187), hP10-Ru₂B₃ (SG#194), and the hP6-RuB₂ (SG#194) phases are stable, while hP20-Ru₇B₃ remains unstable (by 39 meV/atom).

7. Rh-B

The Rh-B system contains hP20-Rh₇B₃ (SG#186)¹⁹⁸, oP12-Rh₂B (SG#62)¹⁹⁹, hP18-Rh₅B₄ (SG#194)²⁰⁰, and hP4-RhB_{1.1} (SG#194)^{198,201}. The first two match our calculated ground states. The oP12-Rh₂B is found to be unstable by 70 meV/atom and the lowest-energy structure at this composition in our database is oP6 (SG#58), a (Pd₂B prototype) metastable by 6 meV/atom. We

constructed and simulated supercell structures of hP2 and hP4 for RhB_x ($0.80 < x < 1.285$) and found all of them to be above the tie line, e.g. the hP15-Rh₈B₇ derivative of hP4 is metastable by 15 meV/atom. It appears that, in contrast to the case of IrB_{0.9}, there is no thermodynamic force for the stable hP4-RhB phase to go off-stoichiometry. At 30 GPa our calculations show that hP20-Rh₇B₃ remains stable, hP4-RhB gives way to oP8-RhB (SG#62), and the hP18-Rh₅B₄ phase at 55% metal content is replaced by a low-symmetry aP30-Rh₃B₂ (SG#2) phase at 60%.

8. Pd-B

All observed compounds in the Pd-B systems are metal-rich: Pd₁₆B₃²⁰², Pd₆B²⁰², Pd₅B²⁰², oP6-Pd₂B (SG#58)^{203,204}, oP16-Pd₃B (SG#62)^{203,205}, and mS28-Pd₅B₂ (SG#15)^{203,205}. Gusev²⁰² discusses the consensus that the three compounds with the highest Pd content are in fact disordered and ordered solid solutions of fcc Pd. For this reason, their simulation is beyond the scope of this study. The stability of oP16-Pd₃B is consistent with our DFT results. The mS28-Pd₅B₂ phase is metastable in the GGA (by 8 meV/atom) but stable in the LDA (by 4 meV/atom below the tie line defined by oP6-Pd₂B and oP16-Pd₃B). While it has been demonstrated that Pd₂B is amorphous²⁰³, the ordered oP6-Pd₂B (SG#62) phase reported by Tergenius and Lundstroem²⁰⁴ is stable in our calculations. According to our calculations at 30 GPa, the Pd-B system contains only the oP16-Pd₃B and mS28-Pd₅B₂ stable phases.

9. Ag-B

There have been reports on the formation of the AgB₂ compound¹⁰²⁻¹⁰⁴, but its long-term instability has been acknowledged by Massalski *et al.*⁹ and Islam *et al.*¹⁰³. Our DFT calculations indicate the immiscibility of Ag and B at both 0 or 30 GPa. The hP3-AgB₂ (SG#191) phase, in particular, has a positive formation energy of 0.52 eV/atom at ambient pressure. The lowest formation energy AgB₂ structure in our calculations was the hR18 (SG#166) structure, but it still retained a positive formation energy.

10. Cd-B

No known intermediate compounds are found for the B-Cd system⁹. This agrees with our convex hull which shows all formation energies are positive.

D. Row 5 Transition metals

The 5d transition metals are discussed below with Fig. (8) containing the corresponding phase diagrams.

1. La-B

The La-B system contains the cP7-LaB₆ (SG#221)²⁰⁶ and tP20-LaB₄ (SG#127) phases²⁰⁷, which agrees with this study. At 30 GPa, an additional hP8-LaB (SG#194) phase defines the convex hull. Among the considered binaries, the predicted hP8 (metal sandwich) structure^{18,51} is found to become stable only for LiB and LaB in the considered pressure range.

2. Hf-B

Several compounds have been reportedly observed in the Hf-B system: cF52-HfB₁₂ (SG#225), hP3-HfB₂ (SG#191), cF8-HfB (SG#225), and oP8-HfB (SG#53)^{151,208-210}. However, Rogl and Potter²¹⁰ demonstrated that cF8-HfB is C stabilized, while oP8-HfB is stable at high temperatures. Our calculations show that only hP3-HfB₂ is stable. The cF52-HfB₁₂ and cF8-HfB phases are above the tie line at 44 meV/atom and 350 meV/atom, respectively. The lowest-energy structure at the 1:1 composition in our database, oP8-HfB (SG#62), is still 34 meV/atom above the tie line agreeing with experiment²¹⁰ that neither cF8 nor oP8 are stable at low temperature. hP3-HfB₂ is the only calculated stable phase at 30 GPa as well.

3. Ta-B

The oS8-TaB (SG#63)⁹⁸, oS22-Ta₅B₆ (SG#65)^{98,211}, oI14-Ta₃B₄ (SG#71)^{97,98} and tP10-Ta₃B₂ (SG#127)¹⁴³ phases reported in the literature agree with our database. However, we have found several discrepancies. For the TaB₂ composition hP3-TaB₂ (SG#191) has been observed experimentally^{98,99}. The employed DFT approximations order the known competing structure types differently. The GGA favors the hP12 (SG#194) structure over hR18 (SG#166) by 6 meV/atom and over hP3 (SG#191) by 15 meV/atom, while the LDA favors the hP3(SG#191) structure over hP12 (SG#194) by 12 meV/atom and over hR18 (SG#166) by 18 meV/atom. The oS20-Ta₂B₃ (SG#63) phase is calculated to be marginally stable (2 meV/atom below the tie line defined by hP12-TaB₂ and oI14-Ta₃B₄), but has not been reported experimentally. See Section IV for further details. Finally, the tI12-Ta₂B (SG#140) reported phase¹⁶¹ is not stable in our calculations at 35 meV above the tie line, which is consistent with Chad *et al.*²¹² who found it to be a high temperature phase. At 30 GPa the stable Ta-B structures do not change from their ambient state

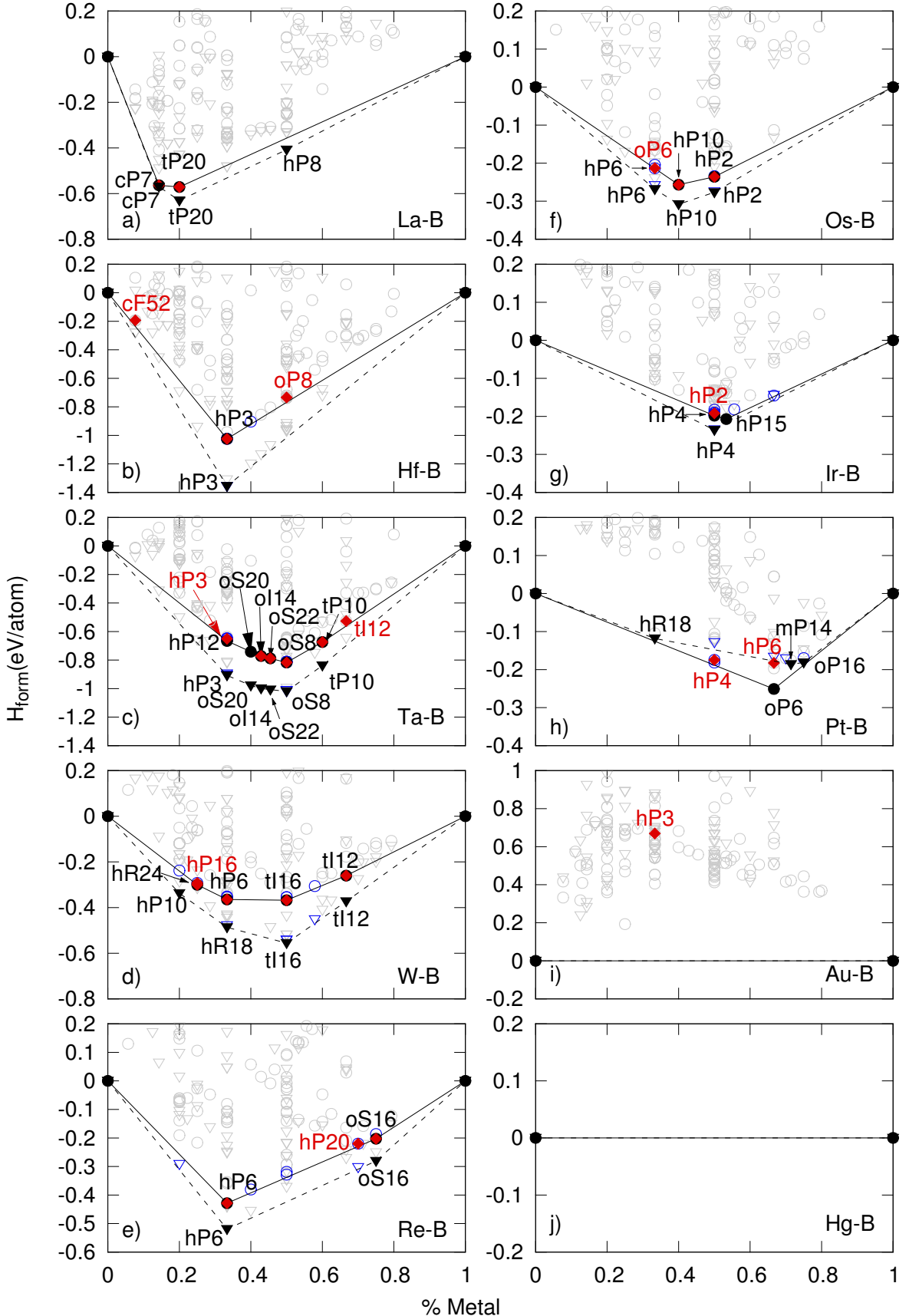


FIG. 8: The tie lines and convex hulls of the 5d TM (La through Hg). Circles are 0 GPa calculations, triangles are 30 GPa calculations, and diamonds are 0 GPa reported experiments. Black shapes are stable, gray shapes are unstable, and blue shapes are marginally-stable systems. Black labels are stable Pearson symbols from this work, while red labels are the Pearson symbols from experiment. If the label corresponds to both this work and literature the label is black. For Os-B the hP6 for ambient pressures is stable in LDA and not GGA.

except that hP3-TaB₂ is found to be stable with both functionals.

4. W-B

The W-rich portion of the W-B system is well established in literature with tI12-W₂B^{30,41,80} and tI16-WB^{30,80,186} reported both experimentally and theoretically. A β phase of WB, oS8 (SG#63), has also been reported¹⁹⁰. The calculated stability of tI12-W₂B (SG#140) and tI16-WB (SG#141) as well as the metastability of oS8-WB (SG#63) (by 13 meV/atom) are consistent with these experimental observations. The B-rich phases show less agreement between theory and experiment. For the WB₂ composition, experiments indicate formation of the hP12 (SG#194) structure⁴¹, while alternative hP6 (SG#194)^{30,80} and oP6 (SG#59)²⁹ solutions have been proposed as lowest-energy structures theoretically. In our calculations, hP6 is stable while the oP6 and hP12 structures are metastable by 9 meV/atom and 30 meV/atom, respectively. It is worth noting that the previously reported W₂B₅ composition is now viewed to be the hP12-WB₂ phase⁸⁰. A debate has recently sparked regarding the true composition and structure of a known (possibly super hard)^{31,185} boron-rich W-B compound, with theory (this study included) predicting hP16-WB₃ (SG#194) and experiment finding hP20-WB₄ (SG#194)^{30,31,80,213} or hP-W_{1-x}B₃²¹⁴ (where $x \sim 0.2$ and is isotypic with hP20-WB₄). The hP16-WB₃ phase can be morphed into hP20-WB₄ by inserting a B dimer that converts the 2D boron network into the 3D one. Zhang *et al.*²⁸ have demonstrated that the structures' similarity has caused confusion in the analysis of experimental XRD^{215,216} data due to all of the WB₃ XRD peaks existing in the WB₄ data. In addition, the high pressure stability of WB₄⁸⁰ obfuscates comparison of the DFT and experimental results. Finally, Liang *et al.*³² have proposed an additional WB₃ prototype, hR24 (SG#166), which is expected to be slightly more energetically favorable than the previously known hP16 structure at zero temperature, agreeing with our calculations. Cheng *et al.*²¹⁷ showed that inclusion of the vibrational entropy term to the free energy destabilizes hR24 with respect to hP16 at 660-680°C. Then experimentally and theoretically, they demonstrated the existence of a WB_{3+x} phase that contains B interstitials in the W plane voids. Within our calculations we considered both B interstitials (single and double) and W vacancies within the hP16-WB₃ phase to understand the hP-W_{1-x}B₃ and hP-WB_{3+x} phases and saw that both defects increased the formation energy within a single conventional cell.

At 30 GPa the calculated convex hull changes to hP10-WB₄, hR18-WB₂, tI16-WB, and tP6-W₂B. This contradicts the study of Xie *et al.*²¹³ who compressed WB₄ up to 60 GPa demonstrating a structural change at 42 GPa with the structure not changing phase before this

transition.

5. Re-B

The Re₃B, Re₇B₃, ReB₃, and ReB₂ compositions have been reported^{9,198,218,219}, with ReB₃ suggested theoretically as unstable at ambient conditions due to a positive formation energy²²⁰. Additionally, the Re₂B, ReB, Re₂B₃, Re₂B₅, and ReB₄ compositions have all been studied with computational techniques²²⁰⁻²²³ and are generally considered unstable or metastable²²⁰. Therefore, from the experimental and theoretical studies it appears that oS16-Re₃B (SG#53), hP20-Re₇B₃ (SG#186), and hP6-ReB₂ (SG#194) are the stable phases for the Re-B system. We calculate hP6-ReB₂ and oS16-Re₃B to be stable structures with the hP20-Re₇B₃ structure being metastable (12 meV/atom above the tie line). A metastable hP6-ReB (SG#156) structure (at 10 meV/Atom above the tie line) consisting of alternating buckled hexagonal and closed packed B layers was found using evolutionary search. Further hP6-ReB₂ and oS16-Re₃B are stable at 30GPa in GGA and LDA.

6. Os-B

The Os-B system has three reported phases, hP2-OsB (SG#51), hP10-Os₂B₃ (SG#194), and oP6-OsB₂ (SG#59)^{194,195}. At the OsB₂ composition, the oP6 (SG#59) structure¹⁹⁵ is found to be 9 meV/atom above the hP6 (SG#194) structure that effectively lies on the α -B \leftrightarrow hP10-Os₂B₃ tie line. The hP10-Os₂B₃ phase was studied by neutron diffraction by Frotscher *et al.*¹⁹⁴ and demonstrated to have an approximate composition of OsB_{1.6}. The stoichiometric structure is found to be stable in our calculations. The obtained stability of the hP2-OsB phase is in agreement with both the experimental⁹ and previous *ab initio* studies²²⁴ of α -OsB. The β -OsB phase⁹ has only (cubic) cell parameters reported which does not match any phases with negative formation energies in our database. The 30-GPa convex hull is defined by the same set of phases.

7. Ir-B

Several off-stoichiometric Ir-B phases near 1:1 composition have been reported and are shown in the most recent phase diagram⁸¹: hP2-IrB_{0.9} (SG#187) (often referred to as β -IrB), oS16-IrB_{0.9} (SG#36) (often referred to as α -IrB), tI12-IrB_{1.1} (SG#141), and mS-IrB_{1.26-1.5} (SG#12)^{9,81,195,198,225,226}. The last three have been suggested to be high-temperature phases⁹. To investigate the stoichiometry-dependent stabilization effect we simulated IrB_x ($0.875 < x < 1.25$) phases by creating B or Ir vacancies in hP2-IrB (SG#187) supercells. The Ir-rich

hP15-Ir₈B₇ phase was indeed found to be stable rendering possible Ir₂B candidate compounds metastable. Although hP4-IrB still appears below the α -B \leftrightarrow hP15-Ir₈B₇ tie line, a more systematic simulation of the off-stoichiometric compounds may lead to a different outcome. The report on synthesized Ir₃B₂ contained no structural information⁹ and we have not observed a stable phase at this composition among the considered prototypes. Application of pressure has been found to destabilize the constructed hP15 off-stoichiometric phase and only hP4-IrB is seen to be stable at 30 GPa.

8. Pt-B

Our findings raise questions about all three reported compounds in the Pt-B system⁹. No structural model is available for the tetragonal Pt₃B phase⁹, and the only relevant structure at this composition in our calculations is oP16 (SG#62), Pd₃B-type) that is metastable by 18 meV/atom. The reported hP4-PtB (SG#194)^{9,198} phase with linear boron chains was considered in our previous study and noted to be in poor agreement with experiment⁵¹. The exceptionally high B-B bond length mismatch of over 10% observed previously⁵¹ and the positive formation energy of 55 meV/atom calculated presently call for a more detailed study of this compound. Our evolutionary search identified an unrelated hP4-PtB (SG#164) phase, just 7 meV/atom above the tie line, comprised of buckled hexagonal sheets of boron (Wyckoff positions are in the Supplementary Materials⁸⁴). Finally, the observed Pt₂B phase is reported to be hP6 (SG#194)⁹, which is found in our calculations to be 68 meV/atom above the oP6 (SG#58), Pd₂B-type) structure. An orthorhombic PtB_{0.67} has also been observed experimentally. Simulation of this disordered phase is outside the scope of our study. The only stable phase, oP6-Pt₂B, obtained in our calculations at 0 GPa is replaced by a set of hR18-PtB₂, mP14-Pt₅B₂, and oP16-Pt₃B phases at 30 GPa. Interestingly, Pt-B is found to be the only considered M-B binary for which the formation enthalpy reduces with pressure. Although pressure-induced disproportionation has been seen in some systems^{227,228} we have not been able to identify factor(s) that make this system special.

9. Au-B

The hP3-AuB₂ (SG#191) phase was first reported by Obrowski¹⁰², but Massalski *et al.*⁹ describe it as a metastable. In a previous study⁵¹ the authors showed that hP3-AuB₂ not only has a large positive formation energy, but is also unstable with respect to a proposed lower-symmetry δ -AuB₂ derivative. All the considered phases have been found to have positive formation energies at both 0- and 30-GPa pressures.

10. Hg-B

The Hg-B system contains no stable compounds⁹, which is consistent with our calculations at both pressures considered.

formula	H_f (eV/atom)	dH (meV/atom)	Pearson
	GGA	LDA	
	GGA	LDA	Sym.
Li ₃ B ₁₄	-0.2326	-0.2453	0.0
Li ₂ B ₃	-0.2378	-0.2313	6.6
Li ₈ B ₇	-0.1907	-0.2093	0.0
Be ₂₉ B ₈₁	-0.1240	-0.1320	0.0
Na ₃ B ₂₀	-0.0594	-0.0305	0.0
Mg ₇ B ₇	-0.1317	-0.1444	0.0
MgB ₄	-0.1402	-0.1490	0.0
MgB ₂	-0.1321	-0.1496	0.0
AlB ₂	-0.0447	-0.0756	0.0
KB ₆	-0.0162	-0.0072	13.5
CaB ₆	-0.4122	-0.4098	0.0
CaB ₄	-0.3997	-0.4381	0.0
ScB ₁₂	-0.2105	-0.2167	0.0
ScB ₂	-0.8376	-0.9098	0.0
TiB ₂	-1.0600	-1.1425	0.0
Ti ₃ B ₄	-0.9357	-1.0002	0.0
TiB	-0.8358	-0.8863	0.0
VB ₂	-0.7402	-0.7999	0.0
V ₂ B ₃	-0.7990	-0.8535	0.0
V ₃ B ₄	-0.8202	-0.8708	0.0
V ₅ B ₆	-0.8312	-0.8796	0.0
VB	-0.8497	-0.8935	0.0
V ₃ B ₂	-0.7249	-0.7604	0.0
CrB ₄	-0.3098	-0.3533	0.0
CrB ₂	-0.4206	-0.4639	0.0
CrB	-0.5321	-0.5819	0.0
Cr ₅ B ₃	-0.4570	-0.7147	0.0
Cr ₂ B	-0.3753	-0.4109	0.0
MnB ₄	-0.2971	-0.3460	0.0
MnB ₃	-0.5184	-0.5031	0.0
Mn ₂ B	-0.4338	-0.4935	0.0
FeB ₂	-0.3001	-0.3877	0.0
FeB	-0.3802	-0.4084	0.0
Fe ₂ B	-0.3152	-0.3096	14.6
CoB	-0.4006	-0.5287	0.0
Ni ₄ B ₃	-0.2818	-0.3532	0.0
Ni ₂ B ₂	-0.2916	-0.3636	0.0
Ni ₅ B ₂	-0.2800	-0.3331	3.3
Ni ₃ B	-0.2640	-0.3160	0.0
SrB ₆	-0.4510	-0.4604	0.1
YB ₁₂	-0.2432	-0.2555	0.0
YB ₄	-0.5899	-0.6266	0.0
YB ₂	-0.5633	-0.5633	0.0
ZrB ₂	-0.9928	-1.0579	0.0
NbB ₂	-0.6961	-0.7456	0.0
Nb ₂ B ₃	-0.7507	-0.7909	0.0
Nb ₃ B ₄	-0.7659	-0.8013	0.0
NbB	-0.7745	-0.7991	0.0
Nb ₃ B ₂	-0.6346	-0.6546	0.0
MoB ₂	-0.4366	-0.4726	0.0
MoB	-0.5002	-0.5384	0.0
TcB ₂	-0.4409	-0.4673	0.0
Tc ₇ B ₃	-0.3164	-0.3237	0.0
Tc ₃ B ₂	-0.2677	-0.2764	0.0
RuB ₂	-0.2859	-0.3033	0.0
Ru ₂ B ₃	-0.3337	-0.3569	0.0
RuB	-0.3260	-0.3471	0.0
RhB	-0.3868	-0.4108	0.0
Rh ₅ B ₄	-0.3680	-0.3782	0.0
Rh ₇ B ₃	-0.2488	-0.2499	5.4
Pd ₂ B ₂	-0.2687	-0.2838	0.0
Pd ₃ B ₁	-0.2590	-0.2913	0.0
BaB ₆	-0.4096	-0.4251	0.0
LaB ₆	-0.5637	-0.5710	0.0
LaB ₄	-0.5713	-0.5877	0.0
HfB ₂	-1.0244	-1.1097	0.0
TaB ₂	-0.6658	-0.7004	12.3
Ta ₂ B ₃	-0.7417	-0.7944	0.0
Ta ₃ B ₄	-0.7717	-0.8197	0.0
Ta ₃ B ₆	-0.7884	-0.8335	0.0
TaB	-0.8168	-0.8544	0.0
Ta ₃ B ₂	-0.6734	-0.7048	0.0
WB ₃	-0.3001	-0.3194	0.0
WB ₂	-0.3644	-0.3854	0.0
WB	-0.3679	-0.4150	0.0
W ₂ B	-0.2602	-0.2828	0.0
ReB ₂	-0.4287	-0.4549	0.0
Re ₃ B	-0.2028	-0.2148	0.0
Os ₂ B ₃	-0.2567	-0.2743	0.0
OsB	-0.2359	-0.2496	0.0
IrB	-0.1982	-0.2008	4.3
Ir ₈ B ₇	-0.2071	-0.2058	0.0
Pt ₂ B	-0.2509	-0.2379	0.0

TABLE II: The compounds calculated to be stable within GGA at ambient pressures with the corresponding dH of the LDA calculations. Here dH is the stability in relation to phase separation as defined by distance of H_f to the tie line. Compounds with $dH=0$ are ground states. Compounds with $0 < dH < 20$ meV/atom are termed metastable (only for LDA). A 20 meV/atom cutoff, a typical size of the *relative* contribution to the Gibbs energy from the vibrational entropy term at $T \sim 1000$ K⁵, is chosen to distinguish between possible metastable and unstable phases. Compounds with dH values greater than 20 meV/atom are not included here.

formula	H_f (eV/atom) GGA	dH (meV/atom) GGA	Pearson LDA	Symbol
Li ₁₀ B ₉	-0.1913	-0.2058	0.6	4.1 hP19
Li ₆ B ₅	-0.1808	-0.2064	5.0	0.0 hP11
Be ₃ B ₅₀	-0.0255	-0.0173	1.1	11.0 aP53
BeB ₂	-0.0994	—	12.8	oP12
BeB ₂	-0.0991	—	13.1	oS12
Be ₂ B	-0.0165	-0.0211	17.2	tP10
NaB ₆	-0.0393	-0.0258	19.3	7.1 oS28
NaB ₃	-0.0448	-0.0537	6.4	0.0 tP16
MgB ₂	-0.1302	-0.1479	1.9	1.8 hP3
MgB ₂	-0.1313	-0.1486	0.8	1.0 oP12
MgB	-0.0892	-0.1444	9.9	0.0 hP8
MgB	-0.0906	-0.1087	8.4	3.5 hR4
Mg ₃ B ₂	-0.0608	-0.0771	18.5	12.6 hP5
K ₃ B ₂₀	-0.0113	-0.0209	3.5	0.0 oS46
ScB	-0.6122	—	16.0	hP8
Sc ₂ B	-0.8146	-0.6634	13.6	18.9 hP4
Tl ₂ B ₃	-0.9712	-1.0414	1.8	1.7 oS20
Tl ₅ B ₆	-0.8961	-0.9564	3.3	2.5 oS22
TiB	-0.8306	-0.8826	3.1	3.9 oS8
VB ₂	-0.7270	-0.7870	13.2	12.9 tI12
VB	-0.8409	-0.8826	8.8	10.9 oP8
VB	-0.8380	-0.8824	11.7	11.1 tI16
VB	-0.8406	-0.8826	9.1	10.9 oP8
CrB ₄	-0.3043	-0.4276	9.5	8.2 mS20
Cr ₅ B ₆	-0.4854	-0.6013	16.2	0.0 oS22
CrB	-0.5224	-0.7773	9.6	10.8 oS8
Cr ₃ B ₂	-0.4301	-0.7223	11.2	7.0 tP10
Cr ₂ B	-0.3744	-0.6852	1.0	0.6 tI12
MnB ₂	-0.3763	-0.4256	19.2	0.0 hP6
MnB ₄	-0.2791	—	18.0	— oI10
MnB ₄	-0.2888	-0.5276	8.2	18.1 oP10
MnB ₄	-0.2775	—	19.6	— mS5
MnB ₄	-0.2857	-0.5316	11.4	14.1 mS20
MnB ₄	-0.2954	-0.5437	1.6	2.0 oF80
MnB	-0.5000	-1.0019	18.3	0.3 tI16
MnB	-0.5111	—	7.3	— oS8
Mn ₂ B	-0.3111	-0.9952	6.9	7.1 oS8
Mn ₂ B	-0.4286	-1.1549	3.1	4.1 tI12
Mn ₃ B	-0.3063	-1.1590	19.1	0.0 oP16
Mn ₂₃ B ₆	-0.2518	-1.0630	17.4	0.0 cF29
FeB ₄	-0.1698	-0.2218	10.2	10.8 oP10
FeB ₄	-0.1635	—	16.6	— mS30
Fe ₂ B ₇	-0.1895	-0.2414	10.6	17.0 oP72
FeB	-0.3746	-0.4187	5.6	4.4 oP8
FeB	-0.3747	-0.4230	3.5	0.0 oS8
Fe ₂ B	-0.2183	—	18.1	— oP16
Fe ₃ B	-0.2169	—	19.5	— oS16
Fe ₂₃ B ₆	-0.1758	—	19.8	— cF116
NiB	-0.2386	-0.3044	8.0	4.6 oP8
NiB	-0.2282	-0.2934	18.3	15.6 tI16
NiB	-0.2414	-0.3085	3.2	0.5 oS8
Ni ₄ B ₃	-0.2796	-0.3459	2.2	7.3 mS14

Ni ₃ B ₂	-0.2673	—	17.4	—	aP30
Ni ₇ B ₃	-0.2695	-0.3252	14.0	19.3	hP20
YB	-0.4032	—	19.3	—	oS8
ZrB ₁₂	-0.2147	—	14.4	—	tI26
Nb ₅ B ₆	-0.7689	-0.8008	0.2	0.0	oS22
NbB	-0.7681	-0.6546	6.4	0.0	oP8
MoB ₄	-0.2341	-0.2812	7.8	2.4	hP10
MoB ₃	-0.3086	—	18.9	—	hP16
MoB ₃	-0.3144	—	13.0	—	hR24
MoB ₂	-0.4338	-0.4693	2.7	3.3	hP12
MoB	-0.4892	-0.5265	11.1	11.9	oS8
Tc ₃ B	-0.2582	-0.2610	9.4	15.4	oP16
RuB ₂	-0.2759	-0.2991	10.0	4.2	hP6
Rh ₈ B ₇	-0.3609	—	14.6	—	hP15
Rh ₂ B	-0.2702	—	6.0	—	oP6
Rh ₅ B ₂	-0.2215	-0.2234	15.4	19.7	mS28
Rh ₃ B	-0.1928	-0.1942	14.5	18.6	oP16
Rh ₃ B	-0.2018	-0.2010	5.5	11.7	oS16
Pd ₅ B ₂	-0.2554	-0.2926	7.8	0.0	mS28
Pd ₃ B ₃	-0.2444	-0.2717	14.6	19.7	oS16

Hf ₂ B ₃	-0.9031	—	18.9	—	oS20
TaB ₂	-0.6508	—	15.0	0.0	hP3
TaB ₂	-0.6599	-0.6943	5.9	18.3	hR18
TaB ₂	-0.6468	-0.7093	19.0	3.3	oP12
TaB	-0.8114	-0.8482	5.4	6.2	oP8
WB ₄	-0.2380	-0.2673	2.1	0.0	hP10
WB ₃	-0.2923	-0.3109	7.8	8.5	hP16
WB ₂	-0.3555	-0.3773	8.9	8.1	oP6
WB ₂	-0.3512	-0.3719	13.2	13.5	hR9
WB	-0.3541	-0.4005	13.8	14.5	oS8
W ₁₁ B ₈	-0.3056	-0.3408	11.3	11.6	oP38
Re ₂ B ₃	-0.3806	-0.4026	12.0	13.9	hP10
ReB	-0.3187	—	19.6	—	tI8
ReB	-0.3283	-0.3448	10.0	14.1	hP6
Re ₇ B ₃	-0.2201	-0.2313	9.8	12.3	hP20
Re ₂ B	-0.1865	—	16.3	—	oP16
OsB ₂	-0.2045	-0.2240	9.4	4.6	hP6
OsB ₂	-0.2134	-0.2261	0.5	2.5	oP6
IrB	-0.1825	—	15.8	—	tP4
IrB	-0.1918	-0.1967	6.4	8.5	hP2
IrB	-0.1842	-0.2032	2.2	8.0	tI8
Ir ₅ B ₄	-0.1817	-0.1764	15.6	6.0	hP18
Ir ₂ B	-0.1454	—	2.6	—	hP6
PtB	-0.1747	-0.1764	13.5	10.4	hR4
PtB	-0.1813	-0.1868	8.0	0.0	hP4
Pt ₃ B	-0.1699	-0.1713	18.2	7.1	oP16

TABLE III: The compounds calculated to be metastable at ambient pressures within GGA with the corresponding dH from LDA. Here dH is the stability in relation to phase separation as defined by distance of H_f to the tie line. Compounds with $dH=0$ are ground states. Compounds with $0 < dH < 20$ meV/atom are termed metastable. A 20 meV/atom cutoff, a typical size of the *relative* contribution to the Gibbs energy from the vibrational entropy term at $T \sim 1000$ K⁵, is chosen to distinguish between possible metastable and unstable phases. Compounds with dH values greater than 20 meV/atom are not included here.

Acknowledgements

A.N.K. acknowledges partial support from the EPSRC (CAF EP/G04072/1).

¹ B. Albert, European Journal of Inorganic Chemistry **2000**, 1679 (2000), ISSN 1099-0682, URL [http://dx.doi.org/10.1002/1099-0682\(200008\)2000:8<1679::AID-EJIC1679>3.0.CO;2-K](http://dx.doi.org/10.1002/1099-0682(200008)2000:8<1679::AID-EJIC1679>3.0.CO;2-K).

² J. R. Etourneau, P. Rogl, T. Lundström, P. Peshevand, and H. Pastor, *Inorganic Reactions and Methods* (John Wiley & Sons, Inc., Hoboken, NJ, USA, 2007), chap. 6.7 Formation of Borides, pp. 84–245, ISBN 9780470145289, URL <http://dx.doi.org/10.1002/9780470145289.ch19>.

³ D. G. Pettifor, *Bonding and Structure of Molecules and Solids* (Oxford University Press, New York, New York, USA., 1995).

⁴ G. Parakhonskiy, N. Dubrovinskaia, E. Bykova, R. Wirth, and L. Dubrovinsky, Sci. Rep. **1** (2011).

⁵ O. O. Kurakevych, Y. Le Godec, T. Hammouda, and C. Goujon, High Pressure Research **32**, 30 (2012), URL <http://www.tandfonline.com/doi/abs/10.1080/08957959.2011.635145>.

⁶ B. Albert and H. Hillebrecht, *Angewandte Chemie International Edition* **48**, 8640 (2009), ISSN 1521-3773, URL <http://dx.doi.org/10.1002/anie.200903246>.

⁷ A. R. Oganov, J. Chen, C. Gatti, Y. Ma, Y. Ma, C. W. Glass, Z. Liu, T. Yu, O. O. Kurakevych, and V. L. Solozhenko, *Nature* **457**, 863 (2009).

⁸ E. Y. Zarechnaya, L. Dubrovinsky, N. Dubrovinskaia, N. Miyajima, Y. Filinchuk, D. Chernyshov, and V. Dmitriev, *Science and Technology of Advanced Materials* **9**, 044209 (2008), URL <http://stacks.iop.org/1468-6996/9/i=4/a=044209>.

⁹ T. B. Massalski, H. Okamoto, and L. Kacprzak, eds., *Binary Alloy Phase Diagrams*, vol. 1 (ASM International, Materials Park, OH, USA., 1990), 2nd ed.

¹⁰ N. N. Jun Nagamatsu and, T. Muranaka, Y. Zenitani, and J. Akimitsu, *Nature* pp. 63–64 (2001).

¹¹ K. Arima, K. Matano, S. Harada, G. Z. Bao, Y. Inada, and G. Q. Zheng, *Journal of Physics: Conference Series* **449**, 012034 (2013), URL <http://stacks.iop.org/1742-6596/449/i=1/a=012034>.

¹² S. Bose and E. Zijlstra, *Physica C: Superconductivity* **432**, 173 (2005), ISSN 0921-4534, URL <http://www.sciencedirect.com/science/article/pii/S0921453405006106>.

¹³ L. Fang, H. Yang, X. Zhu, G. Mu, Z.-S. Wang, L. Shan, C. Ren, and H.-H. Wen, *Phys. Rev. B* **79**, 144509 (2009), URL <http://link.aps.org/doi/10.1103/PhysRevB.79.144509>.

¹⁴ H. Gou, N. Dubrovinskaia, E. Bykova, A. A. Tsirlin, D. Kasinathan, W. Schnelle, A. Richter, M. Merlini, M. Hanfland, A. M. Abakumov, *et al.*, *Phys. Rev. Lett.* **111**, 157002 (2013), URL <http://link.aps.org/doi/10.1103/PhysRevLett.111.157002>.

¹⁵ K. Togano, P. Badica, Y. Nakamori, S. Orimo, H. Takeya, and K. Hirata, *Phys. Rev. Lett.* **93**, 247004 (2004), URL <http://link.aps.org/doi/10.1103/PhysRevLett.93.247004>.

¹⁶ P. Badica, T. Kondo, T. Kudo, Y. Nakamori, S. Orimo, and K. Togano, *Applied Physics Letters* **85**, 4433 (2004), URL <http://link.aip.org/link/?APL/85/4433/1>.

¹⁷ H. Rosner, A. Kitagorodsky, and W. E. Pickett, *Phys. Rev. Lett.* **88**, 127001 (2002), URL <http://link.aps.org/doi/10.1103/PhysRevLett.88.127001>.

¹⁸ A. N. Kolmogorov and S. Curtarolo, *Phys. Rev. B* **73**, 180501 (2006), URL <http://link.aps.org/doi/10.1103/PhysRevB.73.180501>.

¹⁹ A. N. Kolmogorov, M. Calandra, and S. Curtarolo, *Phys. Rev. B* **78**, 094520 (2008), URL <http://link.aps.org/doi/10.1103/PhysRevB.78.094520>.

²⁰ A. N. Kolmogorov, S. Shah, E. R. Margine, A. F. Bialon, T. Hammerschmidt, and R. Drautz, *Phys. Rev. Lett.* **105**, 217003 (2010), URL <http://link.aps.org/doi/10.1103/PhysRevLett.105.217003>.

²¹ A. Oganov and V. Solozhenko, *Journal of Superhard Materials* **31**, 285 (2009), ISSN 1063-4576, URL <http://dx.doi.org/10.3103/S1063457609050013>.

²² J. B. Levine, S. H. Tolbert, and R. B. Kaner, *Advanced Functional Materials* **19**, 3519 (2009), ISSN 1616-3028, URL <http://dx.doi.org/10.1002/adfm.200901257>.

²³ H.-Y. Chung, M. B. Weinberger, J. B. Levine, A. Kavner, J.-M. Yang, S. H. Tolbert, and R. B. Kaner, *Science* **316**, 436 (2007), URL <http://www.sciencemag.org/content/316/5823/436.full.pdf>, URL <http://www.sciencemag.org/content/316/5823/>

436.abstract.

²⁴ H. Niu, J. Wang, X.-Q. Chen, D. Li, Y. Li, P. Lazar, R. Podloucky, and A. N. Kolmogorov, *Phys. Rev. B* **85**, 144116 (2012), URL <http://link.aps.org/doi/10.1103/PhysRevB.85.144116>.

²⁵ N. Dubrovinskaia, L. Dubrovinsky, and V. L. Solozhenko, *Science* **318**, 1550 (2007), URL <http://www.sciencemag.org/content/318/5856/1550.3.full.pdf>, URL <http://www.sciencemag.org/content/318/5856/1550.3.abstract>.

²⁶ J. Qin, D. He, J. Wang, L. Fang, L. Lei, Y. Li, J. Hu, Z. Kou, and Y. Bi, *Advanced Materials* **20**, 4780 (2008), ISSN 1521-4095, URL <http://dx.doi.org/10.1002/adma.200801471>.

²⁷ A. Knappschneider, C. Litterscheid, D. Dzivenko, J. A. Kurzman, R. Seshadri, N. Wagner, J. Beck, R. Riedel, and B. Albert, *Inorganic Chemistry* **52**, 540 (2013), URL <http://pubs.acs.org/doi/pdf/10.1021/ic3020404>, URL <http://pubs.acs.org/doi/abs/10.1021/ic3020404>.

²⁸ R. F. Zhang, D. Legut, Z. J. Lin, Y. S. Zhao, H. K. Mao, and S. Veprek, *Phys. Rev. Lett.* **108**, 255502 (2012), URL <http://link.aps.org/doi/10.1103/PhysRevLett.108.255502>.

²⁹ X.-Q. Chen, C. L. Fu, M. Krčmar, and G. S. Painter, *Phys. Rev. Lett.* **100**, 196403 (2008), URL <http://link.aps.org/doi/10.1103/PhysRevLett.100.196403>.

³⁰ Y. Liang, X. Yuan, and W. Zhang, *Phys. Rev. B* **83**, 220102 (2011), URL <http://link.aps.org/doi/10.1103/PhysRevB.83.220102>.

³¹ Y. Liang, Z. Fu, X. Yuan, S. Wang, Z. Zhong, and W. Zhang, *EPL (Europhysics Letters)* **98**, 66004 (2012), URL <http://stacks.iop.org/0295-5075/98/i=6/a=66004>.

³² Y. Liang, Y. Gou, X. Yuan, Z. Zhong, and W. Zhang, *Chemical Physics Letters* **580**, 48 (2013), ISSN 0009-2614, URL <http://www.sciencedirect.com/science/article/pii/S0009261413008518>.

³³ I. Shein, K. Shein, and A. Ivanovskii, *Physica B: Condensed Matter* **387**, 184 (2007), ISSN 0921-4526, URL <http://www.sciencedirect.com/science/article/pii/S0921452606007964>.

³⁴ M. Zhang, H. Wang, H. Wang, T. Cui, and Y. Ma, *The Journal of Physical Chemistry C* **114**, 6722 (2010), URL <http://pubs.acs.org/doi/pdf/10.1021/jp100225c>, URL <http://pubs.acs.org/doi/abs/10.1021/jp100225c>.

³⁵ Y. Liang, X. Yuan, Z. Fu, Y. Li, and Z. Zhong, *Applied Physics Letters* **101**, 181908 (pages 5) (2012), URL <http://link.aip.org/link/?APL/101/181908/1>.

³⁶ T. Lundström, *Pure Appl. Chem.* **57**, 1383 (1985).

³⁷ X. Ji, Q. Zhang, J. Xu, and Y. Zhao, *Progress in Solid State Chemistry* **39**, 51 (2011), ISSN 0079-6786, URL <http://www.sciencedirect.com/science/article/pii/S0079678611000033>.

³⁸ K. Yada, H. Masaoka, Y. Shoji, and T. Tanji, *J Electron Microscrosc Tech.* **12**, 252 (1989).

³⁹ L. Lanier, G. Metauer, and M. Moukassi, *Microchimica Acta* **114-115**, 353 (1994), ISSN 0026-3672, URL <http://dx.doi.org/10.1007/BF01244562>.

⁴⁰ O. Gutfleisch, M. A. Willard, E. Brück, C. H. Chen, S. G. Sankar, and J. P. Liu, *Advanced Materials* **23**, 821 (2011), ISSN 1521-4095, URL <http://dx.doi.org/10.1002/adma.201002180>.

⁴¹ B. Aronsson, T. Lundstroem, and I. Engstroem, *Anisotropy in single-crystal refractory* **1**, 3 (1968).

⁴² B. Aronsson, T. Lundström, and S. Rundqvist, *Borides, Silicides, and Phosphides* (Spottiswoode, Ballantyne, and Co. Ltd., London, UK., 1965).

⁴³ V. Matkovic, J. Economy, R. Giese, jr, and R. Barrett, *Acta Crystallographica* **19**, 1056 (1965).

⁴⁴ P. F. Walch, D. E. Ellis, and F. M. Mueller, *Phys. Rev. B* **15**, 1859 (1977), URL <http://link.aps.org/doi/10.1103/PhysRevB.15.1859>.

⁴⁵ J. K. Burdett and E. Canadell, *Inorganic Chemistry* **27**, 4437 (1988), <http://pubs.acs.org/doi/pdf/10.1021/ic00297a021>, URL <http://pubs.acs.org/doi/abs/10.1021/ic00297a021>.

⁴⁶ S. Okada, T. Atoda, and I. Higashi, *Journal of Solid State Chemistry* **68**, 61 (1987).

⁴⁷ J. P. Perdew, K. Burke, and M. Ernzerhof, *Phys. Rev. Lett.* **77**, 3865 (1996), URL <http://link.aps.org/doi/10.1103/PhysRevLett.77.3865>.

⁴⁸ J. P. Perdew and A. Zunger, *Phys. Rev. B* **23**, 5048 (1981), URL <http://link.aps.org/doi/10.1103/PhysRevB.23.5048>.

⁴⁹ G. Kresse and D. Joubert, *Phys. Rev. B* **59**, 1758 (1999), URL <http://link.aps.org/doi/10.1103/PhysRevB.59.1758>.

⁵⁰ T. Oguchi, *Journal of the Physical Society of Japan* **71**, 1495 (2002), URL <http://jpsj.ipap.jp/link?JPSJ/71/1495/>.

⁵¹ A. N. Kolmogorov and S. Curtarolo, *Phys. Rev. B* **74**, 224507 (2006), URL <http://link.aps.org/doi/10.1103/PhysRevB.74.224507>.

⁵² S. Curtarolo, D. Morgan, and G. Ceder, *Calphad* **29**, 163 (2005), ISSN 0364-5916, URL <http://www.sciencedirect.com/science/article/pii/S0364591605000064>.

⁵³ O. Levy, G. L. W. Hart, and S. Curtarolo, *Phys. Rev. B* **81**, 174106 (2010), URL <http://link.aps.org/doi/10.1103/PhysRevB.81.174106>.

⁵⁴ O. Levy, G. L. Hart, and S. Curtarolo, *Acta Materialia* **58**, 2887 (2010), ISSN 1359-6454, URL <http://www.sciencedirect.com/science/article/pii/S1359645410000315>.

⁵⁵ A. Jain, G. Hautier, C. J. Moore, S. P. Ong, C. C. Fischer, T. Mueller, K. A. Persson, and G. Ceder, *Computational Materials Science* **50**, 2295 (2011), ISSN 0927-0256, URL <http://www.sciencedirect.com/science/article/pii/S0927025611001133>.

⁵⁶ A. Jain, G. Hautier, S. P. Ong, C. J. Moore, C. C. Fischer, K. A. Persson, and G. Ceder, *Phys. Rev. B* **84**, 045115 (2011), URL <http://link.aps.org/doi/10.1103/PhysRevB.84.045115>.

⁵⁷ A. Bil, B. Kolb, R. Atkinson, D. G. Pettifor, T. Thonhauser, and A. N. Kolmogorov, *Phys. Rev. B* **83**, 224103 (2011), URL <http://link.aps.org/doi/10.1103/PhysRevB.83.224103>.

⁵⁸ S. Curtarolo, W. Setyawan, G. L. Hart, M. Jahnatek, R. V. Chepulskii, R. H. Taylor, S. Wang, J. Xue, K. Yang, O. Levy, *et al.*, *Computational Materials Science* **58**, 218 (2012), ISSN 0927-0256, URL <http://www.sciencedirect.com/science/article/pii/S0927025612000717>.

⁵⁹ S. Curtarolo, G. L. W. Hart, M. B. Nardelli, N. Mingo, S. Sanvito, and O. Levy, *Nat Mater* **12**, 191 (2013).

⁶⁰ T. S. Bush, C. R. A. Catlow, and P. D. Battle, *J. Mater. Chem.* **5**, 1269 (1995), URL <http://dx.doi.org/10.1039/JM9950501269>.

⁶¹ N. L. Abraham and M. I. J. Probert, *Phys. Rev. B* **73**, 224104 (2006), URL <http://link.aps.org/doi/10.1103/PhysRevB.73.224104>.

⁶² A. R. Oganov and C. W. Glass, *The Journal of Chemical Physics* **124**, 244704 (pages 15) (2006), URL <http://link.aip.org/link/?JCP/124/244704/1>.

⁶³ G. Trimarchi and A. Zunger, *Phys. Rev. B* **75**, 104113 (2007), URL <http://link.aps.org/doi/10.1103/PhysRevB.75.104113>.

⁶⁴ D. J. Wales and J. P. K. Doye, *The Journal of Physical Chemistry A* **101**, 5111 (1997), <http://pubs.acs.org/doi/pdf/10.1021/jp970984n>, URL <http://pubs.acs.org/doi/abs/10.1021/jp970984n>.

⁶⁵ D. J. Wales and H. A. Scheraga, *Science* **285**, 1368 (1999), <http://www.sciencemag.org/content/285/5432/1368.full.pdf>, URL <http://www.sciencemag.org/content/285/5432/1368.abstract>.

⁶⁶ M. Amsler and S. Goedecker, *The Journal of Chemical Physics* **133**, 224104 (pages 8) (2010), URL <http://link.aip.org/link/?JCP/133/224104/1>.

⁶⁷ C. J. Pickard and R. J. Needs, *Phys. Rev. Lett.* **97**, 045504 (2006), URL <http://link.aps.org/doi/10.1103/PhysRevLett.97.045504>.

⁶⁸ Y. Wang, J. Lv, L. Zhu, and Y. Ma, *Phys. Rev. B* **82**, 094116 (2010), URL <http://link.aps.org/doi/10.1103/PhysRevB.82.094116>.

⁶⁹ Y. Wang, J. Lv, L. Zhu, and Y. Ma, *Computer Physics Communications* **183**, 2063 (2012), ISSN 0010-4655, URL <http://www.sciencedirect.com/science/article/pii/S0010465512001762>.

⁷⁰ G. Trimarchi, A. J. Freeman, and A. Zunger, *Phys. Rev. B* **80**, 092101 (2009), URL <http://link.aps.org/doi/10.1103/PhysRevB.80.092101>.

⁷¹ B. Meredig and C. Wolverton, *Nat Mater* **12**, 123 (2013).

⁷² A. O. Lyakhov, A. R. Oganov, and M. Valle, *Computer Physics Communications* **181**, 1623 (2010), ISSN 0010-4655, URL <http://www.sciencedirect.com/science/article/pii/S0010465510001840>.

⁷³ A. O. Lyakhov, A. R. Oganov, H. T. Stokes, and Q. Zhu, *Computer Physics Communications* **184**, 1172 (2013), ISSN 0010-4655, URL <http://www.sciencedirect.com/science/article/pii/S0010465512004055>.

⁷⁴ A. N. Kolmogorov, S. Shah, E. R. Margine, A. K. Kleppe, and A. P. Jephcoat, *Phys. Rev. Lett.* **109**, 075501 (2012), URL <http://link.aps.org/doi/10.1103/PhysRevLett.109.075501>.

⁷⁵ A. F. Bialon, T. Hammerschmidt, R. Drautz, S. Shah, E. R. Margine, and A. N. Kolmogorov, *Applied Physics Letters* **98**, 081901 (pages 3) (2011), URL <http://link.aip.org/link/?APL/98/081901/1>.

⁷⁶ A. Hermann, A. McSorley, N. W. Ashcroft, and R. Hoffmann, *Journal of the American Chemical Society* **134**, 18606 (2012), <http://pubs.acs.org/doi/pdf/10.1021/ja308492g>, URL <http://pubs.acs.org/doi/abs/10.1021/ja308492g>.

⁷⁷ F. Peng, M. Miao, H. Wang, Q. Li, and Y. Ma, *Journal of the American Chemical Society* **134**, 18599 (2012), <http://pubs.acs.org/doi/pdf/10.1021/ja308490a>, URL <http://pubs.acs.org/doi/abs/10.1021/ja308490a>.

⁷⁸ S. Shah and A. N. Kolmogorov, *Phys. Rev. B* **88**, 014107 (2013), URL <http://link.aps.org/doi/10.1103/PhysRevB.88.014107>.

⁷⁹ G. Bergerhoff and I.D.Brown, *Crystallographic Databases* (International Union of Crystallography, Chester, UK., 1987).

⁸⁰ E. Zhao, J. Meng, Y. Ma, and Z. Wu, *Phys. Chem.*

Chem. Phys. **12**, 13158 (2010), URL <http://dx.doi.org/10.1039/C004122J>.

⁸¹ P. Rogl, G. Effenberg, and S. Ilenco, *Phase diagrams of ternary metal-boron-carbon systems* (Materials Park, OH : ASM International ; Stuttgart, Germany : MSI, 1998), ISBN 0871706601, includes bibliographical references.

⁸² P. Rogl and J. Schuster, *Phase Diagrams of Ternary Boron Nitride and Silicon Nitride Systems*, Monograph series on alloy phase diagrams (ASM International, Materials Park, OH, USA., 1992), ISBN 9780871702302, URL <http://books.google.com/books?id=0Z0UuZUS4BsC>.

⁸³ E. Rudy, Tech Rept. No. AFML-TR-65-2, Part V Compendium of phase diagram data pp. 1-690 (1969).

⁸⁴ See supplemental material at link for the wyckoff positions of the stable structures, the wyckoff positions of select metastable structures, the compositions considered with evolutionary search, and a discussion of the ground states of magnetic metals selected.

⁸⁵ G. Kresse and J. Furthmüller, Phys. Rev. B **54**, 11169 (1996), URL <http://link.aps.org/doi/10.1103/PhysRevB.54.11169>.

⁸⁶ D. Vanderbilt, Phys. Rev. B **41**, 7892 (1990), URL <http://link.aps.org/doi/10.1103/PhysRevB.41.7892>.

⁸⁷ J. D. Pack and H. J. Monkhorst, Phys. Rev. B **16**, 1748 (1977), URL <http://link.aps.org/doi/10.1103/PhysRevB.16.1748>.

⁸⁸ H. J. Monkhorst and J. D. Pack, Phys. Rev. B **13**, 5188 (1976), URL <http://link.aps.org/doi/10.1103/PhysRevB.13.5188>.

⁸⁹ D. Alfè, Computer Physics Communications **180**, 2622 (2009), ISSN 0010-4655, URL <http://www.sciencedirect.com/science/article/pii/S0010465509001064>.

⁹⁰ I. I. Mazin, Nature **464**, 183 (2010).

⁹¹ R. Fruchart and A. Michel, Compt. Rend. **251**, 2953 (1960).

⁹² S. Andersson, Acta Chem. Scand. **23**, 687 (1969).

⁹³ S. Andersson and J. Carlsson, Acta Chemica Scandinavica **24**, 1791 (1970).

⁹⁴ S. Andersson and T. Lundström, Acta Chem. Scand. **22**, 3103 (1968).

⁹⁵ A. Knappschneider, C. Litterscheid, J. Kurzman, R. Seashadri, and B. Albert, Inorganic Chemistry **50**, 10540 (2011), <http://pubs.acs.org/doi/pdf/10.1021/ic2018083>, URL <http://pubs.acs.org/doi/abs/10.1021/ic2018083>.

⁹⁶ Further details of the crystal structure investigation may be obtained from fachinformationszentrum karlsruhe (fax: (+49)7247-808-666; e-mail: crysdata@fiz-karlsruhe.de, http://www.fiz-karlsruhe.de/request_for_deposited_data.html) on quoting the deposition number [csd-426691](http://www.fiz-karlsruhe.de/request_for_deposited_data.html).

⁹⁷ R. Kiessling, Acta Chemica Scandinavica **3**, 603 (1949).

⁹⁸ S. Okada, K. Kudou, I. Higashi, and T. Lundström, Journal of Crystal Growth **128**, 1120 (1993), ISSN 0022-0248, [jcrysgrowth.1992.1120](http://dx.doi.org/10.1006/jcrys.1992.1120), URL <http://www.sciencedirect.com/science/article/pii/S0022024807801096>.

⁹⁹ J. Norton, H. Blumenthal, and S. Sindeband, Transactions of the American Institute of Mineralogy **185**, 749 (1949).

¹⁰⁰ T. Bjurstroem, Arkiv foer Kemi Mineralogi och Geologi **11**, 1 (1933).

¹⁰¹ S. Rundqvist and S. Pramatus, Acta Chemica Scandinavica **21**, 191 (1967).

¹⁰² W. Obrowski, Naturwissenschaften **48**, 428 (1961).

¹⁰³ A. Islam, F. Parvin, F. Islam, M. Islam, A. Islam, and I. Tanaka, Physica C: Superconductivity **466**, 76 (2007), ISSN 0921-4534, URL <http://www.sciencedirect.com/science/article/pii/S0921453407011021>.

¹⁰⁴ J. R. Tobin, ed., *Superconductivity: Research Developments*, New York, New York, USA. (Nova Science Publishers, Inc., 2008).

¹⁰⁵ R. Caputo, F. Guzzetta, and A. Angerhofer, Inorganic Chemistry **49**, 8756 (2010), <http://pubs.acs.org/doi/pdf/10.1021/ic100896a>, URL <http://pubs.acs.org/doi/abs/10.1021/ic100896a>.

¹⁰⁶ R. V. Chepulskii and S. Curtarolo, Phys. Rev. B **79**, 134203 (2009), URL <http://link.aps.org/doi/10.1103/PhysRevB.79.134203>.

¹⁰⁷ N. Vojteer, J. Stauffer, H. Hillebrecht, K. Hofmann, M. Panda, and B. Albert, Zeitschrift fuer Anorg. und Allgemeine C **635**, 653 (2009).

¹⁰⁸ H. von Schnerring, G. Mair, M. Woerle, and R. Nesper, Zeitschrift fuer Anorg. und Allgemeine C **625**, 1207 (1999).

¹⁰⁹ G. Mair, R. Nesper, von, and H. Schnerring, Journal of Solid State Chemistry **75**, 30 (1988).

¹¹⁰ Z. Liu, X. Qu, B. Huang, and Z. Li, Journal of Alloys and Compounds **311**, 256 (2000), ISSN 0925-8388, URL <http://www.sciencedirect.com/science/article/pii/S0925838800010768>.

¹¹¹ M. Wörle and R. Nesper, Angewandte Chemie International Edition **39**, 2349 (2000), ISSN 1521-3773, URL [http://dx.doi.org/10.1002/1521-3773\(20000703\)39:13<2349::AID-ANIE2349>3.0.CO;2-U](http://dx.doi.org/10.1002/1521-3773(20000703)39:13<2349::AID-ANIE2349>3.0.CO;2-U).

¹¹² H. Rosner and W. E. Pickett, Phys. Rev. B **67**, 054104 (2003), URL <http://link.aps.org/doi/10.1103/PhysRevB.67.054104>.

¹¹³ A. N. Kolmogorov, R. Drautz, and D. G. Pettifor, Phys. Rev. B **76**, 184102 (2007), URL <http://link.aps.org/doi/10.1103/PhysRevB.76.184102>.

¹¹⁴ A. Hermann, N. W. Ashcroft, and R. Hoffmann, Inorganic Chemistry **51**, 9066 (2012), <http://pubs.acs.org/doi/pdf/10.1021/ic301215y>, URL <http://pubs.acs.org/doi/abs/10.1021/ic301215y>.

¹¹⁵ A. Hermann, N. W. Ashcroft, and R. Hoffmann, Chemistry – A European Journal **19**, 4184 (2013), ISSN 1521-3765, URL <http://dx.doi.org/10.1002/chem.201203890>.

¹¹⁶ B. Albert and K. Hofmann, Zeitschrift fuer Anorg. und Allgemeine C **625**, 709 (1999).

¹¹⁷ R. Naslain and J. Kasper, Journal of Solid State Chemistry **1**, 150 (1970).

¹¹⁸ B. Albert, K. Hofmann, C. Fild, H. Eckert, M. Schleifer, and R. Gruehn, Chemistry – A European Journal **6**, 2531 (2000), ISSN 1521-3765, URL [http://dx.doi.org/10.1002/1521-3765\(20000717\)6:14<2531::AID-CHEM2531>3.0.CO;2-2](http://dx.doi.org/10.1002/1521-3765(20000717)6:14<2531::AID-CHEM2531>3.0.CO;2-2).

¹¹⁹ B. Albert and K. Schmitt, Chemistry of Materials **11**, 3406 (1999), <http://pubs.acs.org/doi/pdf/10.1021/cm991130d>, URL <http://pubs.acs.org/doi/abs/10.1021/cm991130d>.

¹²⁰ N. Orlovskaya and M. Lugovy, eds., *Boron Rich Solids: Sensors, Ultra High Temperature Ceramics, Thermoelectrics, Armor*, NATO Science for Peace and Security Series- B: Physics and Biophysics (Springer Science, Dordrecht, NL., 2011).

¹²¹ R. Naslain and J. Etourneau, Comptes Rendus Hebdomadaires des Seances de l'Academie des Sciences, Serie C, Sciences Chimiques **264**, 484 (1966).

¹²² K. Walsh, E. E. Vidal, and B. Mishra, *Beryllium Chemistry and Processing* (ASM International, Materials Park, OH, USA., 2009).

¹²³ M. Jones and R. Marsh, *Journal of the American Chemical Society* **76**, 1434 (1954).

¹²⁴ A. Guette, R. Naslain, and J. Galy, *Comptes Rendus Hebdomadaires des Seances* **275**, 41 (1972).

¹²⁵ A. Pediaditakis, M. Schroeder, V. Sagawe, T. Ludwig, and H. Hillebrecht, *Inorganic Chemistry* **49**, 10882 (2010).

¹²⁶ L. Pauling and S. Weinbaum, *Zeitschrift fuer Krist. Kristallgeometrie* **87**, 181 (1934).

¹²⁷ Z. Liu, X. Han, D. Yu, Y. Sun, B. Xu, X.-F. Zhou, J. He, H.-T. Wang, and Y. Tian, *Applied Physics Letters* **96**, 031903 (pages 3) (2010), URL <http://link.aip.org/link/?APL/96/031903/1>.

¹²⁸ R. W. Johnson and A. H. Daane, *The Journal of Physical Chemistry* **65**, 909 (1961), <http://pubs.acs.org/doi/pdf/10.1021/j100824a004>, URL <http://pubs.acs.org/doi/abs/10.1021/j100824a004>.

¹²⁹ R. Schmitt, B. Blaschkowski, K. Eichele, and H.-J. Meyer, *Inorganic Chemistry* **45**, 3067 (2006), <http://pubs.acs.org/doi/pdf/10.1021/ic0518430>, URL <http://pubs.acs.org/doi/abs/10.1021/ic0518430>.

¹³⁰ H. Ott, M. Chernikov, E. Felder, L. Degiorgi, E. Moshopoulou, J. Sarrao, and Z. Fisk, *Zeitschrift fuer Physik B* **102**, 337 (1997).

¹³¹ K. Schmitt, C. Stueckl, H. Ripplinger, and B. Albert, *Solid State Sciences* **3**, 321 (2001).

¹³² H. Duschanek and P. Rogl, *Journal of Phase Equilibria* **15**, 543 (1994), ISSN 1054-9714, URL <http://dx.doi.org/10.1007/BF02649415>.

¹³³ A. Felten, *Journal of the American Chemical Society* **78**, 5977 (1956).

¹³⁴ N. Zhuravlev and A. Stepanova, *Kristallografiya* **3**, 83 (1958).

¹³⁵ A. Pediaditakis, S. Hasseloff, and H. Hillebrecht, *Solid State Sciences* **13**, 1465 (2011), ISSN 1293-2558, URL <http://www.sciencedirect.com/science/article/pii/S1293255811001348>.

¹³⁶ T. Tanaka, S. Okada, and V. Gurin, *Journal of Alloys and Compounds* **267**, 211 (1998), ISSN 0925-8388, URL <http://www.sciencedirect.com/science/article/pii/S0925838897004908>.

¹³⁷ M. Przybyska, A. H. Reddoch, and G. J. Ritter, *Journal of the American Chemical Society* **85**, 407 (1963), <http://pubs.acs.org/doi/pdf/10.1021/ja00887a008>, URL <http://pubs.acs.org/doi/abs/10.1021/ja00887a008>.

¹³⁸ V. I. Matkovich, J. Economy, R. F. Giese, Jnr, and R. Barrett, *Acta Crystallographica* **19**, 1056 (1965), URL <http://dx.doi.org/10.1107/S0365110X65004954>.

¹³⁹ B. Decker and J. Kasper, *Acta Crystallographica* **7**, 77 (1954).

¹⁴⁰ Y. Nakama, H. Ohtani, and M. Hasebe, *MA-TERIALS TRANSACTIONS* **50**, 984 (2009), URL https://www.jstage.jst.go.jp/article/matertrans/50/5/50_MC200820/_article.

¹⁴¹ Y. Yu, L. Tergenius, T. Lundstroem, and S. Okada, *Journal of Alloys Compd.* **221**, 86 (1995).

¹⁴² K. Spear and P. Gilles, *High Temperature Science* **1**, 86 (1969).

¹⁴³ H. Nowotny and A. Wittmann, *Monatshefte fuer Chemie* **89**, 221 (1958).

¹⁴⁴ O. Schob and E. Parthe, *Acta Crystallographica* **19**, 214 (1965).

¹⁴⁵ G. Effenberg, ed., *Ternary Alloy Systems: Phase Diagrams, Crystallographic and Thermodynamic Data*, vol. 11 (Springer Berlin Heidelberg New York, 2009).

¹⁴⁶ A. Riabov, V. Yartys, B. Hauback, P. Guegan, G. Wiesinger, , and I. Harris, *Journal of Alloys Compd.* **293**, 93 (1999).

¹⁴⁷ C. A. Nunes, B. B. de Lima, G. C. Coelho, P. Rogl, and P. A. Suzuki, *Journal of Alloys and Compounds* **370**, 164 (2004), ISSN 0925-8388, URL <http://www.sciencedirect.com/science/article/pii/S0925838803010211>.

¹⁴⁸ K. Portnoi and V. Romashov, *Soviet powder metallurgy and metal ceram* **8**, 298 (1969).

¹⁴⁹ F. Bertaut and P. Blum, *Comptes Rendus Hebdomadaires des Seances* **236**, 1055 (1953).

¹⁵⁰ C. Guy and A. Uraz, *Journal of the Less-Common Metals* **48**, 199 (1976).

¹⁵¹ B. Post, F. Glaser, and D. Moskowitz, *Acta Metallurgica* **2**, 20 (1954).

¹⁵² A. Frueh, *Acta Crystallographica* **4**, 66 (1951).

¹⁵³ G. Pradelli and C. Gianoglio, *Metallurgia Italiana* **68**, 191 (1976).

¹⁵⁴ G. Papesch, H. Nowotny, and F. Benesovsky, *Monatshefte fuer Chemie und verwandte Te* **104**, 933 (1973).

¹⁵⁵ M. Elfstroem, *Acta Chemica Scandinavica* **15**, 1178 (1961).

¹⁵⁶ E. Lugscheider, O. Knotek, and H. Reimann, *Monatshefte fuer Chemie und verwandte Te* **105**, 80 (1974).

¹⁵⁷ I. Smid, P. Rogl, and F. Weitzer, *The ternary system Manganese-Boron-Nitrogen*, vol. 2 (Proceedings of the 12th International Plansee Seminar, Verlag Tyrolia, Innsbruck, Austria, 1989).

¹⁵⁸ R. Kiessling, *Acta Chemica Scandinavica* **4**, 146 (1950).

¹⁵⁹ L. Tergenius, *Journal of the Less-Common Metals* **82**, 335 (1981).

¹⁶⁰ *Dictionary of Inorganic Compounds*, vol. 1 (Chapman and Hall, London, UK., 1992).

¹⁶¹ E. Havinga, H. Damsma, and P. Hokkeling, *Journal of the Less-Common Metals* **27**, 169 (1972).

¹⁶² B. Aronsson, *Acta Chemica Scandinavica* **14**, 1414 (1960).

¹⁶³ S. Aydin and M. Simsek, *Phys. Rev. B* **80**, 134107 (2009), URL <http://link.aps.org/doi/10.1103/PhysRevB.80.134107>.

¹⁶⁴ H. Okamoto, *Journal of Phase Equilibria and Diffusion* **25**, 297 (2004), ISSN 1547-7037, URL <http://dx.doi.org/10.1007/s11669-004-0128-3>.

¹⁶⁵ K. Balani, A. Agarwal, and N. B. Dahotre, *Journal of Applied Physics* **99**, 044904 (pages 4) (2006), URL <http://link.aip.org/link/?JAP/99/044904/1>.

¹⁶⁶ B. Callmer and T. Lundstrom, *Journal of Solid State Chemistry* **17**, 165 (1976), ISSN 0022-4596, URL <http://www.sciencedirect.com/science/article/pii/0022459676902176>.

¹⁶⁷ S. Watanabe and H. Ohtani, *Iron Steel Inst. Jpn.* **23**, 38 (1983).

¹⁶⁸ Y. Khan, E. Kneller, and M. Sostarich, *Z. Metallkunde* **73**, 624 (1982).

¹⁶⁹ D. Pettifor, B. Seiser, E. Margine, A. Kolmogorov, and R. Drautz, *Philosophical Magazine* **0**, 1 (2013), URL <http://www.tandfonline.com/doi/abs/10.1080/14786435.2013.771824>.

⁸ *Further details of the crystal structure investigation may be obtained from fachinformationszentrum karlsruhe, 76344 eggenstein-leopoldshafen, germany (fax: (+49)7247-808-666; e-mail: crysdata@fiz-karlsruhe.de,*

http://www.fiz-karlsruhe.de/request_for_deposited_data.html on quoting the deposition number csd-426694.

¹⁷¹ R. Fruchart and A. Michel, Bulletin de la Societe Chimique de Franc **1959**, 422 (1959).

¹⁷² Z. Malik, A. Grytsiv, P. Rogl, G. Giester, and J. Buršík, Journal of Solid State Chemistry **198**, 150 (2013), ISSN 0022-4596, URL <http://www.sciencedirect.com/science/article/pii/S0022459612006391>.

¹⁷³ P. Blum, Journal de Physique et du Radium **13**, 430 (1952).

¹⁷⁴ R. Manelis, T. Telyukova, and L. Grishina, Izvestiya Akademii Nauk SSSR Neorganich **6**, 1035 (1970).

¹⁷⁵ R. Giese, jr, V. Matkovic, and J. Economy, Zeitschrift fuer Krist. Kristallgeometr **122**, 423 (1965).

¹⁷⁶ P. Blum and F. Bertaut, Acta Crystallographica **7**, 81 (1954).

¹⁷⁷ T. Tanaka, S. Okada, Y. Yu, and Y. Ishizawa, Journal of Solid State Chemistry **133**, 122 (1997), ISSN 0022-4596, URL <http://www.sciencedirect.com/science/article/pii/S002245969797328X>.

¹⁷⁸ T. Tanaka, S. Okada, and Y. Ishizawa, Journal of Alloys and Compounds **205**, 281 (1994), ISSN 0925-8388, URL <http://www.sciencedirect.com/science/article/pii/0925838894908028>.

¹⁷⁹ K. Schwetz, P. Ettmayer, R. Kieffer, and A. Lipp, Journal of the Less-Common Metals **26**, 99 (1972).

¹⁸⁰ P. Rogl and P. Potter, Calphad **12**, 191 (1988), ISSN 0364-5916, URL <http://www.sciencedirect.com/science/article/pii/0364591688900211>.

¹⁸¹ S. Okada, K. Hamano, T. Lundstrom, and I. Higashi, AIP Conference Proceedings **231**, 456 (1991), URL <http://link.aip.org/link/?APC/231/456/1>.

¹⁸² L. Andersson and R. Kiessling, Acta Chemica Scandinavica **4**, 160 (1950).

¹⁸³ C. A. Nunes, D. Kaczorowski, P. Rogl, M. R. Baldissera, P. A. Suzuki, G. C. Coelho, A. Grytsiv, G. André, F. Bouréé, and S. Okada, Acta Materialia **53**, 3679 (2005), ISSN 1359-6454, URL <http://www.sciencedirect.com/science/article/pii/S1359645405002454>.

¹⁸⁴ A. M. Zakharov, V. P. Pshokin, and E. I. Ivanova, Russ. Metall. **5**, 192 (1985).

¹⁸⁵ V. V. Brazhkin, A. G. Lyapin, and R. J. Hemley, Philosophical Magazine A, **82**, 231 (2002).

¹⁸⁶ R. Kiessling, Acta Chemica Scandinavica **1**, 893 (1947).

¹⁸⁷ T. Lundstroem and I. Rosenberg, Journal of Solid State Chemistry **6**, 299 (1973).

¹⁸⁸ F. Galasso and J. Pinto, Trans. AIME **242**, 754 (1968).

¹⁸⁹ R. Steinitz, I. Binder, and D. Moskowitz, Transactions of the American Institute of Mining, Metallurgical and Petroleum Engineers **194**, 983 (1952).

¹⁹⁰ H. Haschke, H. Nowotny, and F. Benesovsky, Monatshefte fuer Chemie und verwandte Te **97**, 1459 (1966).

¹⁹¹ E. Rudy, F. Benesovsky, and L. Toth, Zeitschrift fuer Metallkunde **54**, 345 (1963).

¹⁹² W. Trzebiatowski and J. Rudzinski, Journal of the Less-Common Metals **6**, 244 (1964).

¹⁹³ W. Obrowski, Metall **17**, 108 (1963).

¹⁹⁴ M. Frotscher, A. Senyshyn, and B. Albert, Zeitschrift fuer anorganische und allgemeine Chemie **638**, 2078 (2012), ISSN 1521-3749, URL <http://dx.doi.org/10.1002/zaac.201200350>.

¹⁹⁵ B. Aronsson, E. Stenberg, and J. Aselius, Nature **195**, 377 (1962).

¹⁹⁶ B. Aronsson, Acta Chemica Scandinavica **13**, 109 (1959).

¹⁹⁷ J. Aselius, Acta Chemica Scandinavica **14**, 2169 (1960).

¹⁹⁸ B. Aronsson, E. Stenberg, and J. Aselius, Acta Chemica Scandinavica **14**, 733 (1960).

¹⁹⁹ R. W. Mooney and A. J. E. Welch, Acta Crystallographica **7**, 49 (1954), URL <http://dx.doi.org/10.1107/S0365110X54000072>.

²⁰⁰ B. Nolaeng, L. Tergenius, and I. Westman, Journal of the Less-Common Metals **82**, 303 (1981).

²⁰¹ B. Aronsson, J. Aselius, and E. Stenberg, Nature **183**, 1318 (1959).

²⁰² A. Gusev, Physics of the Solid State **53**, 1664 (2011), ISSN 1063-7834, URL <http://dx.doi.org/10.1134/S1063783411080130>.

²⁰³ M. Beck, M. Ellner, and E. J. Mittemeijer, Powder Diffraction **16**, 98 (2001), ISSN 1945-7413, URL http://journals.cambridge.org/article_S0885715600005753.

²⁰⁴ L. Tergenius and T. Lundstroem, Journal of Solid State Chemistry **31**, 361 (1980).

²⁰⁵ E. Stenberg, Acta Chemica Scandinavica **15**, 861 (1961).

²⁰⁶ A. Eliseev, V. Efremov, G. Kuzmicheva, E. Konovalova, V. Lazorenko, Paderno, B. Yu, and S. Khlyustova, Kristallografiya **31**, 803 (1986).

²⁰⁷ K. Kato, I. Kawada, C. Oshima, and S. Kawai, Acta Crystallographica B **30**, 2933 (1974).

²⁰⁸ J. Cannon and P. Farnsworth, Journal of the Less-Common Metals **92**, 359 (1983).

²⁰⁹ F. Glaser, D. Moskowitz, and B. Post, Journal of Metals **5**, 1119 (1953).

²¹⁰ P. Rogl and P. Potter, Calphad **12**, 207 (1988), ISSN 0364-5916, URL <http://www.sciencedirect.com/science/article/pii/0364591688900016>.

²¹¹ H. Bolmgren, T. Lundstroem, L. Tergenius, S. Okada, and I. Higashi, Journal of the Less-Common Metals **161**, 341 (1990).

²¹² V. M. Chad, T. Ramos, E. Coaglia, G. C. Coelho, C. A. Nunes, P. A. Suzuki, F. Ferreira, and P. Rogl, Journal of Phase Equilibria and Diffusion **27**, 452 (2006), ISSN 1547-7037, URL <http://dx.doi.org/10.1007/BF02736442>.

²¹³ M. Xie, R. Mohammadi, Z. Mao, M. M. Armentrout, A. Kavner, R. B. Kaner, and S. H. Tolbert, Phys. Rev. B **85**, 064118 (2012), URL <http://link.aps.org/doi/10.1103/PhysRevB.85.064118>.

²¹⁴ H. Duschanek and P. Rogl, Journal of Phase Equilibria **16**, 150 (1995), ISSN 1054-9714, URL <http://dx.doi.org/10.1007/BF02664852>.

²¹⁵ R. Mohammadi, M. Xie, A. T. Lech, C. L. Turner, A. Kavner, S. H. Tolbert, and R. B. Kaner, Journal of the American Chemical Society **134**, 20660 (2012), <http://pubs.acs.org/doi/pdf/10.1021/ja308219r>, URL <http://pubs.acs.org/doi/abs/10.1021/ja308219r>.

²¹⁶ R. Mohammadi, A. T. Lech, M. Xie, B. E. Weaver, M. T. Yeung, S. H. Tolbert, and R. B. Kaner, Proceedings of the National Academy of Sciences **108**, 10958 (2011), <http://www.pnas.org/content/108/27/10958.full.pdf+html>, URL <http://www.pnas.org/content/108/27/10958.abstract>.

²¹⁷ X. Cheng, W. Zhang, X.-Q. Chen, H. Niu, P. Liu, K. Du, G. Liu, D. Li, H.-M. Cheng, H. Ye, et al., Applied Physics Letters **103**, 171903 (2013), URL <http://scitation.aip.org/content/aip/journal/apl/103/17/10.1063/1.4826485>.

²¹⁸ B. Aronsson, M. Bacmann, and S. Rundqvist, Acta Chemica Scandinavica **14**, 1001 (1960).

²¹⁹ S. la Placa and B. Post, *Acta Crystallographica* **15**, 97 (1962).

²²⁰ E. Zhao, J. Wang, J. Meng, and Z. Wu, *Journal of Computational Chemistry* **31**, 1904 (2010), ISSN 1096-987X, URL <http://dx.doi.org/10.1002/jcc.21477>.

²²¹ E. Zhao, J. Wang, J. Meng, and Z. Wu, *Journal of Solid State Chemistry* **182**, 960 (2009), ISSN 0022-4596, URL <http://www.sciencedirect.com/science/article/pii/S0022459609000358>.

²²² A. Ivanovskii, *Journal of Superhard Materials* **34**, 75 (2012), ISSN 1063-4576, URL <http://dx.doi.org/10.3103/S1063457612020013>.

²²³ G. Soto, M. Moreno-Armenta, and A. Reyes-Serrato, *Computational Materials Science* **44**, 628 (2008), ISSN 0927-0256, URL <http://www.sciencedirect.com/science/article/pii/S0927025608002346>.

²²⁴ H.-H. Chen, Z. Li, Y. Cheng, Y. Bi, and L.-C. Cai, *Physica B: Condensed Matter* **406**, 3338 (2011), ISSN 0921-4526, URL <http://www.sciencedirect.com/science/article/pii/S0921452611005436>.

²²⁵ P. Rogl, H. Nowotny, and F. Benesovsky, *Monatshefte fuer Chemie* **102**, 678 (1971).

²²⁶ B. Aronsson, *Acta Chemica Scandinavica* **17**, 2036 (1963).

²²⁷ Q. Williams and R. Jeanloz, *Phys. Rev. Lett.* **59**, 1132 (1987), URL <http://link.aps.org/doi/10.1103/PhysRevLett.59.1132>.

²²⁸ E. Skelton, S. Qadri, A. Webb, R. Ingalls, and J. Traquada, *Physics Letters A* **94**, 441 (1983), ISSN 0375-9601, URL <http://www.sciencedirect.com/science/article/pii/0375960183908496>.

VII. SUPPLEMENTAL MATERIAL

In support of the main paper this supplementary material contains the following descriptions and datasets:

- A description of the magnetic ordering in elemental ground state structures for selected 3d transition metals;
- A list of compositions searched using the evolutionary algorithm for 0 GPa and 30 GPa (Table IV);
- A description of the high-throughput density functional theory framework in MAISE;
- Full structural information of all the stable structures at 0 GPa (Table V);
- Full structural information of select metastable structures at 0 GPa (Table VI);
- Full structural information of all the stable structures at 30 GPa (Table VII).

TABLE IV: The compositions run with evolutionary search, excluding the Fe-B, Cr-B, and Ca-B systems studied in the author's previous papers⁴⁻⁷

Pressure:	Compositions					
0 GPa:	BeB ₆	Cu ₄ B ₈	Cu ₄ B ₄	La ₈ B ₈	LaB	Mg ₂ B ₁₂
	Mg ₄ B ₂₄	MgB ₆	Mn ₂ B ₄	Mn ₄ B ₁₆	Mn ₂ B ₈	Os ₈ B ₈
	Os ₃ B ₃	Os ₄ B ₄	Pt ₂ B ₂	Pt ₂ B ₄	Pt ₄ B ₄	Pt ₆ B ₆
	Pt ₃ B ₃	Pt ₆ B ₄	Rh ₄ B ₄	W ₂ B ₆	W ₂ B ₈	W ₃ B ₁₂
	W ₄ B ₁₂	W ₂ B ₈	Zn ₄ B ₄	Zn ₄ B ₈	Hf ₈ B ₈	Hf ₄ B ₁₆
	Ir ₃ B ₂	Ir ₆ B ₄	Ir ₉ B ₆	Ir ₁₂ B ₈	K ₄ B ₄	K ₈ B ₈
	K ₁ B ₁	Mo ₄ B ₁₀	Mo ₈ B ₂₀	Mo ₂ B ₅	Mo ₄ B ₁₂	MoB ₃
	Mo ₂ B ₆	Mo ₂ B ₈	Mo ₄ B ₁₆	MoB ₄	Ni ₄ B ₁₂	Ni ₆ B ₁₈
	Ni ₈ B ₂₄	Ni ₂ B ₆	Ni ₈ B ₈			
30 GPa:	Ba ₄ B ₄	Ba ₄ B ₈	Ba ₈ B ₄	Be ₂ B ₆	Be ₃ B ₆	Be ₈ B ₈
	Be ₂ B ₈	Be ₄ B ₈	K ₄ B ₄	K ₂ B ₈	K ₂ B ₁₂	K ₄ B ₁₂
	Li ₆ B ₂	Li ₈ B ₂	Li ₁₆ B ₄	Li ₂ B ₆	Li ₂ B ₈	Li ₄ B ₈
	Li ₈ B ₈	Li ₂ B ₁₂	Li ₄ B ₁₂	Li ₄ B ₁₆	Li ₆ B ₁₆	Li ₂ B ₂
	Li ₃ B ₃	Na ₄ B ₈	Na ₂ B ₆	Na ₂ B ₁₂	Sr ₄ B ₄	Sr ₄ B ₈
	Sr ₂ B ₁₂	Sr ₁₆ B ₄	Y ₂ B ₈	Y ₄ B ₁₆	Y ₂ B ₈	Cs ₄ B ₄
	Cs ₄ B ₈					

The chemical potentials of each metal at the respective pressure are determined for the calculation of the formation enthalpy (Eqn. (1)). For the majority of these metals the lowest energy phase was either bcc, fcc, or hcp. However, the 3d Cr, Mn, Fe, Co, and Ni metals require more detailed calculations to account for the ground state magnetic configurations. Cr is calculated to be antiferromagnetic (AFM) in a two-atom bcc unit cell. Fe is ferromagnetic bcc. Co is ferromagnetic hcp. Ni is ferromagnetic fcc. The known ground state for Mn is a large complex non-collinear distorted bcc structure^{1,2}.

However, due to the size and complexity of α -Mn the energetically preferred structure of the bcc, fcc, and hcp structures was selected. It is known that for GGA this correctly favors an AFM fcc structure, while LDA incorrectly favors AFM hcp^{2,3}. Therefore, in this work we use the antiferromagnetic fcc structure for both GGA and LDA (forced). We have checked that the 215 meV/atom difference for the LDA does not affect the stability of the Mn-rich compounds.

The high-throughput density functional theory framework (implemented under the auspices of MAISE) used

to study the structures for each system performed three geometry optimizations with progressively strict convergent criteria to allow structures determined for other systems to converge to realistic cell parameters and atomic positions. Each optimization converged to a strain below 2-3 kbar (0.2 - 0.3 GPa) with interatomic forces below 0.01 eV/Å. Spot checks were performed to determine that the electronic steps converged appropriately with the convergence criteria changed accordingly (usually increased) to converge the structure.

Pearson Symbol	Chemical Formula	Space Group	a (Å)	b (Å)	c (Å)	pos. lab.	pos. lab.	pos. lab.	Metal		
tP136	Li ₃ B ₁₄	81 (P $\bar{4}$)	10.780		8.980	4h (0.05487, 0.05352, 0.85365) 4h (0.41004, 0.07505, 0.70531) 4h (0.17715, 0.08413, 0.54605) 4h (0.12220, 0.14133, 0.71500) 4h (0.28506, 0.16525, 0.64910) 4h (0.28061, 0.27079, 0.96649) 4h (0.05980, 0.29879, 0.70898) 4h (0.55712, 0.55247, 0.35240) 4h (0.91222, 0.58148, 0.21330) 4h (0.67733, 0.58935, 0.04288) 4h (0.62567, 0.64438, 0.21862) 4h (0.78548, 0.66952, 0.15316) 4h (0.77912, 0.77542, 0.46643) 4h (0.55708, 0.80149, 0.21057) 4h (0.44546, 0.05326, 0.89412) 4h (0.08923, 0.07873, 0.03996) 4h (0.32487, 0.08406, 0.20616) 4h (0.37873, 0.14074, 0.03445) 4h (0.21581, 0.16569, 0.10007) 4h (0.22154, 0.27083, 0.78357) 4h (0.44268, 0.29954, 0.04108) 4h (0.94257, 0.55216, 0.40171) 4h (0.58824, 0.57863, 0.54114) 4h (0.81963, 0.58992, 0.70597) 4h (0.87365, 0.64440, 0.53305) 4h (0.71347, 0.66914, 0.59851) 4h (0.71972, 0.77534, 0.28446) 4h (0.94052, 0.80062, 0.53904)	4h (0.55768, 0.77620, 0.46860) 4h (0.44536, 0.27053, 0.77767) 4h (0.10276, 0.39951, 0.94190) 4h (0.89907, 0.90453, 0.31271) 4h (0.05788, 0.75019, 0.12615) 2f ($\frac{1}{2}$, $\frac{1}{2}$, 0.12734) 2g (0., $\frac{1}{2}$, 0.64786)				
tP16	LiB ₃	127 (P4/mmbm)	5.983		4.163	4e (0., 0., 0.29384) 8i (0.66199, 0.63471, 0.)	4h (0.81839, 0.31839, $\frac{1}{2}$)				
hP15	Li ₈ B ₇	187 (P $\bar{6}$ m2)	3.992		11.048	1a (0., 0., 0.) 2g (0., 0., 0.85707) 2g (0., 0., 0.71417) 2g (0., 0., 0.57139) 2h ($\frac{1}{3}$, $\frac{2}{3}$, 0.87618)	2i ($\frac{2}{3}$, $\frac{1}{3}$, 0.75164) 2h ($\frac{1}{3}$, $\frac{2}{3}$, 0.62613) 1e ($\frac{2}{3}$, $\frac{1}{3}$, 0.) 1f ($\frac{2}{3}$, $\frac{1}{3}$, $\frac{1}{2}$)				
hP110	Be ₂₉ B ₈₁	187 (P $\bar{6}$ m2)	9.779		9.523	6l (0.16494, 0.49394, 0.) 12o (0.34861, 0.99722, 0.09510) 6n (0.44640, 0.55360, 0.15235) 12o (0.19187, 0.00164, 0.18604) 6n (0.39447, 0.60553, 0.30570) 6n (0.22870, 0.77130, 0.40404) 6l (0.83675, 0.50696, 0.) 6n (0.55246, 0.44754, 0.84730) 6n (0.60531, 0.39469, 0.69442) 6n (0.77263, 0.22737, 0.59704) 3k (0.93837, 0.06163, $\frac{1}{2}$) 6n (0.87562, 0.12438, 0.65529)	12o (0.63287, 0.63501, 0.32024) 6n (0.11334, 0.88666, 0.37200) 2g (0., 0., 0.87278) 3k (0.56211, 0.43789, $\frac{1}{2}$) 3j (0.86739, 0.13261, 0.) 3k (0.43664, 0.56336, $\frac{1}{2}$) 6l (0.83675, 0.50696, 0.) 6n (0.55246, 0.44754, 0.84730) 6n (0.60531, 0.39469, 0.69442) 6n (0.77263, 0.22737, 0.59704) 3k (0.93837, 0.06163, $\frac{1}{2}$) 6n (0.87562, 0.12438, 0.65529)				
oS46	Na ₃ B ₂₀	65 (Cmmm)	18.678	5.703	4.141	8o (0.82590, 0., 0.79201) 4l (0., $\frac{1}{2}$, 0.79904) 8q (0.45303, 0.15586, $\frac{1}{2}$) 8q (0.38469, 0.35025, $\frac{1}{2}$) 8q (0.29766, 0.27102, $\frac{1}{2}$) 4h (0.74395, 0., $\frac{1}{2}$)	2a (0., 0., 0.) 4g (0.63624, 0., 0.)				
oI64	MgB ₇	74	5.973	10.466	8.111	16j (0.74666, 0.92214, 0.45526)	4e (0., $\frac{1}{4}$, 0.36429)				

						(Imma)			
						16j (0.15560, 0.43633, 0.16340)	4d		($\frac{1}{4}$, $\frac{1}{4}$, $\frac{3}{4}$)
						8h (0., 0.41770, 0.82366)			
						8h { 0., 0.33383, 0.02439 }			
						8h { 0., 0.35919, 0.61519 }			
oP20	MgB ₄	62 (Pnma)	5.480	4.397	7.434	4c (0.27738, $\frac{1}{4}$, 0.65404)	4c		(0.45260, $\frac{1}{4}$, 0.36237)
						4c (0.44614, $\frac{1}{4}$, 0.85326)			
						8d (0.63231, 0.55805, 0.93663)			
oS12	MgB ₂	63 (Cmcm)	3.075	5.328	7.054	4c (0., 0.16699, $\frac{1}{4}$)	4b		(0., $\frac{1}{2}$, 0.)
						4c (0., 0.83341, $\frac{1}{4}$)			
hP3	AlB ₂	191 (P6/mmm)	3.00932		3.28376	2c ($\frac{1}{3}$, $\frac{2}{3}$, 0.)	2b		(0., 0., $\frac{1}{2}$)
cP7	KB ₆	221 (Pm $\bar{3}$ m)	4.233			6f (0.19918, $\frac{1}{2}$, $\frac{1}{2}$)	1a		(0., 0., 0.)
cP7	CaB ₆	221 (Pm $\bar{3}$ m)	4.148			6f (0.20172, $\frac{1}{2}$, $\frac{1}{2}$)	1a		(0., 0., 0.)
tP20	CaB ₄	127 (P4/mbm)	7.158		4.094	4e (0., 0., 0.79422)	4g		(0.81383, 0.31383, 0.)
						4h (0.58555, 0.08555, $\frac{1}{2}$)			
						8j (0.03599, 0.17531, $\frac{1}{2}$)			
cF52	ScB ₁₂	225 (Fm $\bar{3}$ m)	7.412			48i ($\frac{1}{2}$, 0.16932, 0.16932)	4a		(0., 0., 0.)
hP3	ScB ₂	191 (P6/mmm)	3.145		3.526	2c ($\frac{1}{3}$, $\frac{2}{3}$, 0.)	1b		(0., 0., $\frac{1}{2}$)
hP3	TiB ₂	191 (P6/mmm)	3.033		3.229	2c ($\frac{1}{3}$, $\frac{2}{3}$, 0.)	1b		(0., 0., $\frac{1}{2}$)
oI14	Ti ₃ B ₄	71 (Immm)	13.751	3.041	3.263	4e (0.63171, 0., 0.)	2d		($\frac{1}{2}$, 0., $\frac{1}{2}$)
						4f (0.56439, $\frac{1}{2}$, 0.)	4e		(0.18524, 0., 0.)
oP8	TiB	62 (Pnma)	6.120	3.054	4.568	4c (0.47014, $\frac{1}{4}$, 0.40110)	4c		(0.82256, $\frac{1}{4}$, 0.62209)
hP3	VB ₂	191 (P6/mmm)	2.999		3.028	2c ($\frac{1}{3}$, $\frac{2}{3}$, 0.)	1b		(0., 0., $\frac{1}{2}$)
oS20	V ₂ B ₃	63 (Cmcm)	3.040	18.422	2.982	4c (0., 0.02359, $\frac{1}{4}$)	4c		(0., 0.70500, $\frac{1}{4}$)
						4c (0., 0.11772, $\frac{1}{4}$)	4c		(0., 0.42941, $\frac{1}{4}$)
						4c (0., 0.83123, $\frac{1}{4}$)			
oI14	V ₃ B ₄	71 (Immm)	13.223	2.980	3.042	4e (0.63641, 0., 0.)	2d		($\frac{1}{2}$, 0., $\frac{1}{2}$)
						4f (0.56559, $\frac{1}{2}$, 0.)	4e		(0.18750, 0., 0.)
oS22	V ₅ B ₆	65 (Cmmm)	21.234	2.977	3.047	4h (0.08483, 0., $\frac{1}{2}$)	4g		(0.38337, 0., 0.)
						4g (0.27376, 0., 0.)	4h		(0.19428, 0., $\frac{1}{2}$)
						4h (0.45915, 0., $\frac{1}{2}$)	2a		(0., 0., 0.)
oS8	VB	63 (Cmcm)	3.046	8.046	2.970	4c (0., 0.43777, $\frac{1}{4}$)	4c		(0., 0.14760, $\frac{1}{4}$)
tP10	V ₃ B ₂	127 (P4/mbm)	5.729		3.017	4g (0.88942, 0.38942, 0.)	4h		(0.67844, 0.17844, $\frac{1}{2}$)
						2a (0., 0., 0.)			
oP10	CrB ₄	58 (Pnnm)	4.723	5.474	2.851	4g (0.66432, 0.63297, 0.)	2d		(0., $\frac{1}{2}$, $\frac{1}{2}$)
						4g (0.27601, 0.67926, 0.)			
hP12	CrB ₂	194 (P6 ₃ /mmc)	2.912		12.849	2b (0., 0., $\frac{1}{4}$)	4f		($\frac{1}{3}$, $\frac{2}{3}$, 0.36156)
						2d ($\frac{1}{3}$, $\frac{2}{3}$, $\frac{3}{4}$)			
						4f ($\frac{1}{3}$, $\frac{2}{3}$, 0.52463)			
tI16	CrB	141 (I4 ₁ /amd)	2.921		15.693	8e (0., $\frac{1}{4}$, 0.03238)	8e		(0., $\frac{1}{4}$, 0.57254)
tI32	Cr ₅ B ₃	140 (I4/mcm)	5.440		9.958	4a (0., 0., $\frac{1}{4}$)	4c		(0., 0., 0.)
						8h (0.38218, 0.88218, 0.)	16l		(0.67129, 0.17129, 0.35381)
oF48	Cr ₂ B	70 (Fddd)	4.215	7.351	14.595	16g ($\frac{1}{8}$, $\frac{1}{8}$, 0.75050)	16f		($\frac{1}{8}$, 0.45970, $\frac{1}{8}$)
						16g ($\frac{1}{8}$, $\frac{1}{8}$, 0.04211)			
mP20	MnB ₄	14 (P2 ₁ /c)	5.438	5.357	5.473	4e (0.16273, 0.63036, 0.34239)	4e		(0.72927, 0.99954, 0.72270)
						4e (0.87070, 0.68051, 0.62500)			
						4e (0.67084, 0.86971, 0.32427)			
						4e (0.63568, 0.18621, 0.36151)			
oP8	MnB	62 (Pnma)	5.449	2.983	4.121	4c (0.46658, $\frac{1}{4}$, 0.88502)	4c		(0.82461, $\frac{1}{4}$, 0.12317)
oF48	Mn ₂ B	70 (Fddd)	7.151	4.136	14.283	16g ($\frac{1}{8}$, $\frac{1}{8}$, 0.24892)	16e		(0.29681, $\frac{1}{8}$, $\frac{1}{8}$)
						16g ($\frac{1}{8}$, $\frac{1}{8}$, 0.54416)			
oP12	FeB ₂	62 (Pnma)	4.816	4.807	3.740	8d (0.66112, 0.56930, 0.89297)	4c		(0.48015, $\frac{1}{4}$, 0.62385)
tI16	FeB	141 (I4 ₁ /amd)	2.931		14.971	8e (0., $\frac{1}{4}$, 0.53487)	8e		(0., $\frac{1}{4}$, 0.07090)
tI12	Fe ₂ B	140 (I4/mcm)	5.056		4.237	4a (0., 0., $\frac{1}{4}$)	8h		(0.66649, 0.16649, 0.)

oP8	CoB	62 (Pnma)	5.164	3.066	3.924	4c	(0.46821, $\frac{1}{4}$, 0.87600)	4c	(0.82341, $\frac{1}{4}$, 0.12774)
oP28	Ni ₄ B ₃	62 (Pnma)	11.942	2.996	6.569	4c	(0.47510, $\frac{1}{4}$, 0.93807)	4c	(0.14876, $\frac{1}{4}$, 0.49308)
						4c	(0.03882, $\frac{1}{4}$, 0.97822)	4c	(0.44998, $\frac{1}{4}$, 0.25081)
						4c	(0.25718, $\frac{1}{4}$, 0.18427)	4c	(0.70024, $\frac{1}{4}$, 0.61860)
						4c	(0.87656, $\frac{1}{4}$, 0.83032)		
tI12	Ni ₂ B	140 (I4/mcm)	4.968		4.257	4a	(0., 0., $\frac{1}{4}$)	8h	(0.66956, 0.16956, 0.)
mS28	Ni ₅ B ₂	15 (C2/c)	11.315	4.505	5.147	8f	(0.11190, 0.29730, 0.08042)	8f	(0.09305, 0.11017, 0.42616)
						8f	(0.71810, 0.08044, 0.31414)		
						4e	(0., 0.58393, $\frac{1}{4}$)		
oP16	Ni ₃ B	62 (Pnma)	5.178	6.624	4.384	4c	(0.88201, $\frac{1}{4}$, 0.93916)	4c	(0.52830, $\frac{1}{4}$, 0.13295)
cP7	SrB ₆	221 (Pm $\bar{3}$ m)	4.2001			8d	(0.17983, 0.43734, 0.84386)	1b	($\frac{1}{2}$, $\frac{1}{2}$, $\frac{1}{2}$)
cF52	YB ₁₂	225 (Fm $\bar{3}$ m)	7.501			6e	(0.29681, 0., 0.)		
tP20	YB ₄	127 (P4/mbm)	7.112		4.028	48i	($\frac{1}{2}$, 0.16889, 0.16889)	4a	(0., 0., 0.)
						4e	(0., 0., 0.20309)	4g	(0.31798, 0.81798, 0.)
						4h	(0.08701, 0.58701, $\frac{1}{2}$)		
						8j	(0.53854, 0.67601, $\frac{1}{2}$)		
hP3	VB ₂	191 (P6/mmm)	3.300		3.866	2c	($\frac{1}{3}$, $\frac{2}{3}$, 0.)	1b	(0., 0., $\frac{1}{2}$)
oS6	ZrB ₂	65 (Cmmm)	3.177	5.502	3.554	4i	(0., 0.83330, 0.)	2c	($\frac{1}{2}$, 0., $\frac{1}{2}$)
hP3	NbB ₂	191 (P6/mmm)	3.117		3.345	2c	($\frac{1}{3}$, $\frac{2}{3}$, 0.)	1b	(0., 0., $\frac{1}{2}$)
oS20	Nb ₂ B ₃	63 (Cmcm)	3.326	19.599	3.140	4c	(0., 0.02291, $\frac{1}{4}$)	4c	(0., 0.70248, $\frac{1}{4}$)
						4c	(0., 0.11573, $\frac{1}{4}$)	4c	(0., 0.43103, $\frac{1}{4}$)
						4c	(0., 0.83493, $\frac{1}{4}$)		
oI14	Nb ₃ B ₄	71 (Immm)	14.175	3.154	3.321	4e	(0.63202, 0., 0.)	2d	($\frac{1}{2}$, 0., $\frac{1}{2}$)
						4f	(0.56424, $\frac{1}{2}$, 0.)	4e	(0.18499, 0., 0.)
oS22	Nb ₅ B ₆	65 (Cmmmm)	22.912	3.168	3.322	4h	(0.08157, 0., $\frac{1}{2}$)	4g	(0.38573, 0., 0.)
						4g	(0.27244, 0., 0.)	4h	(0.19433, 0., $\frac{1}{2}$)
						4h	(0.46035, 0., $\frac{1}{2}$)	2a	(0., 0., 0.)
oS8	NbB	63 (Cmcm)	3.313	8.788	3.179	4c	(0., 0.44213, $\frac{1}{4}$)	4c	(0., 0.14531, $\frac{1}{4}$)
tP10	Nb ₃ B ₂	127 (P4/mbm)	6.234		3.314	4g	(0.89474, 0.39474, 0.)	4h	(0.67820, 0.17820, $\frac{1}{2}$)
						2a	(0., 0., 0.)		
hR18	MoB ₂	166 (R $\bar{3}$ m)	3.023		21.006	6c	(0., 0., 0.33221)	6c	(0., 0., 0.07586)
						6c	(0., 0., 0.18152)		
tI16	MoB	141 (I4 ₁ /amd)	3.130		17.073	8e	(0., $\frac{1}{4}$, 0.53015)	8e	(0., $\frac{1}{4}$, 0.07187)
hP6	TcB ₂	194 (P6 ₃ /mmc)	2.904		7.472	4f	($\frac{1}{3}$, $\frac{2}{3}$, 0.95248)	2c	($\frac{1}{3}$, $\frac{2}{3}$, $\frac{1}{4}$)
hP20	Tc ₇ B ₃	186 (P6 ₃ mc)	7.516		4.870	6c	(0.18940, 0.81060, 0.65993)	2b	($\frac{1}{3}$, $\frac{2}{3}$, 0.41718)
						6c	(0.87634, 0.12366, 0.74591)		
						6c	(0.54568, 0.45432, 0.45110)		
oS16	Tc ₃ B	63 (Cmcm)	2.918	9.284	7.269	4c	(0., 0.74349, $\frac{1}{4}$)	4c	(0., 0.42423, $\frac{1}{4}$)
						8f	(0., 0.86531, 0.56189)		
oP6	RuB ₂	59 (Pmmn)	4.663	2.882	4.059	4f	(0.55440, $\frac{1}{4}$, 0.63645)	2b	($\frac{1}{4}$, $\frac{3}{4}$, 0.84798)
hP10	Ru ₂ B ₃	194 (P6 ₃ /mmc)	2.923		12.846	4f	($\frac{1}{3}$, $\frac{2}{3}$, 0.53040)	4f	($\frac{1}{3}$, $\frac{2}{3}$, 0.36003)
						2d	($\frac{1}{3}$, $\frac{2}{3}$, $\frac{3}{4}$)		
hP2	RuB	187 (P $\bar{6}$ m2)	2.875		2.864	1f	($\frac{2}{3}$, $\frac{1}{3}$, $\frac{1}{2}$)	1a	(0., 0., 0.)
oS8	RhB	63 (Cmcm)	3.387	5.868	4.163	4a	(0., 0., 0.)	4c	(0., 0.66677, $\frac{1}{4}$)
hP18	Rh ₅ B ₄	194 (P6 ₃ /mmc)	3.336		20.615	4f	($\frac{1}{3}$, $\frac{2}{3}$, 0.91366)	2c	($\frac{1}{3}$, $\frac{2}{3}$, $\frac{1}{4}$)
						4f	($\frac{1}{3}$, $\frac{2}{3}$, 0.80353)	4f	($\frac{1}{3}$, $\frac{2}{3}$, 0.45243)
						4e	(0., 0., 0.35231)		
hP20	Rh ₇ B ₃	186 (P6 ₃ mc)	7.533		4.863	6c	(0.18879, 0.81121, 0.66655)	2b	($\frac{1}{3}$, $\frac{2}{3}$, 0.42478)
						6c	(0.87693, 0.12307, 0.77225)		
						6c	(0.54402, 0.45598, 0.41560)		
oP6	Pd ₂ B	58 (Pnnm)	4.786	5.161	3.161	2b	(0., 0., $\frac{1}{2}$)	4g	(0.24622, 0.15542, 0.)
oP16	Pd ₃ B	62 (Pnma)	5.536	7.714	4.907	4c	(0.38819, $\frac{1}{4}$, 0.93410)	4c	(0.03970, $\frac{1}{4}$, 0.15903)
						8d	(0.67910, 0.42782, 0.82479)		

cP7	BaB ₆	221 (Pm $\bar{3}$ m)	4.280	6f	(0.20536, $\frac{1}{2}$, $\frac{1}{2}$)	1a	(0., 0., 0.)		
cP7	LaB ₆	221 (Pm $\bar{3}$ m)	4.154	6f	(0.19971, $\frac{1}{2}$, $\frac{1}{2}$)	1a	(0., 0., 0.)		
tP20	LaB ₄	127 (P4/mbm)	7.311	4.183	4e 4h 8j	(0., 0., 0.79404) (0.58848, 0.08848, $\frac{1}{2}$) (0.03892, 0.17350, $\frac{1}{2}$)	4g	(0.81625, 0.31625, 0.)	
hP3	HfB ₂	191 (P6/mmm)	3.144	3.490	2c	($\frac{1}{3}$, $\frac{2}{3}$, 0.)	1b	(0., 0., $\frac{1}{2}$)	
hP12	TaB ₂	194 (P6 ₃ /mmc)	3.053	14.649	2b 2d 4f	(0., 0., $\frac{1}{4}$) ($\frac{1}{3}$, $\frac{2}{3}$, $\frac{3}{4}$) ($\frac{1}{3}$, $\frac{2}{3}$, 0.51994)	4f	($\frac{1}{3}$, $\frac{2}{3}$, 0.36514)	
oS20	Ta ₂ B ₃	63 (Cmcm)	3.313	19.479	3.127	4c 4c 4c	(0., 0.02285, $\frac{1}{4}$) (0., 0.11570, $\frac{1}{4}$) (0., 0.83402, $\frac{1}{4}$)	4c	(0., 0.70253, $\frac{1}{4}$) 4c (0., 0.43104, $\frac{1}{4}$)
oI14	Ta ₃ B ₄	71 (Immm)	14.094	3.142	3.307	4e 4f	(0.63306, 0., 0.) (0.56413, $\frac{1}{2}$, 0.)	2d	($\frac{1}{2}$, 0., $\frac{1}{2}$) 4e (0.18513, 0., 0.)
oS22	Ta ₅ B ₆	65 (Cmmm)	22.767	3.156	3.306	4h 4g 4h	(0.08228, 0., $\frac{1}{2}$) (0.27313, 0., 0.) (0.46041, 0., $\frac{1}{2}$)	4g	(0.38563, 0., 0.) 4h (0.19434, 0., $\frac{1}{2}$) (0., 0., 0.)
oS8	TaB	63 (Cmcm)	3.295	8.733	3.169	4c	(0., 0.44052, $\frac{1}{4}$)	4c	(0., 0.14541, $\frac{1}{4}$)
tP10	Ta ₃ B ₂	127 (P4/mbm)	6.212	3.305	4g 2a	(0.39195, 0.89195, 0.) (0., 0., 0.)	4h	(0.17700, 0.67700, $\frac{1}{2}$)	
hR24	WB ₃	166 (R $\bar{3}$ m)	5.219	9.441	18f	(0.66499, 0., 0.)	6c	(0., 0., 0.83364)	
hP6	WB ₂	194 (P6 ₃ /mmc)	2.935	7.767	4f	($\frac{1}{3}$, $\frac{2}{3}$, 0.95946)	2c	($\frac{1}{3}$, $\frac{2}{3}$, $\frac{1}{4}$)	
tI16	WB	141 (I4 ₁ /amd)	3.146	17.039	8e	(0., $\frac{1}{4}$, 0.53107)	8e	(0., $\frac{1}{4}$, 0.07188)	
tI12	W ₂ B	140 (I4/mcm)	5.589	4.799	4a	(0., 0., $\frac{1}{4}$)	8h	(0.66993, 0.16993, 0.)	
hP6	ReB ₂	194 (P6 ₃ /mmc)	2.918	7.504	4f	($\frac{1}{3}$, $\frac{2}{3}$, 0.95236)	2c	($\frac{1}{3}$, $\frac{2}{3}$, $\frac{1}{4}$)	
oS16	Re ₃ B	63 (Cmcm)	2.909	9.410	7.373	4c 8f	(0., 0.74478, $\frac{1}{4}$) (0., 0.86697, 0.56560)	4c	(0., 0.42347, $\frac{1}{4}$)
oP6	OsB ₂	59 (Pmmn)	4.7035	2.8912	4.0916	4f	(0.05555, $\frac{1}{4}$, 0.63803)	2a	($\frac{1}{4}$, $\frac{1}{4}$, 0.15517)
hP10	Os ₂ B ₃	194 (P6 ₃ /mmc)	2.943	12.933	4f 2c	($\frac{1}{3}$, $\frac{2}{3}$, 0.03074) ($\frac{1}{3}$, $\frac{2}{3}$, $\frac{1}{4}$)	4f	($\frac{1}{3}$, $\frac{2}{3}$, 0.86015)	
hP2	OsB	187 (P $\bar{6}$ m2)	2.900	2.881	1f	($\frac{2}{3}$, $\frac{1}{3}$, $\frac{1}{2}$)	1a	(0., 0., 0.)	
hP4	IrB	194 (P6 ₃ /mmc)	3.502	3.999	2a	(0., 0., 0.)	2c	($\frac{1}{3}$, $\frac{2}{3}$, $\frac{1}{4}$)	
hP15	Ir ₂ B ₀	187 (P $\bar{6}$ m2)	5.921	5.557	1b 3j 3k	(0., 0., $\frac{1}{2}$) (0.49831, 0.50169, 0.) (0.49530, 0.50470, $\frac{1}{2}$)	6n 2i	(0.16475, 0.83525, 0.24864) ($\frac{2}{3}$, $\frac{1}{3}$, 0.25049)	
oP6	Pt ₂ B	58 (Pnnm)	4.328	5.619	3.292	2b	(0., 0., $\frac{1}{2}$)	4g	(0.25201, 0.16264, 0.)

TABLE V: The lattice parameters and Wyckoff positions of the stable structures at P=0 GPa.

Pearson Symbol	Chemical Formula	Space Group	a (Å)	b (Å)	c (Å)	pos. lab.	B	pos. lab.	Metal
oS12	BeB ₂	63 (Cmcm)	2.970	6.042	5.132	8f	(0., 0.272140, 0.910730)	4c	(0., 0.411560, 0.250000)
hP8	ScB	194 (P6 ₃ /mmc)	3.167	12.725	2b 2d	(0., 0., 0.250000) ($\frac{1}{3}$, $\frac{2}{3}$, $\frac{3}{4}$)	4f	($\frac{1}{3}$, $\frac{2}{3}$, 0.385770)	
oS8	CrB	63 (Cmcm)	2.928	7.847	2.916	4c	(0., 0.435490, 0.250000)	4c	(0., 0.145520, 0.250000)
oP16	Fe ₃ B	62 (Pnma)	5.399	6.657	4.380	4c 4c	(0.618100, 0.250000, 0.074840) (0.979660, 0.250000, 0.880390)	8d	(0.824530, 0.444380, 0.351230)
tI32	Fe ₃ B	82 (I4)	8.551	4.239	8g 8g 8g	(0.792340, 0.475280, 0.488150) (0.100750, 0.087150, 0.252190) (0.288140, 0.311670, 0.264780)	8g 8g 8g	(0.641010, 0.013140, 0.490330)	

tP32	Fe ₃ B	86 (P4 ₂ /n)	8.545	4.278	8g (0.704640, 0.544420, 0.976270) 8g (0.112430, 0.285350, 0.979410) 8g (0.532560, 0.422730, 0.235290)	8g (0.166130, 0.641380, 0.775610)	
oP72	Fe ₂ B ₇ ⁸	55 (Pbam)	16.922	10.628	2.882	4g (0.131780, 0.053050, 0.) 4g (0.047780, 0.961790, 0.) 4g (0.197400, 0.391880, 0.) 4g (0.140570, 0.875720, 0.) 4h (0.054970, 0.401220, $\frac{1}{2}$) 4g (0.200810, 0.544590, 0.) 4h (0.289620, 0.787680, $\frac{1}{2}$) 4g (0.035120, 0.805880, 0.) 4g (0.100980, 0.475190, 0.) 4h (0.054020, 0.558100, $\frac{1}{2}$) 4h (0.979980, 0.287880, $\frac{1}{2}$) 4h (0.160970, 0.138830, $\frac{1}{2}$) 4h (0.280590, 0.144310, $\frac{1}{2}$) 4h (0.179790, 0.792270, $\frac{1}{2}$)	4h (0.466690, 0.608390, $\frac{1}{2}$) 4g (0.385510, 0.765770, 0.) 4h (0.221240, 0.968470, $\frac{1}{2}$) 4g (0.121620, 0.679480, 0.)
oS8	Ni ₁ B ₁	63 (Cmcm)	2.943	7.359	2.982	4c (0., 0.433240, 0.250000)	4c (0., 0.147010, 0.250000)
hR24	Mo ₁ B ₃	166 (R $\bar{3}$ m)	5.226		9.396	18f (0.665110, 0., 0.)	6c (0., 0., 0.834890)
hP15	Rh ₈ B ₇	164 (P3m1)	6.537		4.403	1b (0., 0., $\frac{1}{2}$) 3e ($\frac{1}{2}$, 0., 0.) 3f ($\frac{1}{2}$, 0., $\frac{1}{2}$) 2c ($\frac{1}{3}$, $\frac{2}{3}$, 0.)	6i (0.833660, 0.166340, 0.259540) 2d ($\frac{1}{3}$, $\frac{2}{3}$, 0.238790)
hP3	Ta ₁ B ₂	191 (P6/mmm)	3.100		3.334	2c (0., 0., 0.)	1b (0., 0., $\frac{1}{2}$)
hR18	Ta ₁ B ₂	166 (R $\bar{3}$ m)	3.055		21.952	6c (0., 0., 0.334150) 6c (0., 0., 0.179980)	6c (0., 0., 0.076630)
hP16	W ₁ B ₃	194 (P6 ₃ /mmc)	5.205		6.338	12i (0.334750, 0., 0.) 2b (0., 0., 0.250000)	2c ($\frac{1}{3}$, $\frac{2}{3}$, 0.250000)
hP6	Re ₁ B ₁	156 (P3m1)	2.891		8.875	1c ($\frac{2}{3}$, $\frac{1}{3}$, 0.361400) 1b ($\frac{1}{3}$, $\frac{2}{3}$, 0.780120) 1b ($\frac{1}{3}$, $\frac{2}{3}$, 0.440730)	1c ($\frac{2}{3}$, $\frac{1}{3}$, 0.612410) 1c ($\frac{2}{3}$, $\frac{1}{3}$, 0.944000) 1b ($\frac{1}{3}$, $\frac{2}{3}$, 0.189480)
hP6	Ir ₂ B ₁	194 (P6 ₃ /mmc)	2.794		10.737	2c ($\frac{1}{3}$, $\frac{2}{3}$, 0.250000)	4f ($\frac{1}{3}$, $\frac{2}{3}$, 0.887880)
hP4	Pt ₁ B ₁	164 (P3m1)	3.107		5.657	2d ($\frac{1}{3}$, $\frac{2}{3}$, 0.913380)	2d ($\frac{1}{3}$, $\frac{2}{3}$, 0.292770)

TABLE VI: The lattice parameters and Wyckoff positions of select metastable structures at P=0 GPa. The oP72-Fe₂B₇ (SG#55) structure is attributed to Bykova and co-authors based on unpublished single crystal X-ray diffraction data⁸.

Pearson Symbol	Chemical Formula	Space Group	a (Å)	b (Å)	c (Å)	pos. lab.	B		pos. lab	Metal
oS28	LiB ₆	65 (Cmmm)	8.724	4.584	4.573	8q (0.16357, 0.18197, $\frac{1}{2}$) 8n (0., 0.68996, 0.68502) 8o (0.09900, 0., 0.18894)		4g	(0.66518, 0., 0.)	
tP136	Li ₃ B ₁₄	81 (P $\bar{4}$)	10.301		8.603	4h { 0.05566, 0.05376, 0.85206 } 4h { 0.41115, 0.07620, 0.70386 } 4h { 0.17755, 0.08077, 0.54643 } 4h { 0.12443, 0.13992, 0.71629 } 4h { 0.28709, 0.16491, 0.64877 } 4h { 0.27973, 0.27031, 0.96543 } 4h { 0.06127, 0.29829, 0.71006 } 4h { 0.55832, 0.55292, 0.35057 } 4h { 0.91216, 0.58164, 0.21450 } 4h { 0.67803, 0.58748, 0.04176 } 4h { 0.62706, 0.64454, 0.21865 } 4h { 0.78799, 0.67047, 0.15200 } 4h { 0.77810, 0.77654, 0.46589 } 4h { 0.55756, 0.80236, 0.21082 } 4h { 0.44485, 0.05394, 0.89437 } 4h { 0.08858, 0.07930, 0.04004 } 4h { 0.32479, 0.08068, 0.20588 } 4h { 0.37681, 0.13932, 0.03289 } 4h { 0.21362, 0.16542, 0.10048 } 4h { 0.22258, 0.27010, 0.78474 }	4h { 0.55771, 0.77881, 0.47033 } 4h { 0.44509, 0.27345, 0.77570 } 4h { 0.10127, 0.40024, 0.94055 } 4h { 0.89937, 0.90599, 0.31430 } 4h { 0.03607, 0.75005, 0.12755 } 2f ($\frac{1}{2}$, $\frac{1}{2}$, 0.12472) 2g (0., $\frac{1}{2}$, 0.64999)			

cF52	ScB ₁₂	225 (Fm $\bar{3}$ m)	7.138	48i	($\frac{1}{2}$, 0.16953, 0.16953)	4a	(0., 0., 0.)
hP3	ScB ₂	191 (P6/mmm)	3.030	3.356 2c	($\frac{1}{3}$, $\frac{2}{3}$, 0.)	1b	(0., 0., $\frac{1}{2}$)
hP3	TiB ₂	191 (P6/mmm)	2.948	3.097 2d	($\frac{1}{3}$, $\frac{2}{3}$, $\frac{1}{2}$)	1a	(0., 0., 0.)
oI14	Ti ₃ B ₄	71 (Immm)	13.285 2.944	3.132 4e	(0.63269, 0., 0.)	2d	($\frac{1}{2}$, 0., $\frac{1}{2}$)
oP8	TiB	62 (Pnma)	5.884 2.948	4.387 4c	(0.56455, $\frac{1}{2}$, 0.) (0.46904, $\frac{1}{4}$, 0.39777)	4e 4c	(0.18662, 0., 0.) (0.82377, $\frac{1}{4}$, 0.61949)
hP3	VB ₂	191 (P6/mmm)	2.923	2.916 2c	($\frac{1}{3}$, $\frac{2}{3}$, 0.)	1b	(0., 0., $\frac{1}{2}$)
oS20	V ₂ B ₃	63 (Cmcm)	2.932 17.936	2.903 4c	(0., 0.02365, $\frac{1}{4}$) (0., 0.11775, $\frac{1}{4}$) (0., 0.83093, $\frac{1}{4}$)	4c 4c	(0., 0.70552, $\frac{1}{4}$) (0., 0.42933, $\frac{1}{4}$)
oI14	V ₃ B ₄	71 (Immm)	12.867 2.899	2.935 4e	(0.63678, 0., 0.)	2d	($\frac{1}{2}$, 0., $\frac{1}{2}$)
oS22	V ₅ B ₆	65 (Cmmm)	20.655 2.895	2.942 4h	(0.56553, $\frac{1}{2}$, 0.) (0.08511, 0., $\frac{1}{2}$) (0.27397, 0., 0.) (0.45917, 0., $\frac{1}{2}$)	4e 4g 4h 2a	(0.18826, 0., 0.) (0.38284, 0., 0.) (0.19396, 0., $\frac{1}{2}$) (0., 0., 0.)
oS8	VB	63 (Cmcm)	2.945 7.817	2.885 4c	(0., 0.43705, $\frac{1}{4}$)	4c	(0., 0.14855, $\frac{1}{4}$)
tP10	V ₃ B ₂	127 (P4/mbm)	5.557	2.912 4g	(0.38896, 0.88896, 0.)	4h	(0.17898, 0.67898, $\frac{1}{2}$)
oP10	CrB ₄	58 (Pnmm)	4.571 5.359	2.740 4g	(0.65793, 0.37268, 0.)	2d	(0., $\frac{1}{2}$, $\frac{1}{2}$)
hP12	CrB ₂	194 (P6 ₃ /mmc)	2.823	12.510 2b	(0., 0., $\frac{1}{4}$)	4f	($\frac{1}{3}$, $\frac{2}{3}$, 0.36182)
oI14	Cr ₃ B ₄	71 (Immm)	12.708 2.867	2.824 4e	(0.63992, 0., 0.)	2d	($\frac{1}{2}$, 0., $\frac{1}{2}$)
tI16	CrB	141 (I4 ₁ /amd)	2.838	15.289 8e	(0.56636, $\frac{1}{2}$, 0.) (0., $\frac{1}{4}$, 0.03272)	4e 8e	(0.18718, 0., 0.) (0., $\frac{1}{4}$, 0.57318)
oS48	Cr ₂ B	70 (Fddd)	4.096 7.145	14.193 16g	($\frac{1}{8}$, $\frac{1}{8}$, 0.25029) ($\frac{1}{8}$, $\frac{1}{8}$, 0.54280)	16f	($\frac{1}{8}$, 0.95872, $\frac{1}{8}$)
mP20	MnB ₄	14 (P2 ₁ /c)	5.241 5.248	5.280 4e	(0.16458, 0.62644, 0.34251) (0.87374, 0.68336, 0.62035) (0.67318, 0.87393, 0.31983) (0.63491, 0.18817, 0.36114)	4e	(0.73044, 0.99896, 0.72303)
oP8	MnB	62 (Pnma)	5.250 2.903	3.993 4c	(0.46516, $\frac{1}{4}$, 0.88280)	4c	(0.82442, $\frac{1}{4}$, 0.12220)
oS48	Mn ₂ B	70 (Fddd)	7.151 4.136	14.283 16g	($\frac{1}{8}$, $\frac{1}{8}$, 0.24892) ($\frac{1}{8}$, $\frac{1}{8}$, 0.54416)	16e	(0.29681, $\frac{1}{8}$, $\frac{1}{8}$)
oP12	FeB ₂	62 (Pnma)	4.684 4.700	3.625 8d	(0.1632, 0.56851, 0.89135)	4c	(0.9774, $\frac{1}{4}$, 0.62248)
oP8	FeB	62 (Pnma)	5.216 2.877	3.899 4c	(0.9650, $\frac{1}{4}$, 0.87906)	4c	(0.32297, $\frac{1}{4}$, 0.12118)
tI12	Fe ₂ B	140 (I4/mcm)	4.896	4.056 4a	(0., 0., $\frac{1}{4}$)	8h	(0.66404, 0.16404, 0.)
oP8	CoB	62 (Pnma)	4.989 2.989	3.833 4c	(0.46689, $\frac{1}{4}$, 0.37365)	4c	(0.82415, $\frac{1}{4}$, 0.62817)
oS8	NiB	63 (Cmcm)	2.823 7.191	2.894 4c	(0., 0.43166, $\frac{1}{4}$)	4c	(0., 0.14782, $\frac{1}{4}$)
oP28	Ni ₄ B ₃	62 (Pnma)	11.576 2.905	6.366 4c	(0.52567, $\frac{1}{4}$, 0.06472) (0.96024, $\frac{1}{4}$, 0.02179) (0.74235, $\frac{1}{4}$, 0.81870) (0.12396, $\frac{1}{4}$, 0.16742)	4c 4c 4c 4c	(0.85067, $\frac{1}{4}$, 0.50976) (0.55069, $\frac{1}{4}$, 0.75038) (0.2996, $\frac{1}{4}$, 0.37976)
tI12	Ni ₂ B	140 (I4/mcm)	4.828	4.099 4a	(0., 0., $\frac{1}{4}$)	8h	(0.66746, 0.16746, 0.)
oP16	Ni ₃ B	62 (Pnma)	5.004 6.398	4.242 4c	(0.1164, $\frac{1}{4}$, 0.06145)	4c	(0.4743, $\frac{1}{4}$, 0.87095)
oS46	Rb ₃ B ₂₀	65 (Cmmm)	17.931 5.619	4.099 8d	(0.18205, 0.93973, 0.84502)	2a	(0., 0., 0.)
				8o	(0.82549, 0., 0.79073)	4g	(0.6488, 0., 0.)
				4l	(0., $\frac{1}{2}$, 0.79835)		
				8q	(0.45245, 0.15327, $\frac{1}{2}$)		
				8q	(0.38545, 0.35285, $\frac{1}{2}$)		
				8q	(0.29731, 0.27428, $\frac{1}{2}$)		

mS24	RbB ₂	12 (C2/m)	10.780	4.388	6.322	4h 8j 4i 4i 4i	(0.74303, 0., $\frac{1}{2}$) (0.67266, 0.31122, 0.50199) (0.26803, 0., 0.64400) (0.42413, 0., 0.49359) (0., 0.4998, $\frac{1}{4}$)	4i 4i 4i 4c	(0.95429, 0., 0.79234) (0.6561, 0., 0.90384) (0., 0.16665, $\frac{1}{4}$)
oS8	RbB	63 (Cmcm)	4.833	8.381	3.035	4c	(0.20045, $\frac{1}{2}$, $\frac{1}{2}$)	4c	(0., 0., 0.)
cP7	SrB ₆	221 (Pm $\bar{3}$ m)	3.990			6f	(0.20045, $\frac{1}{2}$, $\frac{1}{2}$)	1a	(0., 0., 0.)
tP20	SrB ₄	127 (P4/mbm)	6.950		4.004	4e 4h 8j	(0., 0., 0.79345) (0.58572, 0.08572, $\frac{1}{2}$) (0.03738, 0.17523, $\frac{1}{2}$)	4g	(0.8143, 0.3143, 0.)
oI12	SrB ₂	71 (Immm)	8.158	4.202	4.021	4g 4j	(0., 0.19428, 0.) ($\frac{1}{2}$, 0., 0.21526)	4f	(0.3106, $\frac{1}{2}$, 0.)
mS16	SrB	15 (C2/c)	8.107	4.740	5.859	8f	(0.51595, 0.09552, 0.10967)	8f	(0.83238, 0.10515, 0.27992)
cF52	YB ₁₂	225 (Fm $\bar{3}$ m)	7.224			48i	($\frac{1}{2}$, 0.16911, 0.16911)	4a	(0., 0., 0.)
tP20	YB ₄	127 (P4/mbm)	6.818		3.839	4e 4h 8j	(0., 0., 0.79718) (0.58638, 0.08638, $\frac{1}{2}$) (0.03979, 0.17768, $\frac{1}{2}$)	4g	(0.81743, 0.31743, 0.)
hP3	YB ₂	191 (P6/mmm)	3.145		3.699	2c	($\frac{1}{3}$, $\frac{2}{3}$, 0.)	1b	(0., 0., $\frac{1}{2}$)
hP3	ZrB ₂	191 (P6/mmm)	3.075		3.422	2c	($\frac{1}{3}$, $\frac{2}{3}$, 0.)	1b	(0., 0., $\frac{1}{2}$)
hP3	NbB ₂	191 (P6/mmm)	3.035		3.232	2c	($\frac{1}{3}$, $\frac{2}{3}$, 0.)	1b	(0., 0., $\frac{1}{2}$)
oS20	Nb ₂ B ₃	63 (Cmcm)	3.219	19.032	3.055	4c 4c 4c	(0., 0.02298, $\frac{1}{4}$) (0., 0.11574, $\frac{1}{4}$) (0., 0.83478, $\frac{1}{4}$)	4c 4c	(0., 0.70304, $\frac{1}{4}$) (0., 0.43101, $\frac{1}{4}$)
oI14	Nb ₃ B ₄	71 (Immm)	13.768	3.066	3.212	4e 4f	(0.63233, 0., 0.) (0.56425, $\frac{1}{2}$, 0.)	2d 4e	($\frac{1}{2}$, 0., $\frac{1}{2}$) (0.18567, 0., 0.)
oS22	Nb ₅ B ₆	65 (Cmmm)	22.233	3.076	3.216	4h 4g 4h	(0.08185, 0., $\frac{1}{2}$) (0.27264, 0., 0.) (0.46029, 0., $\frac{1}{2}$)	4g 4h 2a	(0.38525, 0., 0.) (0.19404, 0., $\frac{1}{2}$) (0., 0., 0.)
oS8	NbB	63 (Cmcm)	3.208	8.514	3.086	4c	(0., 0.44142, $\frac{1}{4}$)	4c	(0., 0.14631, $\frac{1}{4}$)
tP10	Nb ₃ B ₂	127 (P4/mbm)	6.032		3.197	4g 2a	(0.39445, 0.89445, 0.) (0., 0., 0.)	4h	(0.17902, 0.67902, $\frac{1}{2}$)
hP10	MoB ₄	194 (P6 ₃ /mmc)	2.849		10.781	4f 4f	($\frac{1}{3}$, $\frac{2}{3}$, 0.45584) ($\frac{1}{3}$, $\frac{2}{3}$, 0.61114)	2c	($\frac{1}{3}$, $\frac{2}{3}$, $\frac{1}{4}$)
hR18	MoB ₂	166 (R $\bar{3}$ m)	2.932		20.524	6c 6c	(0., 0., 0.33211) (0., 0., 0.18179)	6c	(0., 0., 0.07603)
tI16	MoB	141 (I4 ₁ /amd)	3.048		16.618	8e	(0., $\frac{1}{4}$, 0.53042)	8e	(0., $\frac{1}{4}$, 0.07234)
hP10	TcB ₄	194 (P6 ₃ /mmc)	2.830		10.587	4f 4f	($\frac{1}{3}$, $\frac{2}{3}$, 0.45821) ($\frac{1}{3}$, $\frac{2}{3}$, 0.61497)	2c	($\frac{1}{3}$, $\frac{2}{3}$, $\frac{1}{4}$)
hP6	TcB ₂	194 (P6 ₃ /mmc)	2.814		7.323	4f	($\frac{1}{3}$, $\frac{2}{3}$, 0.95234)	2c	($\frac{1}{3}$, $\frac{2}{3}$, $\frac{1}{4}$)
oP8	TcB	62 (Pnma)	5.884	2.889	4.350	4c	(0.46961, $\frac{1}{4}$, 0.39377)	4c	(0.81997, $\frac{1}{4}$, 0.61657)
hP20	Tc ₇ B ₃	186 (P6 ₃ mc)	7.322		4.735	6c 6c 6c	(0.18992, 0.81008, 0.66085) (0.87693, 0.12307, 0.74399) (0.54498, 0.45502, 0.45234)	2b	($\frac{1}{3}$, $\frac{2}{3}$, 0.41646)
oS16	Tc ₃ B	63 (Cmcm)	2.839	9.050	7.077	4c 8f	(0., 0.74365, $\frac{1}{4}$) (0., 0.86545, 0.56078)	4c	(0., 0.4261, $\frac{1}{4}$)
hP6	RuB ₂	194 (P6 ₃ /mmc)	2.825		7.170	4f	($\frac{1}{3}$, $\frac{2}{3}$, 0.94867)	2c	($\frac{1}{3}$, $\frac{2}{3}$, $\frac{1}{4}$)
hP10	Ru ₂ B ₃	194 (P6 ₃ /mmc)	2.829		12.610	4f 2c	($\frac{1}{3}$, $\frac{2}{3}$, 0.03008) ($\frac{1}{3}$, $\frac{2}{3}$, $\frac{1}{4}$)	4f	($\frac{1}{3}$, $\frac{2}{3}$, 0.85966)
hP2	RuB	187 (P6m2)	2.790		2.801	1f	($\frac{1}{3}$, $\frac{2}{3}$, $\frac{1}{2}$)	1a	(0., 0., 0.)
oP8	RhB	62 (Pnma)	5.485	3.240	4.106	4c	(0.47143, $\frac{1}{4}$, 0.38005)	4c	(0.82413, $\frac{1}{4}$, 0.62655)
aP30	Rh ₃ B ₂	2 (P-1)	9.004	6.694	5.372	2i 2i 2i 2i	(0.8162, 0.37247, 0.98435) (0.21327, 0.09004, 0.90911) (0.73358, 0.76298, 0.78924) (0.54756, 0.04442, 0.64581)	2i 2i 2i 2i	(0.02889, 0.47307, 0.73905) (0.28795, 0.8567, 0.71604) (0.45011, 0.26717, 0.47596) (0.51603, 0.80484, 0.03267)

hP20	Rh ₇ B ₃	186 (P6 ₃ mc)	7.304	4.696	2i (0.06123, 0.7707, 0.53912) 2i (0.54644, 0.52199, 0.82412) 2i (0.87223, 0.85598, 0.42828) 2i (0.02452, 0.18323, 0.10039) 2i (0.73846, 0.46597, 0.64959)	2i (0.6956, 0.56311, 0.14522) 2i (0.77314, 0.09675, 0.76981)	
mS28	Pd ₅ B ₂	15 (C2/c)	12.407	4.840	5.343	6c (0.18942, 0.81058, 0.66609) 6c (0.87704, 0.12296, 0.76378) 6c (0.54359, 0.45641, 0.42524) 8f (0.11353, 0.29717, 0.07762) 8f (0.71458, 0.07598, 0.30937) 4e (0., 0.57728, $\frac{1}{4}$)	2b ($\frac{1}{3}$, $\frac{2}{3}$, 0.42268) 8f (0.09537, 0.09884, 0.42288)
oP16	Pd ₃ B	62 (Pnma)	5.341	7.334	4.747	4c (0.38769, $\frac{1}{4}$, 0.93792) 8d (0.68197, 0.43204, 0.83033)	4c (0.03463, $\frac{1}{4}$, 0.14982) 8d (0.96404, 0., 0.78177)
mS24	CsB ₂	12 (C2/m)	10.842	4.347	6.941	8j (0.67302, 0.31172, 0.50303) 4i (0.27538, 0., 0.62927) 4i (0.42367, 0., 0.49363)	4i (0.66684, 0., 0.88551)
cP7	BaB ₆	221 (Pm $\bar{3}$ m)	4.065			6f (0.20216, $\frac{1}{2}$, $\frac{1}{2}$)	1a (0., 0., 0.)
cP7	LaB ₆	221 (Pm $\bar{3}$ m)	3.973			6f (0.19817, $\frac{1}{2}$, $\frac{1}{2}$)	1a (0., 0., 0.)
tP20	LaB ₄	127 (P4/mbm)	6.981	4.001	4e (0., 0., 0.20506) 4h (0.08755, 0.58755, $\frac{1}{2}$) 8j (0.5402, 0.67546, $\frac{1}{2}$)	4g (0.31709, 0.81709, 0.)	
hP8	LaB	194 (P6 ₃ /mmc)	3.160	12.606	2b (0., 0., $\frac{1}{4}$) 2d ($\frac{1}{3}$, $\frac{2}{3}$, $\frac{3}{4}$) 2c ($\frac{1}{3}$, $\frac{2}{3}$, 0.)	4f ($\frac{1}{3}$, $\frac{2}{3}$, 0.40261)	
hP3	HfB ₂	191 (P6/mmm)	3.050	3.364	2c ($\frac{1}{3}$, $\frac{2}{3}$, 0.)	1b (0., 0., $\frac{1}{2}$)	
hP3	TaB ₂	191 (P6/mmm)	3.022	3.228	2c ($\frac{1}{3}$, $\frac{2}{3}$, 0.)	1b (0., 0., $\frac{1}{2}$)	
oS20	Ta ₂ B ₃	63 (Cmcm)	3.213	18.945	3.046	4c (0., 0.97709, $\frac{1}{4}$) 4c (0., 0.88434, $\frac{1}{4}$) 4c (0., 0.16585, $\frac{1}{4}$)	4c (0., 0.29703, $\frac{1}{4}$) 4c (0., 0.56902, $\frac{1}{4}$)
oI14	Ta ₃ B ₄	71 (Immm)	13.707	3.059	3.204	4e (0.63314, 0., 0.) 4f (0.56417, $\frac{1}{2}$, 0.)	2d ($\frac{1}{2}$, 0., $\frac{1}{2}$) 4e (0.1856, 0., 0.)
oS22	Ta ₅ B ₆	65 (Cmmm)	22.138	3.069	3.207	4h (0.0824, 0., $\frac{1}{2}$) 4g (0.27324, 0., 0.) 4h (0.46035, 0., $\frac{1}{2}$)	4g (0.38532, 0., 0.) 4h (0.19417, 0., $\frac{1}{2}$) 2a (0., 0., 0.)
oS8	TaB	63 (Cmcm)	3.196	8.479	3.081	4c (0., 0.44001, $\frac{1}{4}$)	4c (0., 0.1461, $\frac{1}{4}$)
tP10	Ta ₃ B ₂	127 (P4/mbm)	6.024	3.194	4g (0.39203, 0.89203, 0.) 2a (0., 0., 0.)	4h (0.17777, 0.67777, $\frac{1}{2}$)	
hP10	WB ₄	194 (P6 ₃ /mmc)	2.858	10.806	4f ($\frac{1}{3}$, $\frac{2}{3}$, 0.45529) 4f ($\frac{1}{3}$, $\frac{2}{3}$, 0.61060)	2c ($\frac{1}{3}$, $\frac{2}{3}$, $\frac{1}{4}$)	
hR18	WB ₂	166 (R $\bar{3}$ m)	2.934	20.672	6c (0., 0., 0.33189) 6c (0., 0., 0.18182)	6c (0., 0., 0.07656)	
tI16	WB	141 (I4 ₁ /amd)	3.067	16.627	8e (0., $\frac{1}{4}$, 0.53113)	8e (0., $\frac{1}{4}$, 0.07224)	
tI12	W ₂ B	140 (I4/mcm)	5.447	4.678	4a (0., 0., $\frac{1}{4}$)	8h (0.66945, 0.16945, 0.)	
hP6	ReB ₂	194 (P6 ₃ /mmc)	2.834	7.366	4f ($\frac{1}{3}$, $\frac{2}{3}$, 0.95268)	2c ($\frac{1}{3}$, $\frac{2}{3}$, $\frac{1}{4}$)	
oS16	Re ₃ B	63 (Cmcm)	2.845	9.205	7.190	4c (0., 0.74541, $\frac{1}{4}$) 8f (0., 0.8664 $\frac{1}{8}$ 0.56423)	4c (0., 0.42483, $\frac{1}{4}$)
hP6	OsB ₂	194 (P6 ₃ /mmc)	2.843	7.242	4f ($\frac{1}{3}$, $\frac{2}{3}$, 0.94970)	2c ($\frac{1}{3}$, $\frac{2}{3}$, $\frac{1}{4}$)	
hP10	Os ₂ B ₃	194 (P6 ₃ /mmc)	2.857	12.725	4f ($\frac{1}{3}$, $\frac{2}{3}$, 0.53007) 2d ($\frac{1}{3}$, $\frac{2}{3}$, $\frac{3}{4}$)	4f ($\frac{1}{3}$, $\frac{2}{3}$, 0.35988)	
hP2	OsB	187 (P $\bar{6}$ m2)	2.824	2.826	1f ($\frac{2}{3}$, $\frac{1}{3}$, $\frac{1}{2}$)	1a (0., 0., 0.)	
hP4	IrB	194 (P6 ₃ /mmc)	3.448	3.806	2a (0., 0., 0.)	2c ($\frac{1}{3}$, $\frac{2}{3}$, $\frac{1}{4}$)	
hR18	PtB ₂	166 (R $\bar{3}$ m)	2.906	22.004	6c (0., 0., 0.81634) 6c (0., 0., 0.89102)	6c (0., 0., 0.71782)	
mS28	Pt ₅ B ₂	15 (C2/c)	12.610	5.013	5.347	8f (0.11327, 0.29247, 0.07367) 8f (0.71454, 0.06236, 0.30870) 4e (0., 0.57262, $\frac{1}{4}$)	8f (0.09541, 0.09679, 0.42442) 8f (0.18484, 0.43136, 0.32086)
oP16	Pt ₃ B	62 (Pnma)	5.371	7.517	4.859	4c (0.89096, $\frac{1}{4}$, 0.43979) 8d (0.18484, 0.43136, 0.32086)	4c (0.53278, $\frac{1}{4}$, 0.65313)

TABLE VII: The lattice parameters and Wyckoff positions of the stable structures at P=30 GPa.

¹ D. Hobbs, J. Hafner, and D. Spišák, Phys. Rev. B **68**, 014407 (2003), URL <http://link.aps.org/doi/10.1103/PhysRevB.68.014407>.

² J. Hafner and D. Hobbs, Phys. Rev. B **68**, 014408 (2003), URL <http://link.aps.org/doi/10.1103/PhysRevB.68.014408>.

³ N. Stojić and N. Binggeli, Journal of Magnetism and Magnetic Materials **320**, 100 (2008), ISSN 0304-8853, URL <http://www.sciencedirect.com/science/article/pii/S0304885307006841>.

⁴ A. N. Kolmogorov, S. Shah, E. R. Margine, A. K. Kleppe, and A. P. Jephcoat, Phys. Rev. Lett. **109**, 075501 (2012), URL <http://link.aps.org/doi/10.1103/PhysRevLett.109.075501>.

⁵ A. N. Kolmogorov, S. Shah, E. R. Margine, A. F. Bialon, T. Hammerschmidt, and R. Drautz, Phys. Rev. Lett. **105**, 217003 (2010), URL <http://link.aps.org/doi/10.1103/PhysRevLett.105.217003>.

⁶ H. Niu, J. Wang, X.-Q. Chen, D. Li, Y. Li, P. Lazar, R. Podloucky, and A. N. Kolmogorov, Phys. Rev. B **85**, 144116 (2012), URL <http://link.aps.org/doi/10.1103/PhysRevB.85.144116>.

⁷ S. Shah and A. N. Kolmogorov, Phys. Rev. B **88**, 014107 (2013), URL <http://link.aps.org/doi/10.1103/PhysRevB.88.014107>.

⁸ *Further details of the crystal structure investigation may be obtained from fachinformationszentrum karlsruhe, 76344 eggenstein-leopoldshafen, germany (fax: (+49)7247-808-666; e-mail: crysdata@fiz-karlsruhe.de, http://www.fiz-karlsruhe.de/request_for_deposited_data.html) on quoting the deposition number csd-426694.*